Final Report

North Carolina Department of Transportation
Research Project No. 2006-16 (IBRC 2004)

Evaluation of Design and Construction of HPC Deck Girder Bridge in Stanly County, North Carolina

By

Janos Gergely, Ph.D., P.E.
Principal Investigator

Garrett L. Overcash, E.I.
Graduate Research Assistant

Jacob B. Mock, E.I.
Graduate Research Assistant

Chris M. Clark, E.I.
Graduate Research Assistant

Kevin G. Bailey, MSCE, P.E.
Consulting Engineer at RWA

Department of Civil Engineering
University of North Carolina at Charlotte
9201 University City Boulevard
Charlotte, NC 28223

January 4, 2007

Technical Report Documentation Page

1. Report No. **FHWA/NC/2006-18**	2. Government Accession No.	3. Recipient's Catalog No.
4. Title and Subtitle **Evaluation of Design and Construction of HPC Deck Girder Bridge in Stanly County, North Carolina**		5. Report Date **January 4, 2007** 6. Performing Organization Code
7. Author(s) **Janos Gergely, Garrett L. Overcash, Jacob B. Mock, Chris M. Clark, Kevin G. Bailey**		8. Performing Organization Report No.
9. Performing Organization Name and Address **University of North Carolina at Charlotte** **Civil Engineering Department** **9201 University City Blvd** **Charlotte, NC 28223**		10. Work Unit No. (TRAIS) 11. Contract or Grant No.
12. Sponsoring Agency Name and Address **North Carolina Department of Transportation** **Research and Analysis Group** **1 South Wilmington Street** **Raleigh, North Carolina 27601**		13. Type of Report and Period Covered **Final Report** **6/06/05-6/30/06** 14. Sponsoring Agency Code **2006-16**
Supplementary Notes:		

16. Abstract

A current initiative by the Federal Highway Administration (FHWA), and the Innovative Bridge Research and Construction (IBRC) Program, focuses on new materials and technologies in bridge design and construction. Under this program, a recent project awarded to the North Carolina Department of Transportation (NCDOT) concentrates on a high performance concrete (HPC) deck girder system, comprising of a modified AASHTO Type III girder with an additional flange (deck) section, with the objectives to review the design and detailing information, monitor the deck girder fabrication and the bridge construction processes, load test the completed bridge, and to evaluate the embedded stud connection. The load testing of the deck girder bridge was performed using two tandem trucks. The bridge was instrumented using strain transducers, strain gages, and displacement transducers. The instrument layout was designed to experimentally determine the transverse distribution factors, impact factors, strain levels, and displacements of each girder due to different loading conditions.

A finite element (FE) model was also developed, for which, model calibration was performed by comparing vertical displacement and stress values using NCDOT, Larsa™, and ANSYS™ results on a single deck girder. Once calibrated, the single-girder model was then copied to create five identical deck girders. The plate and diaphragm components were created and the appropriate loads were placed on the model. The results were then compared to the actual quasi-static load test performed on the finished bridge. Furthermore, using the working ANSYS model, a parametric study was then performed to investigate the influence of diaphragm and flange connection spacing.

The capacity and failure mechanism of the embedded stud connection used to join the adjacent deck girders is not accurately defined by current PCI specifications. Therefore, the shear and tension capacity of the connection was investigated through FE analysis, followed by laboratory testing of four specimens of each type. Only few of the calculations compared closely to the predicted values from the 6th Edition of the PCI Design Handbook. Hence, in order to accurately assess the capacity of non-traditional connections not resembling the standard headed stud details, experimental and/or FE studies should be performed.

17. Key Words Precast, prestressed, concrete deck girders, AASHTO Type III girders	18. Distribution Statement		
19. Security Classif. (of this report) Unclassified	20. Security Classif. (of this page) Unclassified	21. No. of Pages 178	22. Price

Form DOT F 1700.7 (8-72) **Reproduction of completed page authorized**

Executive Summary

The objectives of the present research project were to: (1) review the design and detailing information; (2) monitor the deck girder fabrication and the bridge construction processes; (3) load test the completed bridge, and (4) evaluate the embedded stud connection. This final report summarizes the findings of the project as a whole, including recommendations and conclusions reached throughout the duration of this project.

The load testing of the deck girder bridge was performed using two tandem trucks with a combined total weight of approximately 100,000 lbs. The bridge was instrumented using strain transducers, strain gages, and displacement transducers. The instrument layout was designed to experimentally determine the distribution factors, impact factors, strain levels, and displacements of each girder due to different loading conditions.

Graphs of the deck girder strain and vertical displacement were obtained as the load test trucks traveled across the bridge. The maximum transverse compressive and tensile stress that occurred in the top extreme fiber of the instrumented plates was also recorded. The instrumented steel diaphragms also resulted in normal stress values at both of the diaphragm ends. The load test revealed that the plate connectors have a safety factor of approximately 2.1. The diaphragm members transmitted a relatively small portion of the load, and had a significantly larger safety margin.

A finite element (FE) model was developed, for which, model calibration was performed by comparing vertical displacement and stress values using NCDOT, Larsa™, and ANSYS™ results on a single deck girder. The FE model was found to match both sets of calculations when the prestress force and self-weight was applied. Once calibrated, the single-girder model was then repeated to create five identical deck girders. The plate and diaphragm components were created and the appropriate loads were placed on the model. The results were then compared to the actual quasi-static load test performed on the finished bridge. The resulting normal stresses and displacements obtained from the computer models were very similar to the actual load test values. The plate and

diaphragm maximum stress values were also very similar to the actual load test results. The maximum stress in the plates was found to be significantly less than the allowed LRFD stress values.

Using the working ANSYS model, a parametric study was then performed to investigate the influence of diaphragms and flange connection spacing. The spacing of the plates was investigated with the spacing increased to 10'-0". The increased spacing resulted in a negligible distribution factor change and increased mid-span diaphragm stress slightly. The stress increase in the plates when spacing was increased was mainly in compression and seemed to be a viable alternative to the 5'-0" original design. The diaphragm stresses were observed at both plate spacing, and resulted in relatively small values compared to the yield stress.

The capacity and failure mechanism of the embedded stud connection used to join the adjacent deck girders is not accurately defined by current PCI specifications. Therefore, the shear and tension capacity of the connection was investigated through FE analysis, followed by laboratory testing of four specimens of each type. The connection capacity was governed by tensile (eccentric) loading, with an average capacity of 12.78 kips. The shear specimens' average ultimate capacity was 24.65 kips. Only few of the calculations compared closely to the predicted values from the 6th Edition of the PCI Design Handbook. Therefore, in order to accurately assess the capacity of non-traditional connections not resembling the standard headed stud details, experimental and/or FE studies should be performed.

Table of Contents

List of Figures

List of Tables

1 Introduction

A current initiative by the Federal Highway Administration (FHWA), and the Innovative Bridge Research and Construction (IBRC) Program, focuses on new materials and technologies in bridge design and construction. Under this program, a recent project awarded to the North Carolina Department of Transportation (NCDOT) concentrates on a high performance concrete (HPC) deck girder system, comprising of a modified AASHTO Type III girder with an additional flange (deck) section. The objectives of the present research project were to review the design and detailing information, monitor the deck girder fabrication and the bridge construction processes, and finally, to load test the completed bridge. Finite Element (FE) models of the entire bridge and the embedded stud connections were also created to better represent the force transmission through the diaphragms and the steel plate connectors.

This final report summarizes the findings and conclusions obtained by documenting the bridge project from the NCDOT design phase to the quasi-static load test on the completed bridge. The load test values are compared to the LRFD design calculations and predictions. The comparison of the FE model and the actual load test is presented to determine the behavior of the components and the distribution of live load on the bridge. A parametric study on the steel connector plates was also completed to validate the number and spacing of the steel plate connectors. The stresses associated with the steel diaphragms were also investigated. The embedded stud connection behavior was discussed based on actual laboratory load tests and an FE connection model. The connection analysis provided a more precise estimate for the shear and tensile capacity of the connection used in the constructed deck girder bridge project. The FE model allowed the change in loading and geometry associated with the connection.

1.1 Literature Review

The primary source of existing literature on deck girders was located in PCI journal articles authored by Anderson. Other related information contained discussions about pry-out capacity and design criteria of headed studs. An article concerning the effects of diaphragms on live load distribution was also located in the Canadian Journal of Civil Engineering.

Little research has been published about deck girders, and no known published research has been found using the AASHTO LRFD Specifications for the design of deck girders using standard AASHTO I-Beams. A PCI Journal article was published by Anderson (1973) describing the longer span capabilities of segmental type construction using a deck girder system with what was then known as AASHO-PCI Beams Type III and IV. The Type III and IV beams were cast integral with the deck portion prior to post-tensioning in the field to achieve maximum span capabilities.

Another PCI Journal article written by Anderson (CTA, 1973) describes how Mr. Anderson and his brother, along with their two former companies developed the deck girder system as we know it today. A technical bulletin from the Concrete Technology Associates (CTA), one of the companies formed by the Anderson brothers, was found to also include a design example demonstrating that long spans can be achieved with segmental deck girders and the use of post-tensioning only (CTA, 1973).

Additional related publications include an article in the Canadian Journal of Civil Engineering by Cheung (1986). This article describes a theoretical approach for computing and evaluating the structural behavior of diaphragms in a beam-and-slab system with two or more diaphragms for short to medium-span bridges. Two, more recent PCI Journal articles were found that discuss pry-out capacities and shear capacities of headed stud anchorages (Anderson and Meinheit, 2000 and 2005).

Deck bulb-tee girders using standard AASHTO I-beams based on the LRFD design method was also reviewed in a thesis authored by Bailey (2006). The thesis discusses the LRFD design method by exploring how deck girder spacing, AASHTO girder type, material strength, and prestress strand pattern affect the applications of the deck girders.

1.2 Research Objectives

The primary focus of this research project was to evaluate a new deck girder bridge system and provide the NCDOT with feedback information to aid in the design and construction of similar bridge systems. The fabrication stage of the bridge project was monitored to provide future fabricators with knowledge addressing common problems and alternative methods for casting the deck girders. The transportation from the casting yard to the bridge site was also documented to further close the gap between the fabrication standards and the requirements for safely transporting the deck girders. The accuracy of the LRFD design was evaluated to compare the design calculations with the actual performance of the deck girder bridge.

The ANSYS™ FE model was created to allow a parametric study to be performed. The influence of the steel plate connectors and the steel diaphragms were then evaluated to provide the NCDOT with data for future deck girder designs. The actual flange connection (as constructed) was then tested and modeled in an FE program to establish capacities that do not exist in the current PCI Design Handbook 6th Edition (2004). It is our hope that the research project will provide the NCDOT with a base of information that can be used to design deck girder systems and the components associated with the bridge systems, with a working knowledge of how well the LRFD design method applies to this particular bridge type.

2 Design and Detailing

2.1 Bridge Description

The deck girder bridge was designed, using the most recent AASHTO LRFD specifications, as a two lane bridge spanning over Long Creek (a clear water creek) in Stanly County, North Carolina. The total bearing to bearing span is 106' with no intermediate supports and with integral end bents. The bridge consists of five 107'-4" independent prestressed deck girders that were connected with steel plates spaced at 5'-0" on center and steel diaphragms at the quarter and half points. The standard type III AASHTO girders were cast first, then the 6'-6" deck section was cast (using the same concrete mix as for the girder section) and allowed to cure to the release strength of 5,500psi. The prestress strands were cut only when the total section had reached the allowable release strength. The net section was then prestressed and acted as a single unit.

Once the girders were placed in the final positions at the construction site, the steel diaphragms were installed and the embedded stud connections were joined by a welded steel plate. The shear key voids between the adjacent deck girder flanges were then filled with a non-shrink grout. The parapet walls were poured and the guardrails were installed. The final asphalt surface was then paved and the bridge was opened to traffic.

2.2 Design Review

A design review was performed on the hand calculations for the deck girder design and was completed in two different stages. The first stage was an initial review of the calculations for the actual deck girders. The second stage consisted of a review of the calculations, plus referring to the LRFD Specifications throughout each step. The girder design hand calculations were studied to help understand the process used for the particular project.

The moment and shear distribution factors for interior and exterior girders were chosen based on the cross section and the criteria in AASHTO LRFD Table 4.6.2.2.1-1. Type "k" describes a bridge design that contains a sufficiently connected deck to act as a unit, such as a monolithic deck girder construction. Type "j" (for the purpose of this report) describes a bridge that consists of individual deck girders connected with flexible connection. The factors represent the connections' ability to transfer load from girder to girder. Upon reviewing the design calculations, the use of bridge type "k" for computing distribution factors was seen, which also includes type "j" bridges appropriately with rigid connection. However, the use of bridge type "j" (with flexible connection) is more common for computing live load distribution factors for bulb tee sections, and it is more appropriate for this bridge. This distribution factor was also confirmed by the bridge test results.

As demonstrated in Figure 2-1, the difference in distribution factors for moment is insignificant when girder spacing is small. In this project the girder spacing of 6.5 ft. is relatively small; therefore, the assumption will have very little effect on the design moment (Case k = 0.513 and Case j = 0.558). However, if in the future larger girder spacing will be desired, the connection details should be more closely investigated and designed for a rigid connection between deck girders.

An independent evaluation of the prestress design and factored deck girder stresses using an in-house spreadsheet program was also performed at Ralph Whitehead Associates, Inc. (RWA) using the more conservative type "j" bridge assuming a more flexible connection. See Figures 2-2 and 2-3 for a sample output of the independent computations performed for this project. This program produced very similar results to the NCDOT hand calculations throughout the computational process in accordance with the AASHTO LRFD specifications.

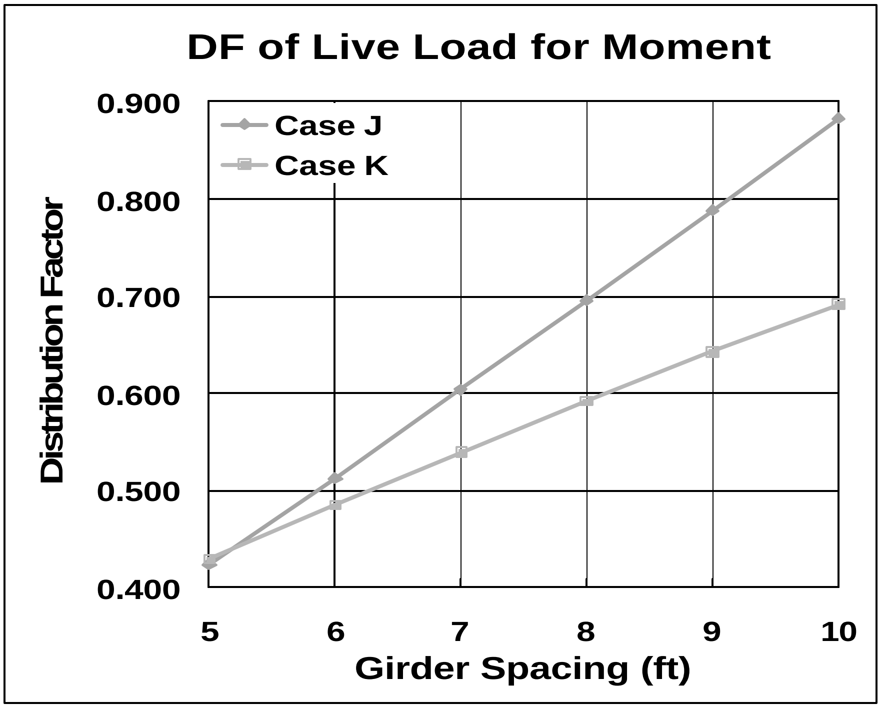

Figure 2-1. Category k and j Moment Distribution Factor Comparison

Cum. No. Strands	? f_{cgp}	ELASTIC SHORTENING ? f_{pES}	INITIAL STRESS f_{pi}	INITIAL JACKING FORCE F_{pi}	SHRINKAGE ? f_{pSR}	? f_{cdp}	CREEP ? f_{pCR}
32	2.521	16.816	185.7	1289.391	5.75	0.636	25.80

Cum. No. Strands	RELAXATION ? f_{pR2}	TOTAL LOSS ? f_{pT}	EFFECTIVE STRESS AFTER LOSSES f_{pe}	EFFECTIVE FORCE F_{pe}
32	2.089	50.457	152.0	1055.784

Figure 2-2. Independent Loss Calculations

Cum. No. Strands	Midspan @ Full Service Loads	PS + DL Gdr @ Release		Allowable Stresses	PS Only	
		Top Gdr	Bot Gdr	O.K.?	Top Gdr	Bot Gdr
	Self DL =	*0.957*	*-1.994*		*0.000*	*0.000*
	Comp DL =				*0.000*	*0.000*
	Comp LL =				*0.000*	*0.000*
32		**0.187**	**2.676**	**O.K.**	**-0.631**	**3.824**

Cum. No. Strands	Midspan @ Full Service Loads	PS + DL Only		Allowable Stresses	PS + DL + LL		Allowable Stresses
		Top Gdr	Bot Gdr	O.K.?	Top Gdr	Bot Gdr	O.K.?
	Self DL =	*0.936*	*-1.950*		*0.936*	*-1.950*	
	Comp DL =	*0.350*	*-0.729*		*0.350*	*-0.729*	
	Comp LL =	*0.000*	*0.000*		*0.844*	*-1.407*	
32		**0.655**	**1.145**	**O.K.**	**1.499**	**-0.262**	**O.K.**

Cum. No. Strands	Midspan @ Full Service Loads	LL + .5*(PS+DL)		Allowable Stresses
		Top Gdr	Bot Gdr	O.K.?
	Self DL =	*0.936*	*-1.950*	
	Comp DL =	*0.350*	*-0.729*	
	Comp LL =	*0.844*	*-1.758*	
32		**1.171**	**-1.186**	**O.K.**

Figure 2-3. Independent Stress Calculations

2.3 Larsa™ Model Construction

A parametric study was conducted using Larsa™ 2000 4^{th} Dimension for Bridges (Larsa™, 2005), a software developed for bridge analysis and design (this software was provided by Larsa™ Inc. free of charge for the duration of the present project). The program allows accurate assembly of the bridge elements as they are fabricated and constructed in the field. This feature allowed all loadings and restraints to be applied in a staged construction order. Once completed, the program reported results (such as member stresses, camber due to prestress, etc...) that were comparable with the design hand calculations performed by the NCDOT. Some of the member output values from Larsa™ were smaller than the hand calculation results, a discrepancy that can be attributed to the fact that in the hand calculations the entire 10 feet wide lane load was applied to a single 6'-6" wide deck girder section (which resulted in a more conservative design).

The first step in completing the Larsa™ model was defining the six different girder cross section types (Figure 2-4). The next step involved extruding the sections to the desired length from bearing to bearing. Figures 2-5 through 2-7 show the connection details, as well as the bridge superstructure model respectively. As it can be seen in Figure 2-7, in this parametric study it was assumed that the bridge is simply supported at both ends (pinned-roller connection). This assumption was also used in the hand calculations; however, the integral end walls will introduce negative moments close to the supports. The Larsa™ model used later in this report to compare with actual load test results had fixed supports at both ends of the deck girders. The design calculations however, were computed with simple supports as was the initial Larsa™ model. This integral end bent contribution to stiffness was also further investigated in the ANSYS™ FE model.

Another limitation of this model was the angle-to-steel plate connections. The current modeling techniques in Larsa™ allowed the plates to be connected to the embedded angles only at the four corners, instead of the fillet weld connection to be performed in the field. Furthermore, the shear keys were not filled with a grout, connecting the deck girder flanges. These limitations resulted in a more flexible and weaker connection details, causing the initial analytical study to predict higher than anticipated forces in the connecting plates. Therefore, the Larsa™ analytical results should be viewed as a qualitative analysis, rather than a quantitative evaluation. The main purpose of the Larsa™ model was to aid the research team when deciding how to instrument the bridge for the load test. The creation of a working ANSYS™ model in this time frame was not feasible. The ANSYS™ FE model was restrained as constructed with the integral end bent and finer connection details were created to provide a more accurate model of the constructed bridge, this is discussed later in Chapter 3. The ANSYS™ FE model was also calibrated to the actual load test.

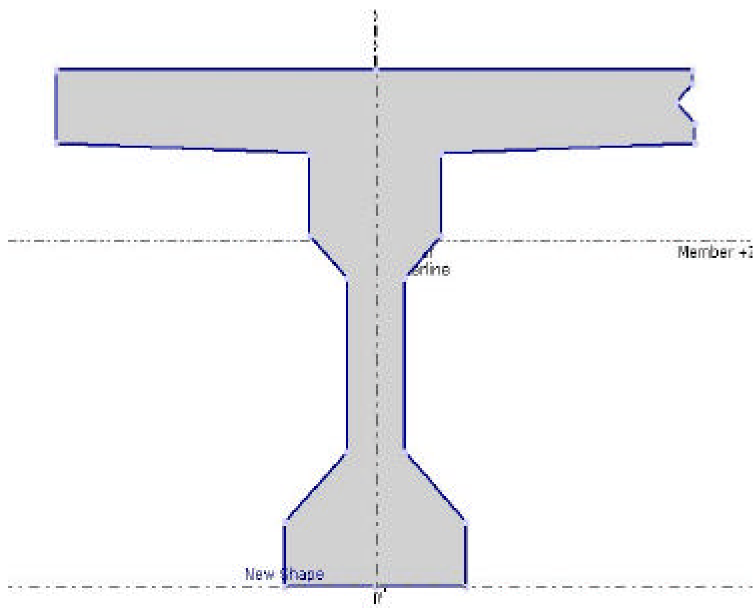

Figure 2-4. Larsa™ Exterior Shear Key Girder Cross Section

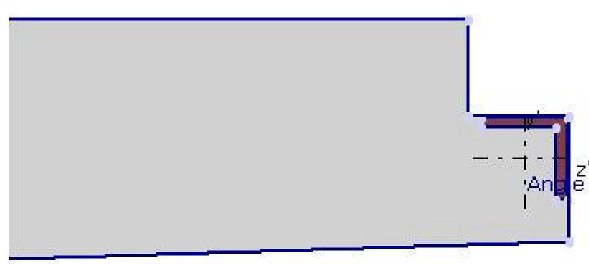

Figure 2-5. Larsa™ Embedded Steel Angle Detail

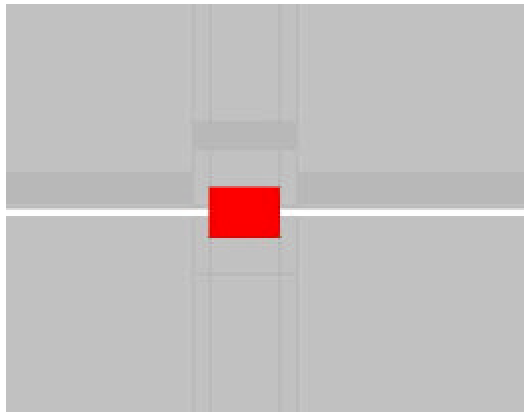

Figure 2-6. Larsa™ Plan View of Plate and Connection Detail

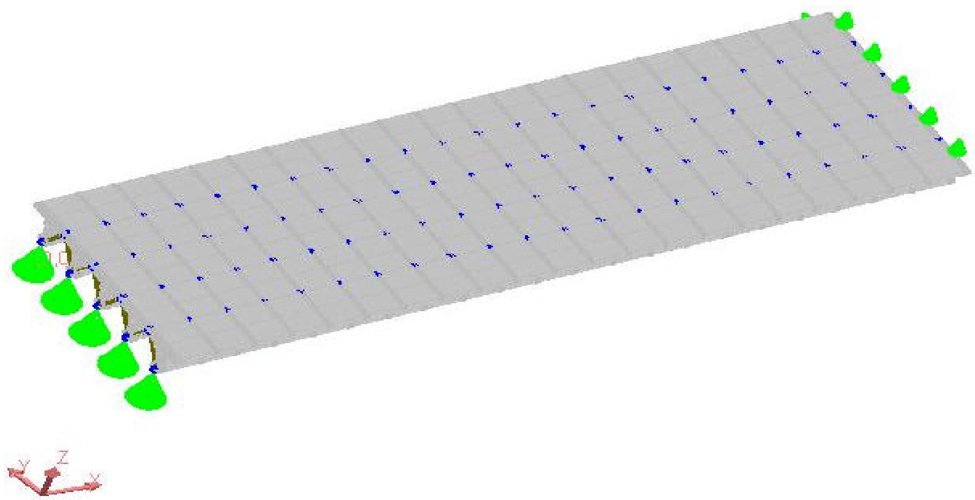

Figure 2-7. Larsa™ Complete Bridge Section

After assembling the deck girders in the model, all connection plates were added at 5’-0” on center along each span. All dead loads generated from structural and non-structural components were applied. The lane paths, which represent the wheel lines of a truck axle, were then generated. The HL-93 design truck and the corresponding 10’-0” wide lane loading was placed at four strategic locations that would result in the highest stresses in the steel plates. The lane loads and the truck wheel paths are shown in Figures 2-8 through 2-11. Additionally, tendon paths were placed at the centroid of the strand group in each deck girder to allow loading from the prestress forces. Figure 2-8 represents the worst case loading condition, when both lanes are loaded and maximum stresses are recorded in the connections.

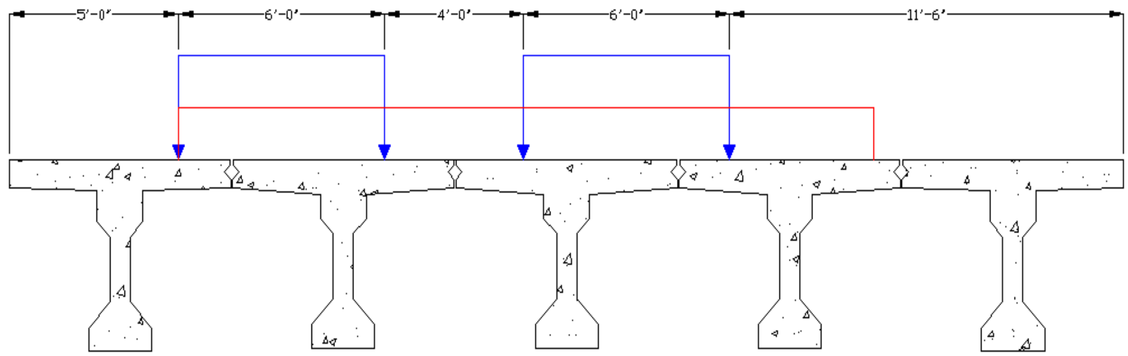

Figure 2-8. Truck 1 and Lane Load Layout

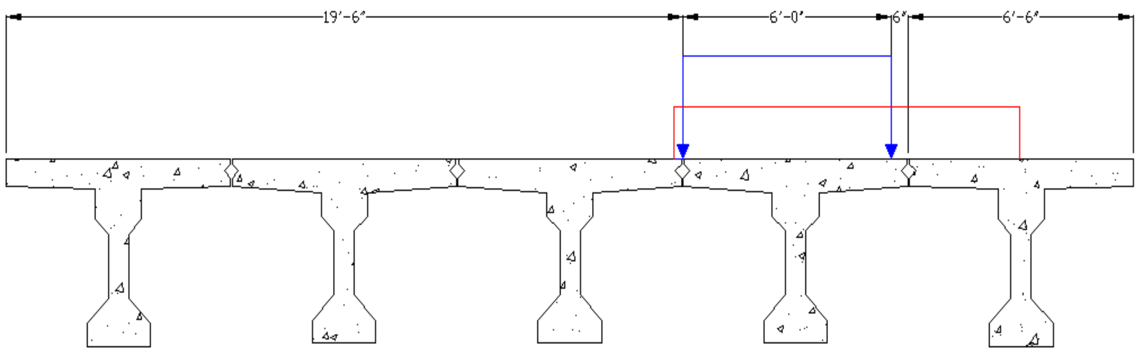

Figure 2-9. Truck 2 and Lane Load Layout

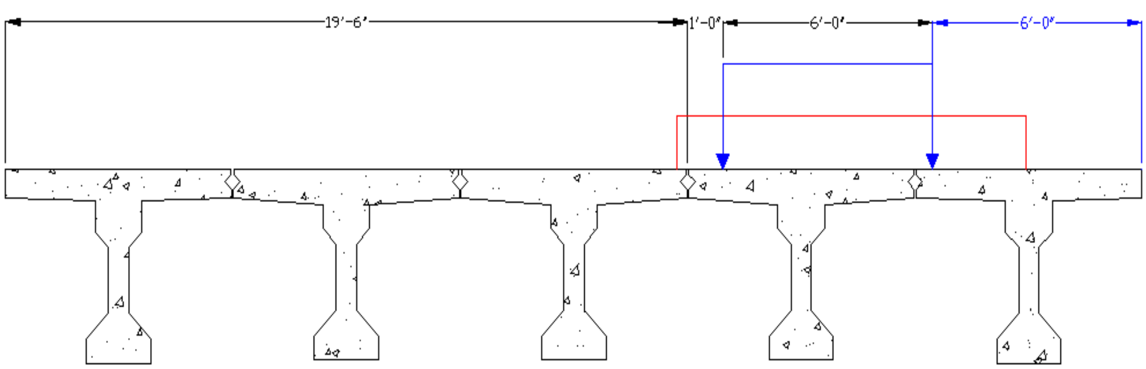

Figure 2-10. Truck 3 and Lane Load Layout

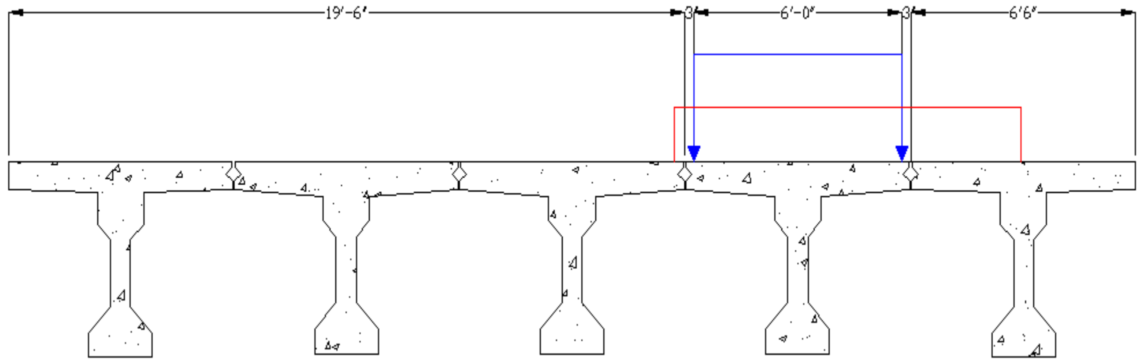

Figure 2-11. Truck 4 and Lane Load Layout

2.4 Larsa™ Model Results

The Larsa 2000™ bridge model provided very similar values for a number of different NCDOT hand calculations presented in the design document (Hanks, 2005). The stresses at release were found to be within 15% at the top fiber and within 2% at the bottom fiber. Small differences, 7% maximum, in stresses at service loads were reported (see Table 2-1). The calculated values for stresses induced under the live loading are shown for each of the four different live load cases. Worst case girder forces were caused by loading conditions that did not correspond with the controlling loading conditions for the plate connectors. Therefore, several load cases were considered in addition to the more standard loading cases performed in hand calculations.

The deflection and camber values provided by the NCDOT also provided an excellent model check. The difference in vertical displacement in the girder at mid-span was only 0.14" (2.46" in NCDOT calculations, and 2.60" Larsa™ results). Only self weight and prestress at release were considered in the next simple comparison (see Table 2-2). A comparison of unfactored shear and moment values from the Larsa™ model and the NCDOT design calculations was also performed (see Table 2-3). As it can be seen, the Larsa™ model results closely matched the hand calculations, and an initial parametric study followed these preliminary model calibrations. The Larsa™ model was used as a preliminary indication of how to instrument the actual bridge and the deck girders were simply supported. As it was stated earlier, due to modeling limitations, these analyses should be viewed as a qualitative evaluation, rather than a quantitative study.

Table 2-1. Deck Girder Member Stress: Larsa 2000™ vs. NCDOT Design

Location	Load Case	Larsa Stress at Top (ksi)	NCDOT Stress at Top (ksi)	Larsa Stress at Bottom (ksi)	NCDOT Stress at Bottom (ksi)
mid-span	Dead + Prestress @ Release	0.165	0.191	2.788	2.725
mid-span	Dead + Prestress @ Service Loads	0.675	0.709	1.165	1.085
mid-span	Dead + Prestress + Live Load	1.265	1.725	0.171	0.572
mid-span	0.5(Dead + Prestress) + Live Load	1.488	1.371	n/a	n/a

Table 2-2. Unfactored Vertical Displacement Comparison: Larsa 2000™ vs. NCDOT Design

Vertical Displacement (in.)	Location Along Span	Larsa Model (in.)	NCDOT Calculations (in.)
P/S Camber @ Release	mid-span	4.62	4.48
Deck Girder Self-weight Deflection	mid-span	-2.02	-2.02
Net Camber	mid-span	2.60	2.46
Rail/Overlay/FWS Deflection	mid-span	-0.67	-0.66

Table 2-3. Unfactored Shear and Moment Comparison: Larsa 2000™ vs. NCDOT Design

Force	Unfactored Applied Loads	Location Along Span	Larsa Model	NCDOT Calculations
Interior/Exterior Beam Shear (kips)	Total DC Load	member end	75.3	76.0
	Total DW Load	member end	22.9	23.0
Interior/Exterior Beam Moment (k- ft)	Total DC Load	mid-span	1994.4	2003.0
	Total DW Load	mid-span	610.9	611.0

Note: DC = Dead Load of Structural Components and Non- Structural Attachments
DW = Dead Load of Structural Overlay and Future Wearing Surfaces

Based on the plate stresses obtained from the Larsa™ model, a connection fatigue analysis was performed. The welded connector plate experiences the highest fatigue stress based on Truck 1 loading condition, and caused a maximum stress in the first plate between girder lines 2 and 3 (see Figure 2-12 for plate numbering). The axis and plane geometry of the plate is shown in Figure 2-13, "X" being the longitudinal axis of the bridge.

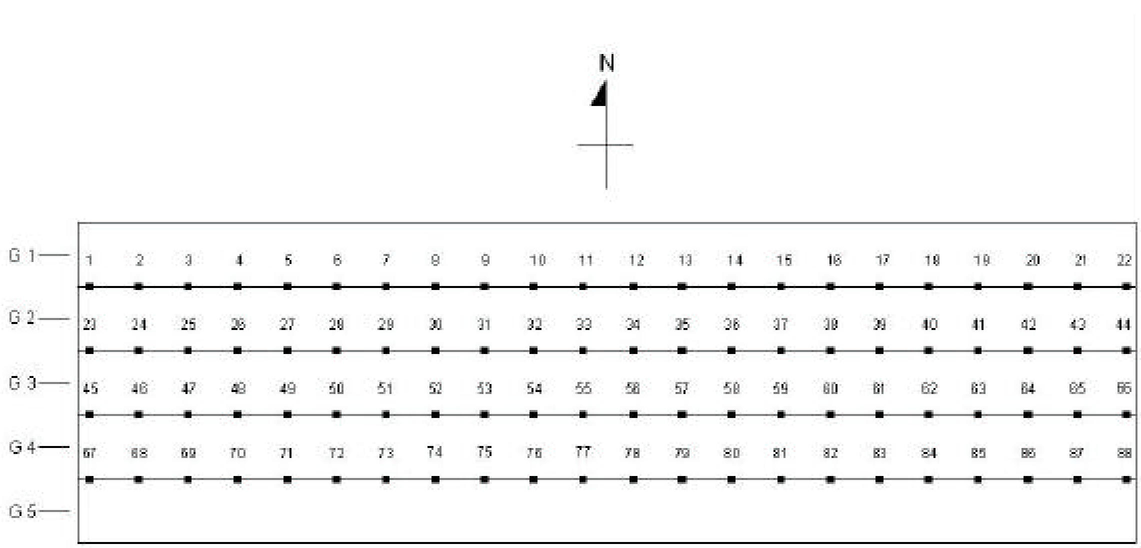

Figure 2-12. Plate Numbering in Plan View

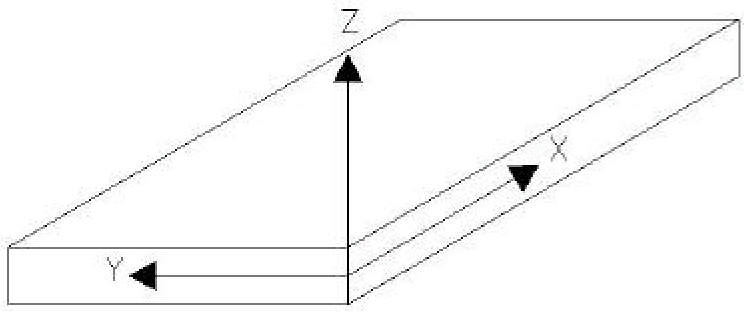

Figure 2-13. Local Plate Axis in Larsa™

For analyzing fatigue in the connector plates (1/2" x 3" x 4"), the Load-Induced Fatigue section (6.6.1.2.2) of the LRFD specifications were considered (using Equations 2-1 through 2-3), since no other specific information was available for these connection details. The LRFD Bridge Design Manual does not contain a method for selecting a detail category; therefore, using Detail 17 in Figure 6.6.1.2.3-1, Detail Category "D" was selected based on similarities with the specified field welding conditions.

The largest live load stress due to fatigue truck loading was 1.38 ksi (see Table 2-4), a value significantly lower than the nominal fatigue resistance for the plate calculated as 3.7 ksi, as shown in the LRFD 6.6.1.2.2-1 design criteria.

$$g(\Delta f) \le (\Delta F)_n \qquad (2\text{-}1)$$

where:

? = load factor specified in LRFD Table 3.4.1-1 for the fatigue load combination

(? f) = force effect, live load stress range due to the passage of the fatigue load as specified in LRFD Article 3.6.1.4

(? F)$_n$ = nominal fatigue resistance as specified in LRFD 6.6.1.2.5 (Equation 2-2)

$$(\Delta F)_n = \left(\frac{A}{N}\right)^{1/3} \ge \frac{1}{2}(\Delta F)_{TH} \qquad (2\text{-}2)$$

and

$$N = (365)(75)n(ADTT)_{SL} \tag{2-3}$$

where:

A = constant from LRFD Table 6.6.1.2.5-1
n = number of stress range cycles per truck passage (LRFD Table 6.6.1.2.5-2)
$(ADTT)_{SL}$ = single – lane ADTT as specified in LRFD Article 3.6.1.4
$(?F)_{TH}$ = constant – amplitude fatigue threshold (LRFD Table 6.6.1.2.5-3)

Fatigue Design Calculations:

? = 0.75
(?f) = 1.38 ksi
A = 22.0 x 10^8 ksi^3
n = 1.0
$(ADTT)_{SL}$ = 0.85 x 1875
$(?F)_{TH}$ = 7.0

$$N = (365)(75)(1.0)(0.85 \times 1875) = 43{,}628{,}906.3$$

$$(\Delta F)_n = \left(\frac{22.0 \times 10^8}{43{,}628{,}906.3} \right)^{1/3} \geq \frac{1}{2}(7.0)$$
$$= 3.7 \geq 3.5 \Rightarrow \underline{\text{OK use 3.7}}$$

$$g(\Delta f) = 0.75(1.38) = \underline{1.04 \text{ ksi} < 3.7 \text{ ksi}} \Rightarrow \textbf{OK}$$

Table 2-4. Maximum Plate Stresses - Truck 1 Fatigue <u>(with Diaphragms)</u>

Plate Id	**Location**	**Sxx** ksi	**Syy** ksi	**Sxy** ksi	**Principal Max** ksi
2	Top	**0.446**	0.289	-0.142	0.529
10	Bottom	0.175	**1.378**	-0.120	1.390
61	Bottom	-0.093	-0.236	**0.848**	0.686
10	Bottom	0.175	1.378	-0.120	**1.390**

In order to investigate the effect of diaphragms on the connection stresses, the diaphragm members were then removed and the same loading conditions were performed to find the effect on the plates during fatigue analysis. The results show that the diaphragm had a considerable effect on the plate stresses, especially in the S_{yy} (transverse) direction (results shown in Table 2-5). These stresses are still lower than the nominal fatigue resistance calculated above.

Table 2-5. Maximum Plate Stresses - Truck 1 Fatigue (<u>Without Diaphragms</u>)

Plate Id	**Location**	**Sxx** ksi	**Syy** ksi	**Sxy** ksi	**Principal Max** ksi
56	Bottom	**-0.624**	-1.812	0.112	-0.613
10	Bottom	0.403	**2.156**	-0.111	2.163
49	Bottom	-0.226	-0.848	**-0.878**	0.394
10	Bottom	0.382	2.132	-0.257	**2.169**

In addition to evaluating fatigue stresses in the connector plates, other stresses due to the LRFD Strength I - Truck 3 loading combination were also considered. Strength I load combination was found to produce the maximum stresses in the connector plates. These results are shown in Tables 2-6 and 2-7. Similarly to the parametric study done for the fatigue analysis, this strength analysis considered both the current design configuration, as well as a bridge without diaphragms.

Table 2-6. Strength I (<u>with Diaphragms</u>) - Connector Plate Stresses

Plate Id	**Location**	**Sxx** ksi	**Syy** ksi	**Sxy** ksi	**Principal Max** ksi
69	Bottom	**2.777**	5.595	1.456	6.212
75	Bottom	2.416	**13.508**	1.761	13.781
39	Bottom	-0.280	-0.424	**-4.018**	3.667
75	Bottom	2.416	13.508	1.761	**13.781**

Table 2-7. Strength I (Without Diaphragms)- Connector Plate Stresses

Plate Id	**Location**	**Sxx** ksi	**Syy** ksi	**Sxy** ksi	**Principal Max** ksi
32	Bottom	**- 4.854**	-9.191	1.537	-4.365
77	Bottom	4.515	**27.131**	0.490	27.142
43	Bottom	-0.963	-1.565	**-10.115**	8.855
77	Bottom	4.515	27.131	0.490	**27.142**

The maximum principal stress in the plate connectors was determined to be 13.781ksi. This value was heavily influenced by the S_{yy} stress of 13.51 ksi in the transverse direction. The maximum stress in each combination is provided in bold text. The tensile (pull-out) force at the contact point between the welded plate and the angle was calculated to be 24.3 kips (48.9 kips). However, as it was mentioned earlier, the Larsa™ model did not truly capture the rigidity of the bridge and the connections detail. Therefore, the initial Larsa™ force values are believed to considerably overestimate plate stresses.

The values from Table 2-7 prove that the absence of diaphragms considerably increases the connection stresses, well beyond their estimated pull-out capacities. The maximum stress in any of the diaphragms under all load conditions considered was found to occur in Strength I Truck I load condition. The stress caused by this load combination was 6.39 ksi, which represented only 18% of the diaphragm material yield stress of 36 ksi. This proves that the diaphragms have ample strength capacity, considering a more flexible Larsa™ model.

2.5 Construction Economical Analysis

The cost for construction of the bridge in Stanly County was an aspect that needed to be addressed for further decisions to use modified AASHTO prestress deck girders for other bridge projects. The NCDOT provided bidding information on two other bridge projects of different types along with the project on Austin Road. The bidding information for the cost of the superstructure is shown in Table 2-8. Projects B-3630 and B-3376 both required a concrete deck to be poured after the girders were placed on site.

The net cost of each project shows that the deck girder bridge was more expensive than using bulb-T beams or steel plate girders. This could have been expected because the AASHTO Type III prestress concrete deck girders had never been fabricated before – and if more sections are fabricated in the future, their cost should be lower based on economy of scale. Though this project was more expensive than similar projects, the traveling public benefited from a significantly reduced road closure period. The construction prices for a deck girder bridge in a more accessible area may decrease the price of the project. However, the construction of this deck girder bridge was roughly 3-4 weeks faster than a normal bridge project where the deck is poured on site (when bulb T or steel girders are used). This could save a significant amount of labor and material cost.

Table 2-8. Price Comparison of NCDOT Type Bridges

Project	Superstructure	Net Cost	Bearing Length (ft.)	Bearing Area (ft.^{2})	Net Cost/ ft.^{2}
B-3630	60" Steel Plate Girder	$315,375.80	120	3,730	$84.55
B-3376	63" Bulb T	$360,253.36	105	3,992	$90.24
B-3700	Type III Prestressed Concrete Deck Girder	$423,561.70	110	3,575	$118.48

3 FE Analysis

An ANSYS™ FE model of the deck girder bridge was created to facilitate a parametric study on the steel plates and steel diaphragms. The model also allowed changes in the material properties and live loading patterns to evaluate the effects on the bridge as a whole. The deck girders were modeled using the ultimate concrete strengths from the cylinders that were tested at the time of the load test. The prestress strands were given the strain values that were present after all losses, because no time analysis was performed in the FE program. The asphalt overlay, parapet rail, and the future wearing surface were omitted because only the live loading effects were recorded during the actual load test.

The use of ANSYS™ was warranted due to the program's ability to report values of stress and displacement at multiple locations within a member. This feature allowed small members (steel plates) to report stress contours throughout the whole cross section, whereas in Larsa™ the extreme fiber stresses are the only available values. The ability to "weld" the plate connectors to the flange surfaces also captured a more accurate fixity of the steel plates. ANSYS™ does not have a moving load option; this was amended by placing the load test truck at mid-span to create near maximum moment and deflection values that coincided with the actual load test stress levels. ANSYS™ also did not allow for staged construction steps, this required fixing the girder ends that were incased by the integral end bents before prestress effects were applied.

3.1 Model Description

The ANSYS™ deck girder bridge model was created by first modeling one deck girder that produced comparable stress and camber values to NCDOT and Larsa™ results. Once the completed girder was verified, the other four girders were generated. The steel plates and diaphragms were then placed on the model, and the prestress and self-weight loads were added. The plates and diaphragms were placed on the bridge before tendon release, because no construction stage option was available in ANSYS™. The stresses in the plates and diaphragms due to the prestress and dead load were recorded in ANSYS™ so that post-construction live load effects could be analyzed separately. The equivalent girder cross section is shown in Figure 3-1.

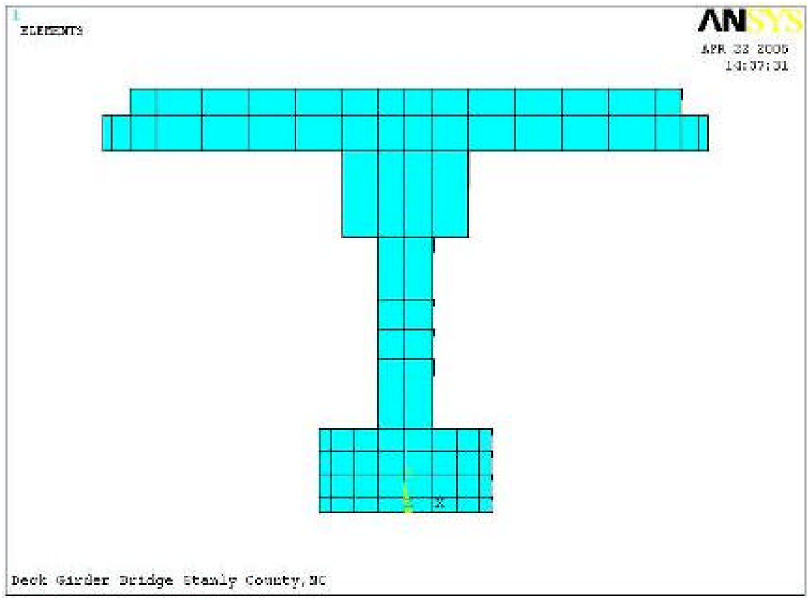

Figure 3-1. Equivalent Deck Girder Cross Section

The simply supported girder was created using SOLID65 elements, which are 3-D reinforced concrete elements with cracking and crushing capabilities. The prestress force was induced by using axial LINK8 elements with an initial strain. The steel plates and diaphragms were modeled using the two-node BEAM4 line elements. The deck girder cross section was modified from the one described in Interim Report III, to allow the plates and diaphragms to be placed between adjacent girders. The steel members were modeled using 36 ksi steel with an elastic – perfectly plastic stress/strain relationship. The deformed girder under the prestress and self-weight conditions is shown in Figure 3-2.

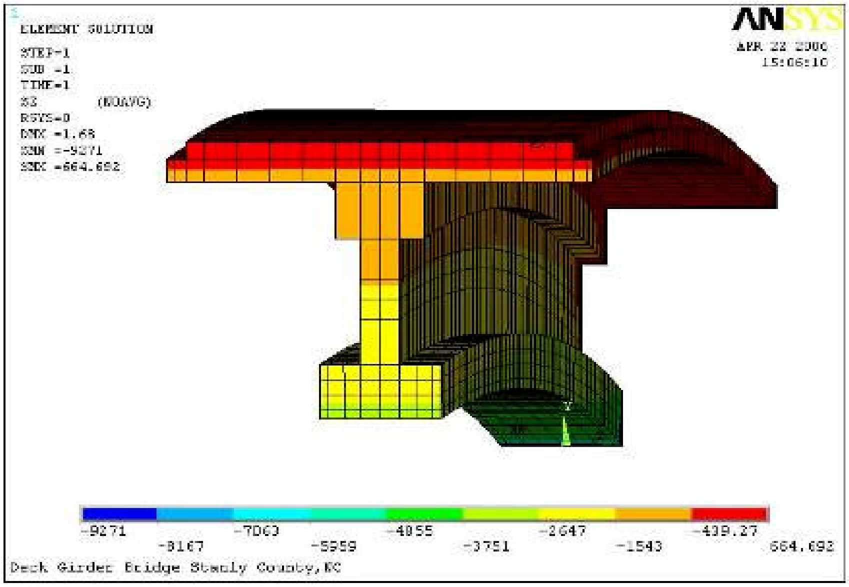

Figure 3-2. Prestress + Self-Weight Normal Stress

The creation of the entire bridge in ANSYS™ proved to be a very time and disk space consuming operation. To alleviate this problem, only half of the bridge was modeled and a symmetry plane was placed at deck girder mid-span perpendicular to the direction of traffic. This allowed the entire bridge to be modeled, while only using half of the computing resources necessary. The five generated deck girders are shown in Figure 3-3.

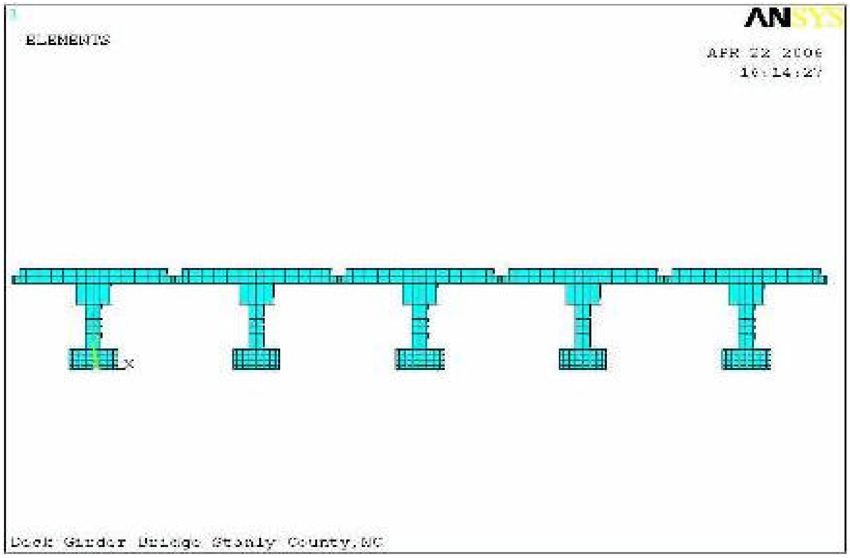

Figure 3-3. Deck Girder Bridge Model

The five deck girders were first connected by the 1/2” steel plates spaced at 5’-0” centers. A typical plate is shown in Figure 3-4 connected between adjacent deck girder flanges. The steel angle and corresponding shear studs were omitted due to the large size contrast and the meshing limitations of ANSYS™. The deck girders were then braced with the line element diaphragms with fixed moment transferring connections. The diaphragms at mid-span and the quarter points are shown in Figure 3-5.

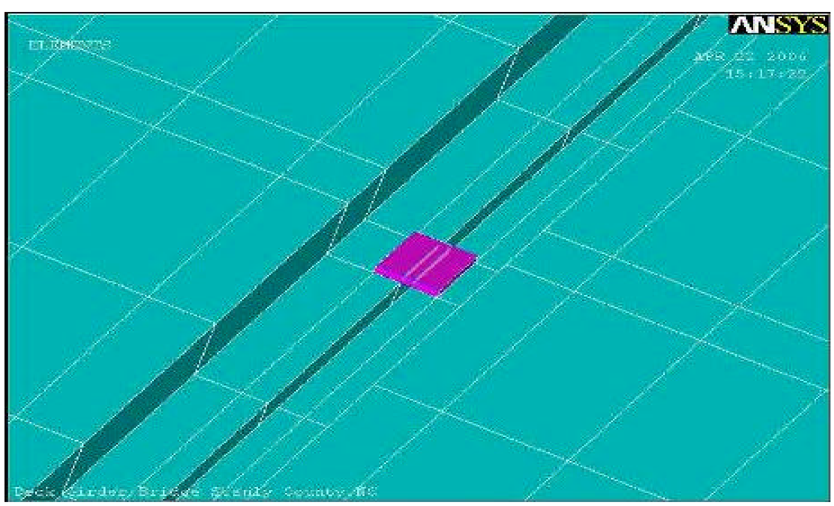

Figure 3-4. Plate Connecting Deck Girder Flanges

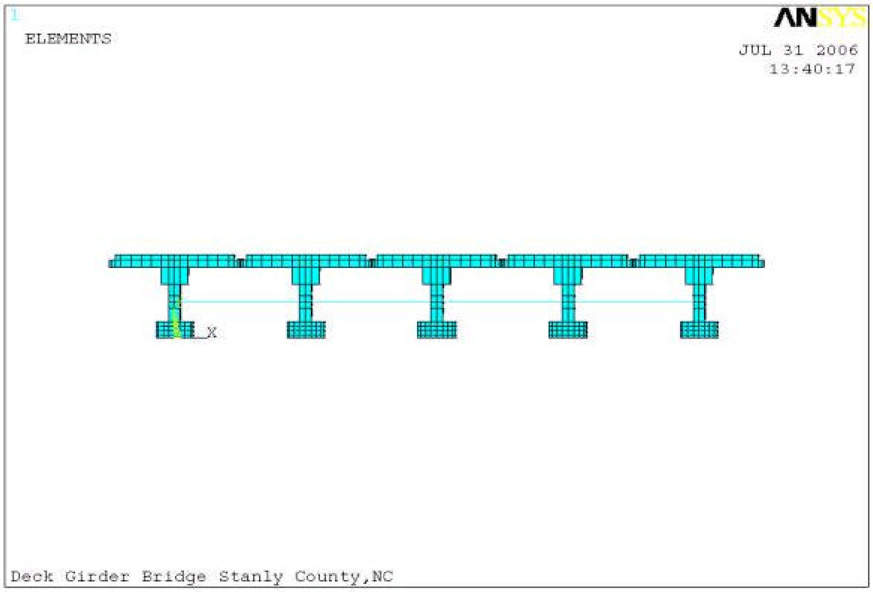

Figure 3-5. Diaphragms on Half-Bridge Model

3.2 Model Calibration

The first step in creating a working ANSYS™ model was generating one deck girder that produced prestress properties that matched the NCDOT and Larsa™ model values. After the individual deck girder was deemed accurate the generation of the entire bridge was then completed. The comparison of the normal stress at extreme fibers at mid-span and the deflection at mid-span were used to verify that the mesh accurately captured the behavior of the girder at the time of construction. The model was restrained with a pin and roller connection as designed by the NCDOT. The model was later restrained by fixing the areas that were enclosed by the integral end bent to capture the bridge behavior at the time of the load test.

The equivalent deck girder normal stress comparisons are shown in Figure 3-6 (prestress + self-weight). The equivalent deck girder deflection and camber are shown in Figure 3-7. It is clear that the modeled deck girder produced comparable results while containing the necessary mesh pattern to include the plates and diaphragms. As expected, the diaphragm and plate additions to the five independent girders resulted in an insignificant effect on the stress and camber of the individual girders before post construction live loads were added.

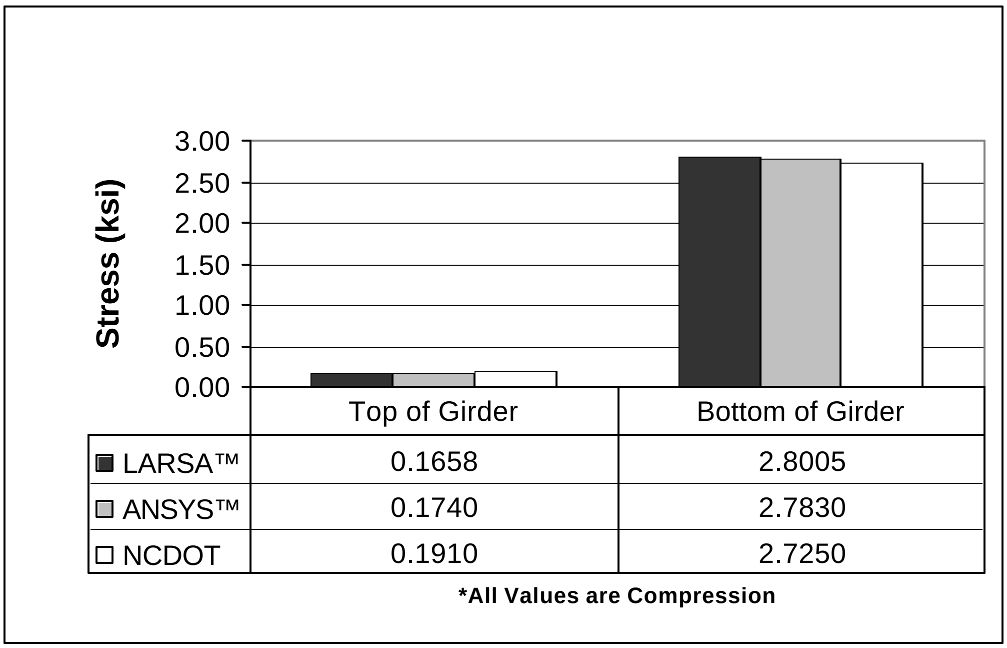

	Top of Girder	Bottom of Girder
LARSA™	0.1658	2.8005
ANSYS™	0.1740	2.7830
NCDOT	0.1910	2.7250

Figure 3-6. Equivalent Deck Girder Stress at Extreme Fiber Comparison

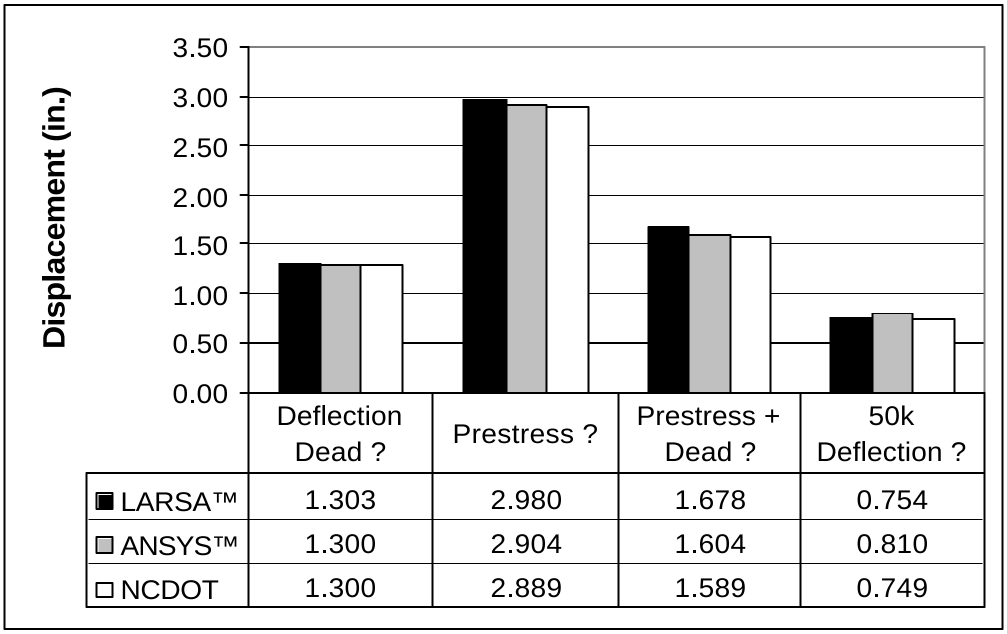

Figure 3-7. Equivalent Deck Girder Displacement Comparison.

The ANSYS™ model was first generated with simple supports and all load test paths were entered into the program. The use of symmetry in the model required the creation of an equivalent truck live load that could be reflected across the symmetry plane of the bridge model. The equivalent truck loading per axle is shown in Figure 3-8, where the center of the equivalent truck was placed on the longitudinal centerline of the bridge (dashed line). This centerline is also the plane of symmetry used in the FE program.

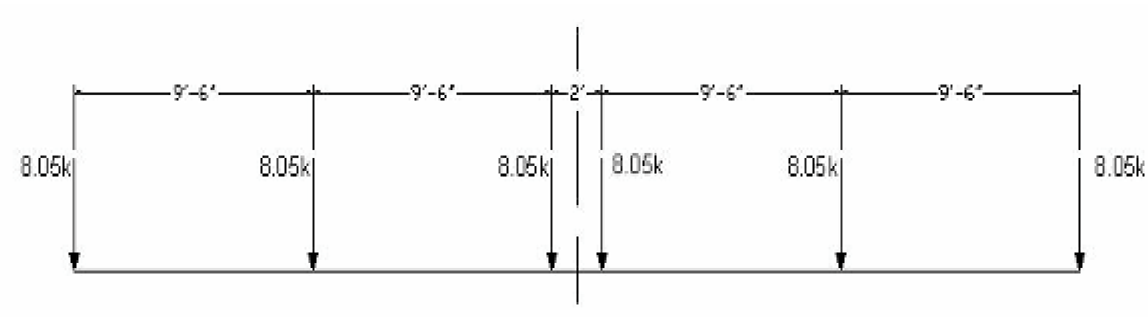

Figure 3-8. Equivalent Truck Live Loading

The ANSYS™ model was then subjected to three of the five load paths that were used when the bridge was load tested. The total amount of load paths was not used due to the symmetry of the FE bridge model. The load paths modeled in ANSYS™ were paths 1, 2, and 4. The quasi-static load testing procedure is discussed in greater depth in the bridge load test section of this paper (chapter 6). The five bridge test truck paths are shown in Figure 3-9.

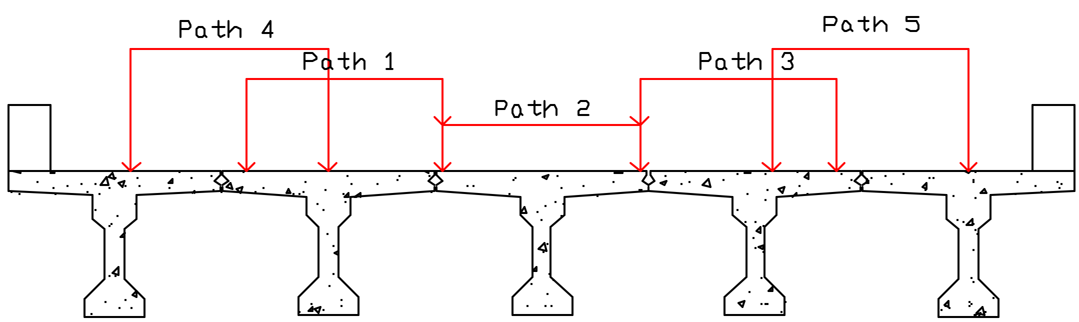

Figure 3-9. Bridge Load Test Truck Paths

The calibrated ANSYS™ and Larsa™ models with simple supports proved to be more flexible than the actual bridge. The simply supported deck girder stresses and displacements in Larsa™ and ANSYS™ were higher than the instruments captured when the bridge was load tested. The simply-supported deck girder model was deemed too flexible and the fixity of the actual bridge was then modeled in the two computer programs. The integral end bent fixity was modeled in ANSYS™ by restraining the areas that were enclosed by the end bent. The decision was made to compare the fixed ANSYS™ and Larsa™ models to the actual load test values. This support condition change yielded deck girder stresses and displacements that were very comparable to the actual load test in both computer models. These comparisons are discussed further in chapter 7.

3.3 Parametric Study

After the FE model was calibrated and the girder results were comparable to the actual load test, a parametric study was performed on the steel plates and diaphragms. The plate stresses were obtained from the fixed-end ANSYS™ model that behaved similarly to the actual load test. The plate spacing was specified at 5’-0” on center. The initial Larsa™ computer model showed that the maximum plate stress occurred in the transverse direction (perpendicular to traffic). Therefore, the considered plate stress values from the load test (later discussed in Chapter 6) and the parametric study were primarily the transverse and principal values.

The plate spacing was increased to 10’-0” on center and the maximum tensile and compressive transverse stress values (peak values from ANSYS not necessarily corresponding to an actual strain gage location on the bridge) in the plates were compared (see Figures 3-10 through 3-11). This was completed to evaluate the effect of connection spacing on the stress in the plates and the diaphragms. The larger spacing increased the plate stresses, and thus reduced the safety factor of these connections significantly – therefore, this modification is not recommended without redesigning the connection detail. The influence of the spacing on the plate principal stress (highest stress at a given location, acting on the principal plane) is shown in Figures 3-12 through 3-13.

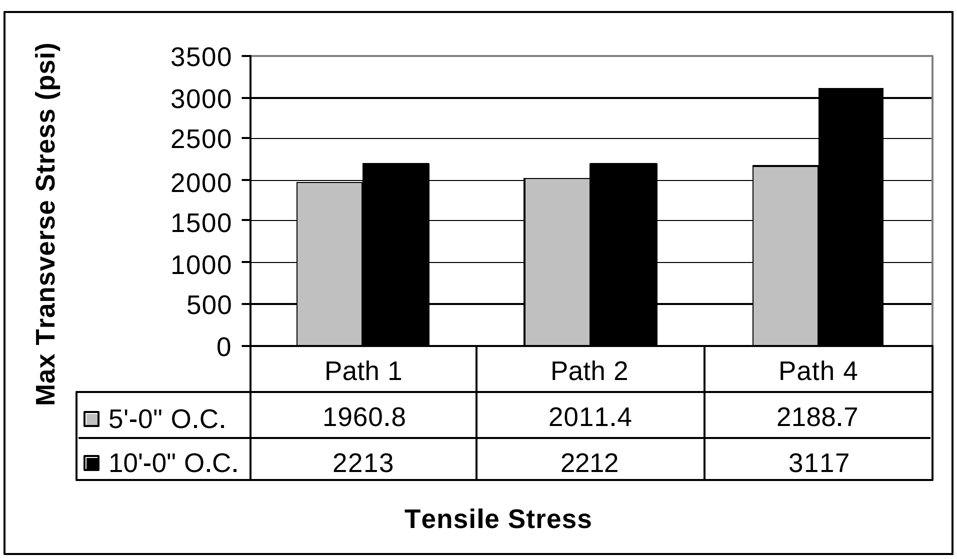

Figure 3-10. ANSYS™ Maximum Tensile Transverse Plate Stress

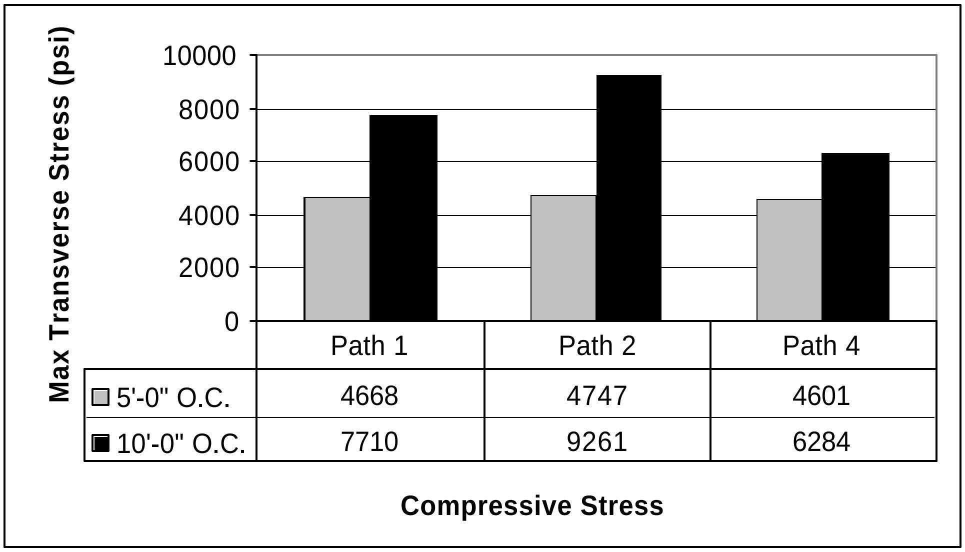

	Path 1	Path 2	Path 4
5'-0" O.C.	4668	4747	4601
10'-0" O.C.	7710	9261	6284

Figure 3-11. ANSYS™ Maximum Compressive Transverse Plate Stress

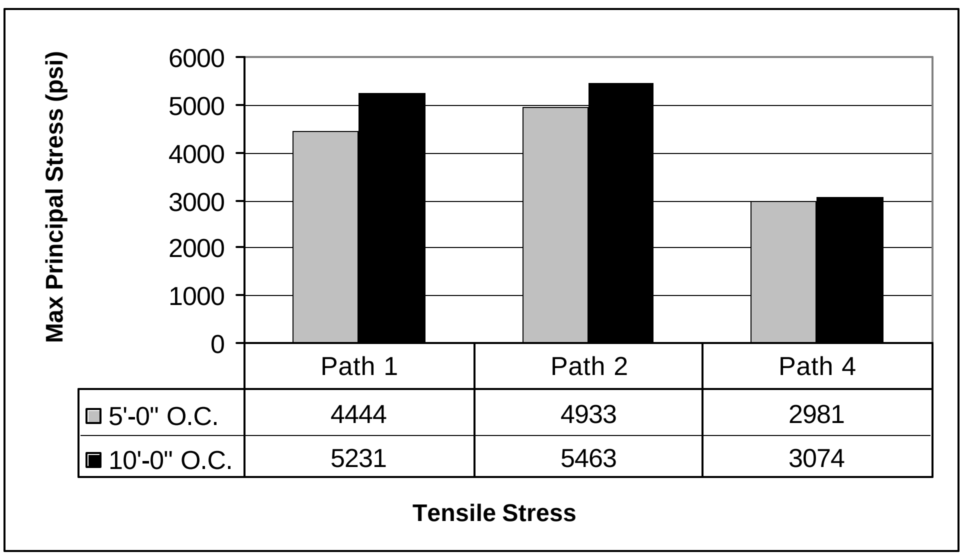

	Path 1	Path 2	Path 4
5'-0" O.C.	4444	4933	2981
10'-0" O.C.	5231	5463	3074

Figure 3-12. ANSYS™ Maximum Tensile Principal Plate Stress

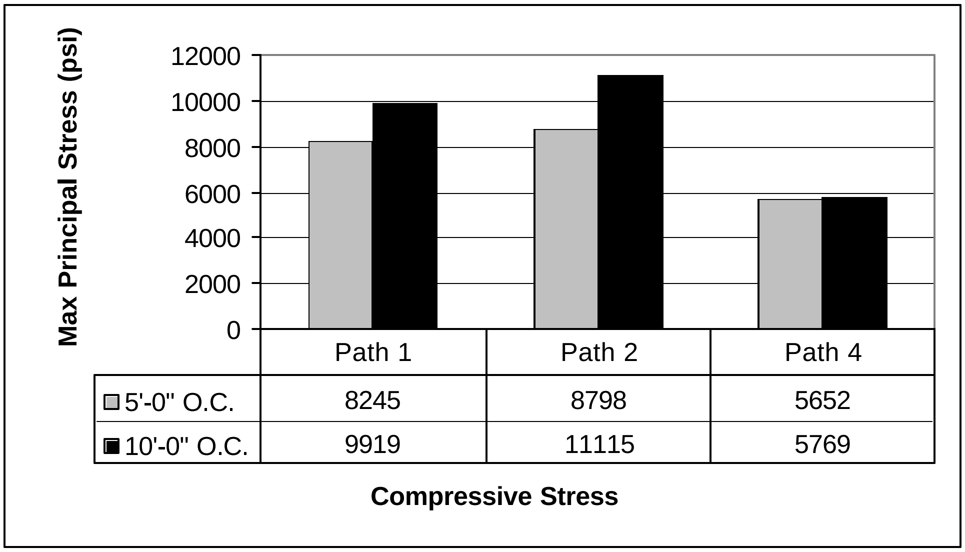

Figure 3-13. ANSYS™ Maximum Compressive Principal Plate Stress

The effect of the diaphragms was then evaluated by running the FE model with the diaphragms at the quarter and half points of the bridge. The diaphragms are numbered and located according to the instrument layout included in Appendix C. The normal stress in the diaphragms is shown in Figures 3-14 through 3-18 with all the plate connectors as constructed in the field and with the connector plates at 10'-0" on center.

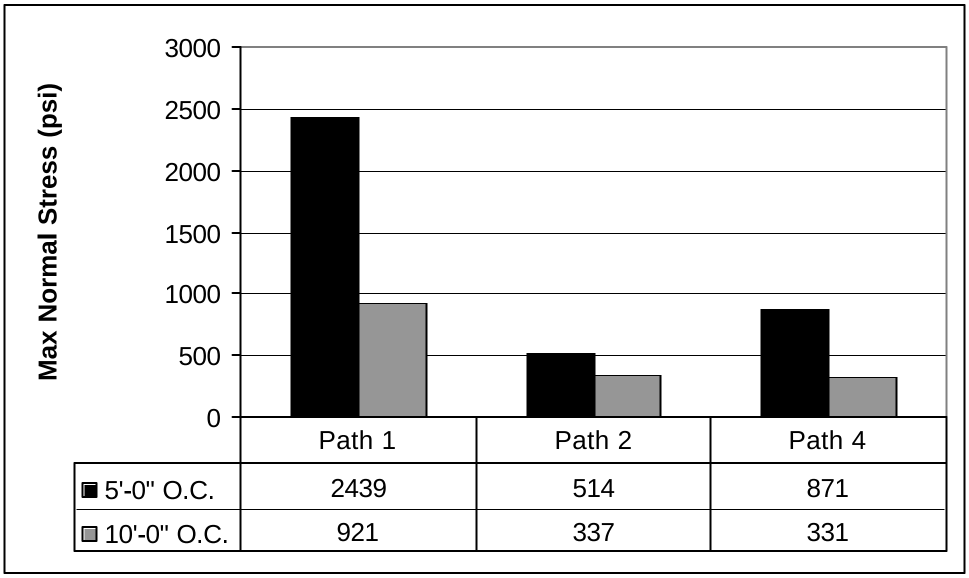

	Path 1	Path 2	Path 4
5'-0" O.C.	2439	514	871
10'-0" O.C.	921	337	331

* (-) = Compression

(+) = Tension

Figure 3-14. ANSYS™ Maximum Normal Stress – Diaphragm D1

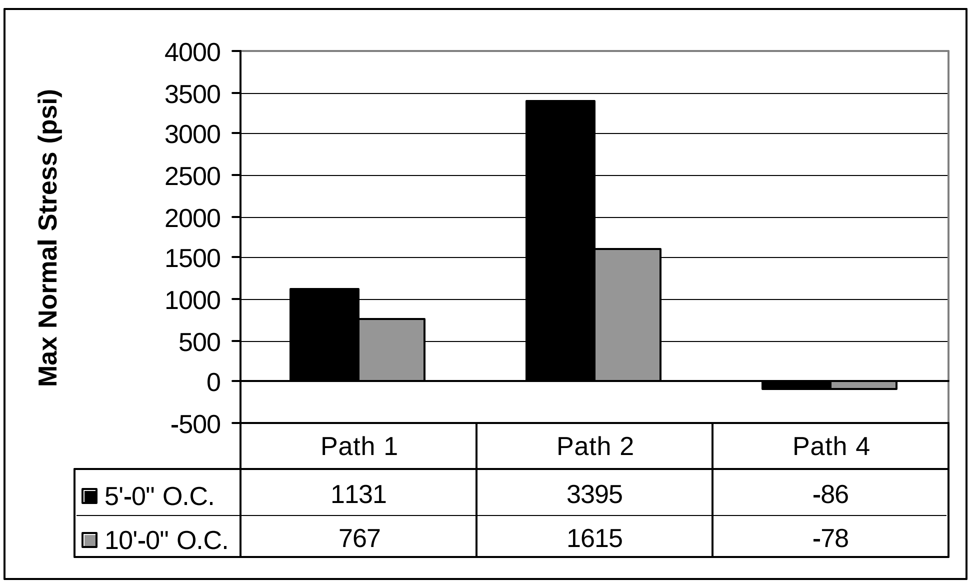

	Path 1	Path 2	Path 4
5'-0" O.C.	1131	3395	-86
10'-0" O.C.	767	1615	-78

* (-) = Compression

(+) = Tension

Figure 3-15. ANSYS™ Maximum Normal Stress – Diaphragm D2

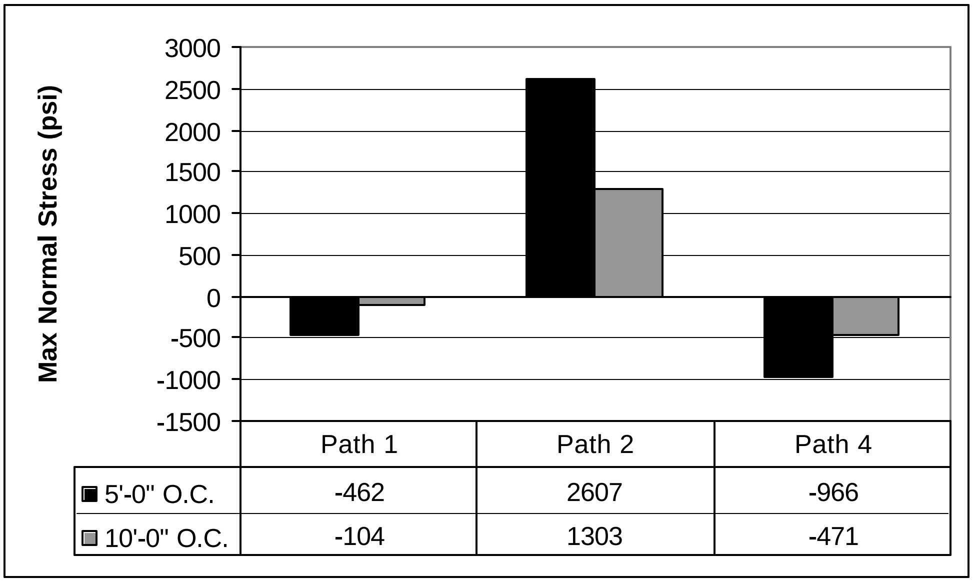

* (-) = Compression

(+) = Tension

Figure 3-16. ANSYS™ Maximum Normal Stress – Diaphragm D3

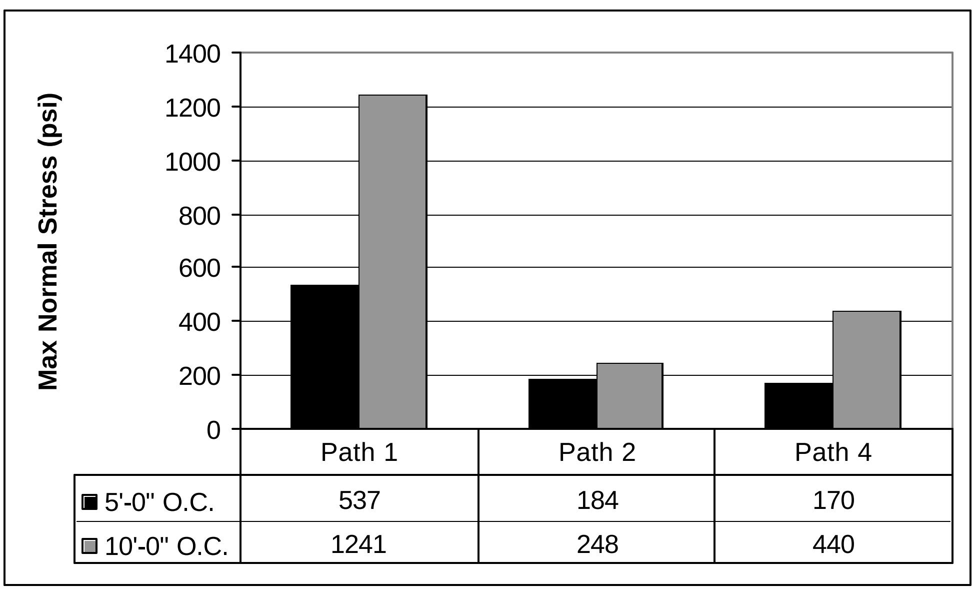

* (-) = Compression

(+) = Tension

Figure 3-17. ANSYS™ Maximum Normal Stress – Diaphragm D5

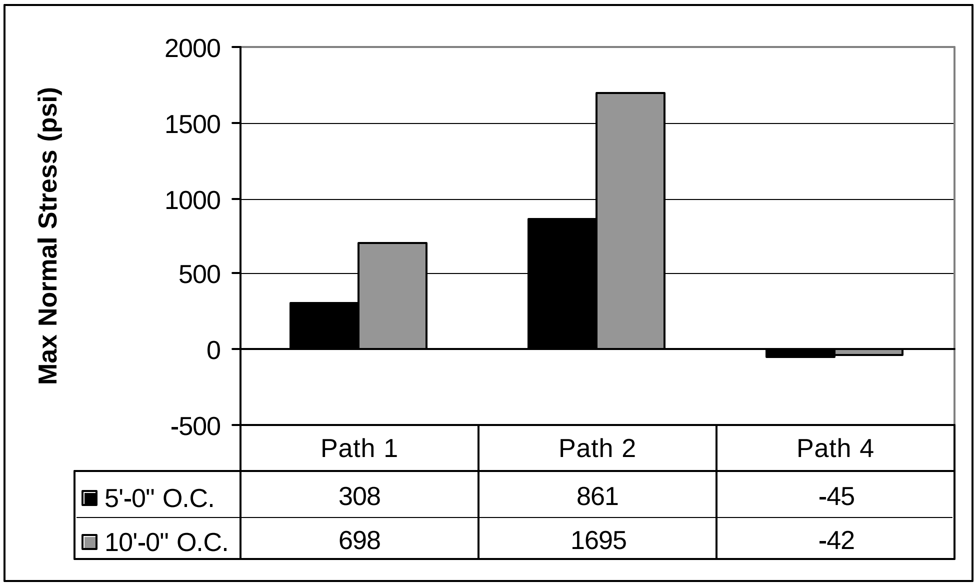

* (-) = Compression

(+) = Tension

Figure 3-18. ANSYS™ Maximum Normal Stress – Diaphragm D6

The effect of the plate spacing on the live load distribution was also investigated (see Figures 3-19 through 3-22). The distribution factors for interior and exterior deck girders were calculated using the 2 and 4-wheel line methods. The methodology of the distribution factor calculations is discussed in depth later in Chapter 6.

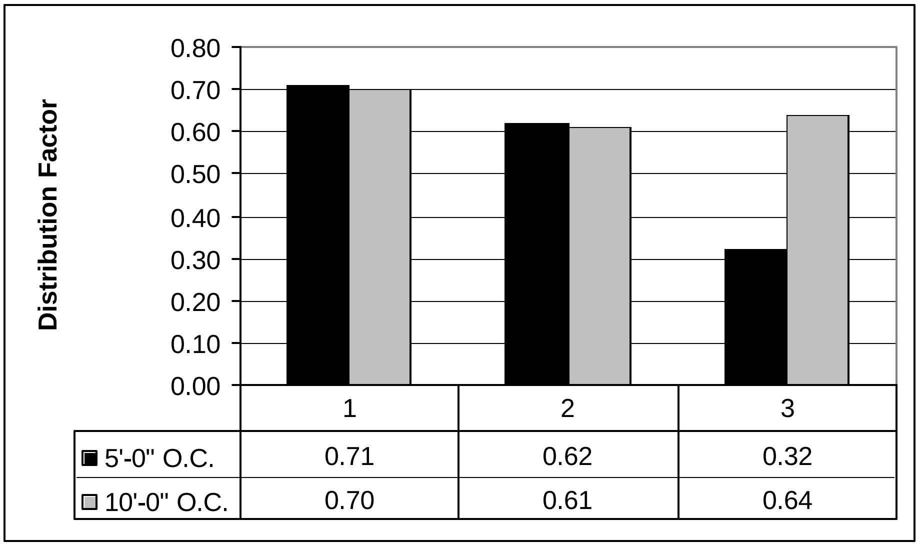

Figure 3-19. 2 –Wheel Lines Distribution Factor for Interior Girder Paths

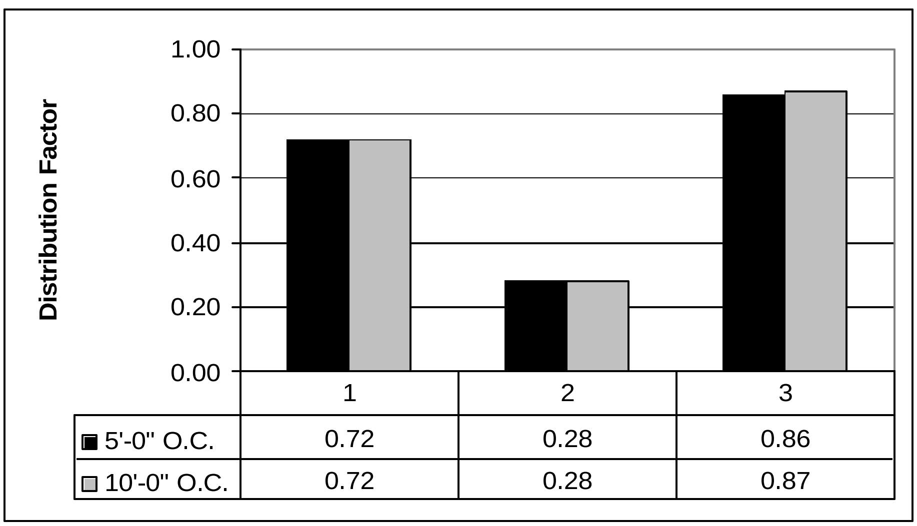

Figure 3-20. 2 –Wheel Lines Distribution Factor for Exterior Girder Paths

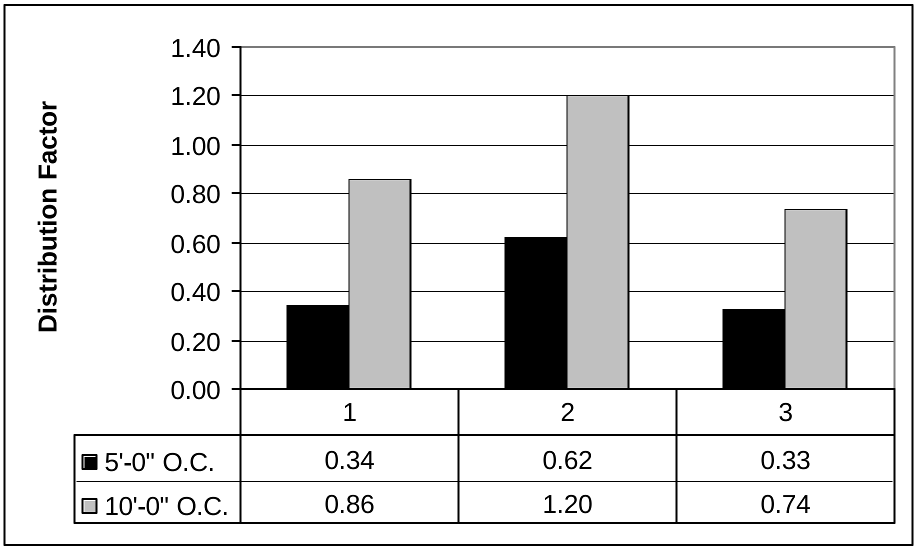

Figure 3-21. 4 –Wheel Lines Distribution Factor for Interior Girder Paths

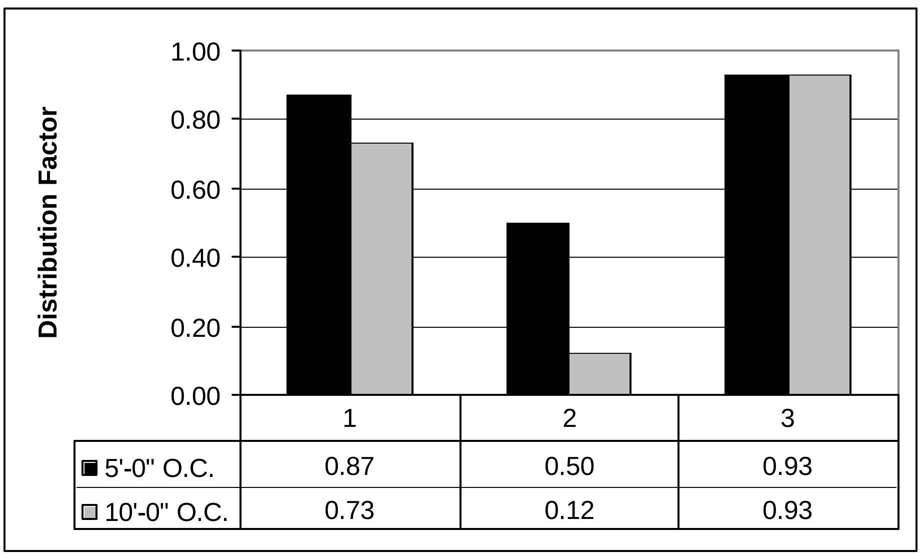

Figure 3-22. 4 –Wheel Lines Distribution Factor for Exterior Girder Paths

The maximum tensile transverse plate stresses with the plates at 10’-0” on center were found to be 200-1000psi higher than the 5’-0” on center plate spacing. The maximum transverse compressive stress was found to be approximately twice as high with the increased plate spacing. The maximum tensile principal stress difference was found to be 700psi. The compressive principal stress comparison resulted in a larger difference ranging from 120-2300psi. The largest stress induced in the plates when spaced at 10’-0” on center was 11,115psi in compression.

The maximum diaphragm normal stresses were similar with both plate spacing arrangements in the diaphragms located at the quarter points of the bridge. However, the diaphragms located at mid-span (D5–D6) experienced roughly twice as much stress with the increased plate spacing. The ANSYS™ model only loaded the deck girders at the worst case location of mid-span, resulting in lower stresses in the quarter point diaphragms. It is apparent that the plate spacing has a significant effect on how much load is transferred through the diaphragms at mid-span. The diaphragm normal stress values are very low with both spacing arrangements, and were not close to the yield strength of 36ksi.

The distribution factors for the interior and exterior deck girders, as expected, proved to differ little when the plate spacing was increased. This would indicate that the smaller number of plates simply transmitted an increased load. This higher load transmission is evident in the increased maximum transverse and principal plate stress comparisons.

Finally, the integral end bent fixity contribution was modeled in ANSYS™ by fixing the deck girder areas that were restrained by the end bent in the finished bridge. The fixity of the model was calibrated by comparing the ANSYS™ model deck girder stresses and displacements to the actual load test. Once the deck girder behavior matched that of the actual bridge test data, the top fiber normal stresses were recorded. The live load stress as a function of distance along deck girder one is shown in Figure 3-23. The stress is graphed on half of the deck girder due to the symmetry plane at the mid-span of the bridge. The fixity of the deck girder is clearly represented by the initial tensile stress near the end bent, the compressive stress at mid-span, and the live load inflection point at about 25'-0" from the support.

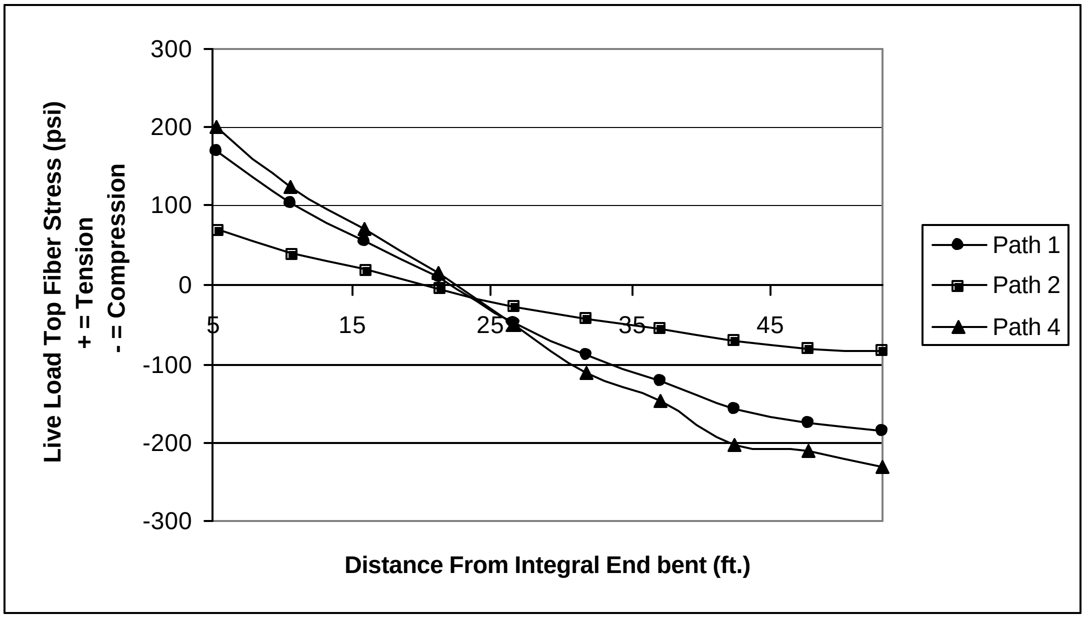

Figure 3-23. Top Fiber Live Load Normal Stress - Deck Girder 1

The maximum tensile stress that occurs due to the live load was found to be 200psi at approximately 5.3 ft. from the integral end bent wall. The deformed shape of deck girder one is shown in Figure 3-24. In this figure, the associated stress values are not adjusted to exclude prestress and self-weight.

The stress in the top of the deck girder, resulting from prestress and self-weight, is shown at the deck girder end and mid-span (see Table 3-1). The total tensile stress at 5'-4" from the end bent wall was found to be 902psi. This value is higher than the 563psi design concrete tensile stress limitation (or 862psi, using actual f'_c=13,202psi measured on the bridge test day, using cylinders made during deck girder fabrication), which is also proven by hairline cracks present in the flanges of the bridge deck girders. The mid-span normal stress is well within the design specified compressive stress limitations. The large stress observed at the 5'-4" length could be slightly higher than the actual value due to the debonding of strands in the actual girder fabrication process. However, the ability to de-bond the prestressing strands was not available in the ANSYS™ FE program.

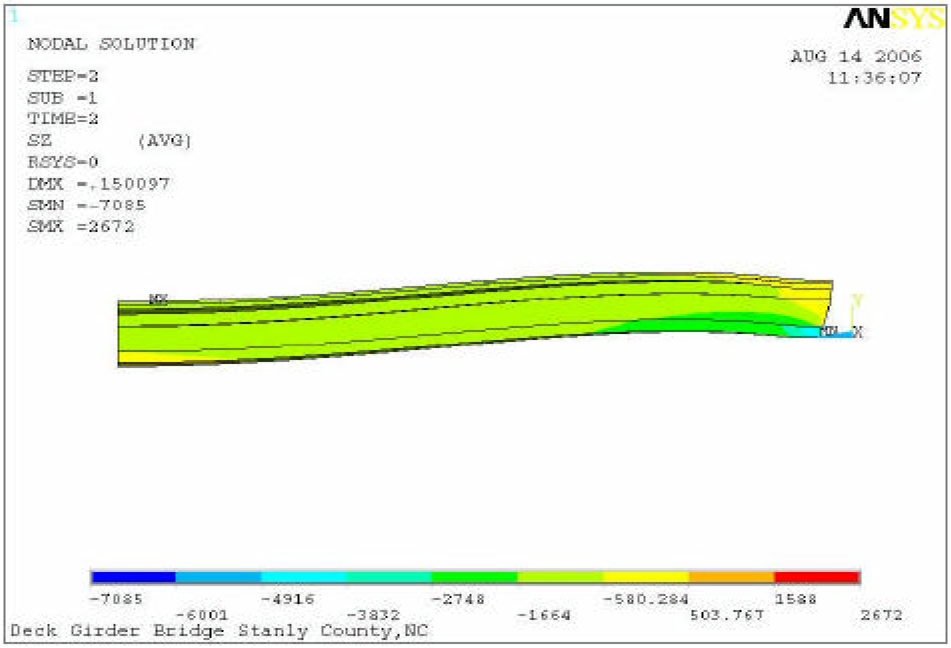

Figure 3-24. Deformed Shape and Un-adjusted Normal Stress- Deck Girder 1

Table 3-1. ANSYS™ Top Fiber Normal Stress Values – Girder 1

Girder Location (ft.)	Live Load Top Fiber Stress (psi)	Self-Weight + Prestress (psi)	Overlay + Parapet Wall (psi)	Total (psi)
5’-4”	200	645	57	902
53’-0”	-231	-174	-307	-712

+ = Tension
- = Compression

4 Flange Connection Analysis

4.1 FE Model

As the flange connection analysis began, an FE model was used to help the research team predetermine material and connection behavior. In order to accurately understand the connection's behavior, a basic model of the studded connection with the steel plate was generated using ANSYS™. The model was a six inch piece of angle with two shear studs attached to the back side, and a 3” x 4” x ½” steel plate welded to the top of the angle (see Figure 4-1).

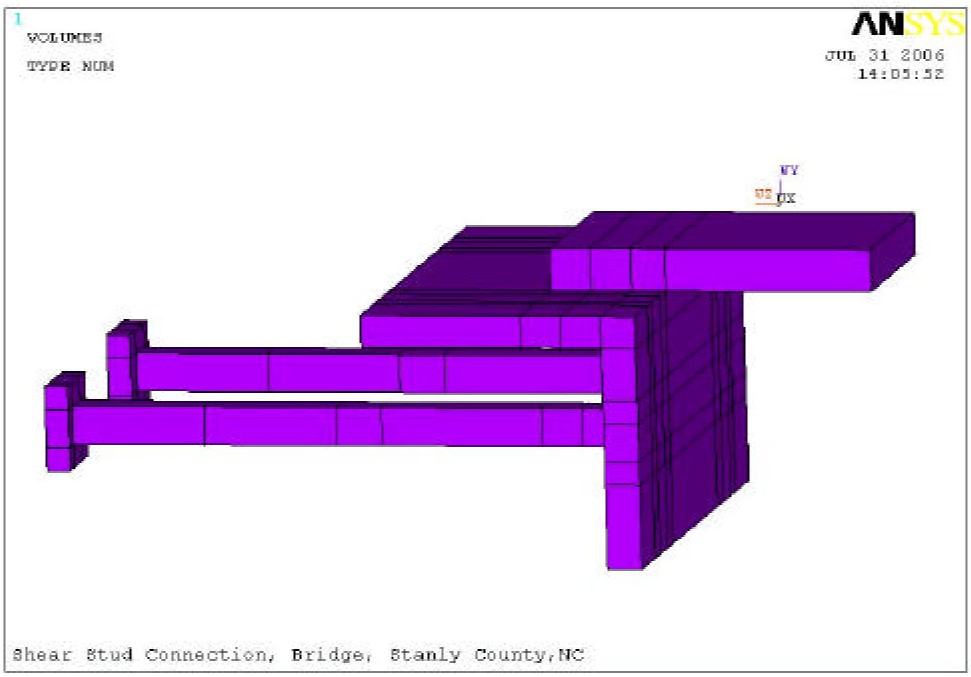

Figure 4-1. Flange Connection Un-deformed Shape

The FE model was created using SOLID45, a 4-node brick element. Simplifications were made when generating the model such as, equating the circular areas to square areas in order to get a simplified mesh within the FE program. The steel properties of the connection were found in the PCI Design Handbook 6th Edition (2004), with an ultimate strength of 65 ksi for tensile members. The FE model was then fixed at the base of the stud head. An eccentric tensile load was then placed on the plate. According to the FE program this particular connection was able to withstand approximately a 1,450 lbs eccentric load before yielding was observed at the front of the two studs where the angle and studs were connected. Figure 4-2 shows connection's deformed shape at a load level of 1,450 lbs.

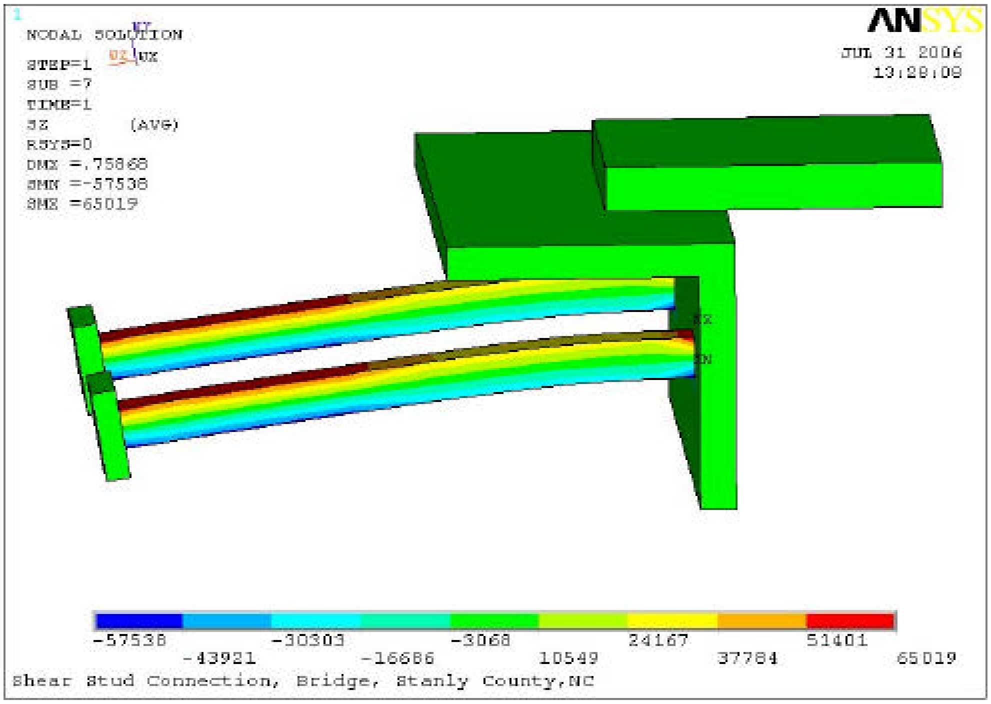

Figure 4-2. Flange Connection Deformed Shape

After testing the connection specimens, the research team re-visited the FE model in order to re-evaluate the experimental results. The laboratory testing showed that the connection was not simply controlled by yielding at the base of the stud (where it meets the angle). As the connection reached failure (defined as loss of at least 30% of peak load), the deformed connection began to rotate rather than translate. Essentially, the bottom of the angle acted as a fulcrum for the connection to pivot on as the angle and plate rotated outward and the studs elongated. The failure was modeled more accurately in ANSYS™ by placing a block just behind the bottom of the angle.

This more accurate FE model showed that the connection can take a much higher load due to the connection of the angle and shank. The revised FE model shows that flexural yielding occurred in the shanks of the shear studs before the load reached ultimate. The plate never attained stresses with the magnitude of those observed in the studs. However, when the loading conditions were at failure, the angle reached similar stresses as the studs.

The load that the revised FE model reached was approximately four to five times what the connection alone could hold, reaching load levels between 6,000 lbs and 7,000 lbs. During the laboratory testing, according to all of the strain gages attached, that initial yielding occurred in the shanks of the shear studs. Similarly, as load was applied to the FE model the first location that yielding occurred was in the shanks of the connection, thus confirming the FE model analysis. Figure 4-3 shows this interaction and how the fulcrum allows for increased load to be applied to the flange connection.

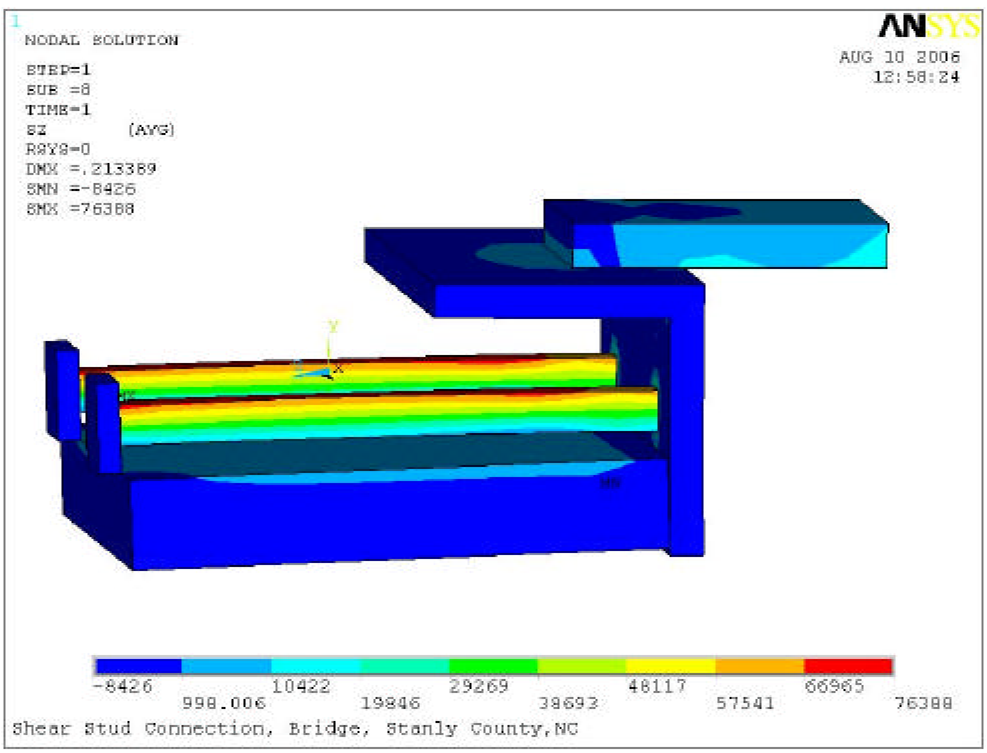

Figure 4-3. Deformed Flange Connection with Pivot Surface

4.2 Testing Procedure

Early in the project it was clear that currently available headed stud connection design methods do not accurately represent the details of the actual deck girder flange connections. This would not have been critical, however, based on the bridge load test, it was clear that most of the live load transfer from deck girder to deck girder was achieved through the flange connections, and not the diaphragms. Therefore, additional experimental and theoretical analyses were performed on the flange connection, considering direct tension and longitudinal shear. The research team also made a decision to neglect the capacity of the grouted shear key between flanges, as this provided some resistance mostly in the out-of-plane direction of the flange only.

The specimens were designed and constructed based on the top flange connection detail provided in the NCDOT bridge design document (Hanks, 2005). The details concerning specimen size and shape were arranged by using a tributary method to simulate the area of influence of one single connection on the actual bridge. The materials in deck girder production, regarding rebar size and placement, concrete strength, and the studded connection were as specified. Four tension and four shear (data from one shear test is disregarded here as it did not follow the load-deformation behavior and load capacity of the other three specimens) specimens were tested during the experimental phase of the connection analysis.

The complete drawings of the specimen design are shown in Figure 4-4 and Figure 4-5. Figure 4-6 is a picture of the rebar assemblies and specimen formwork. These designs were based primarily on the exact replication of the actual NCDOT bridge documents as well as development length of rebar, concrete strength, steel properties, and current ACI 318-05 design requirements.

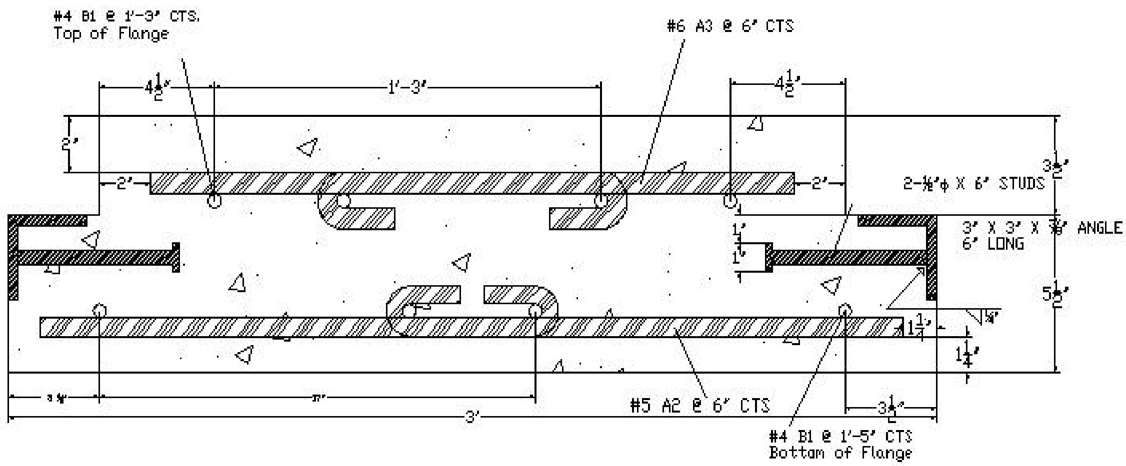

Figure 4-4. Test Specimen Cross-Section View

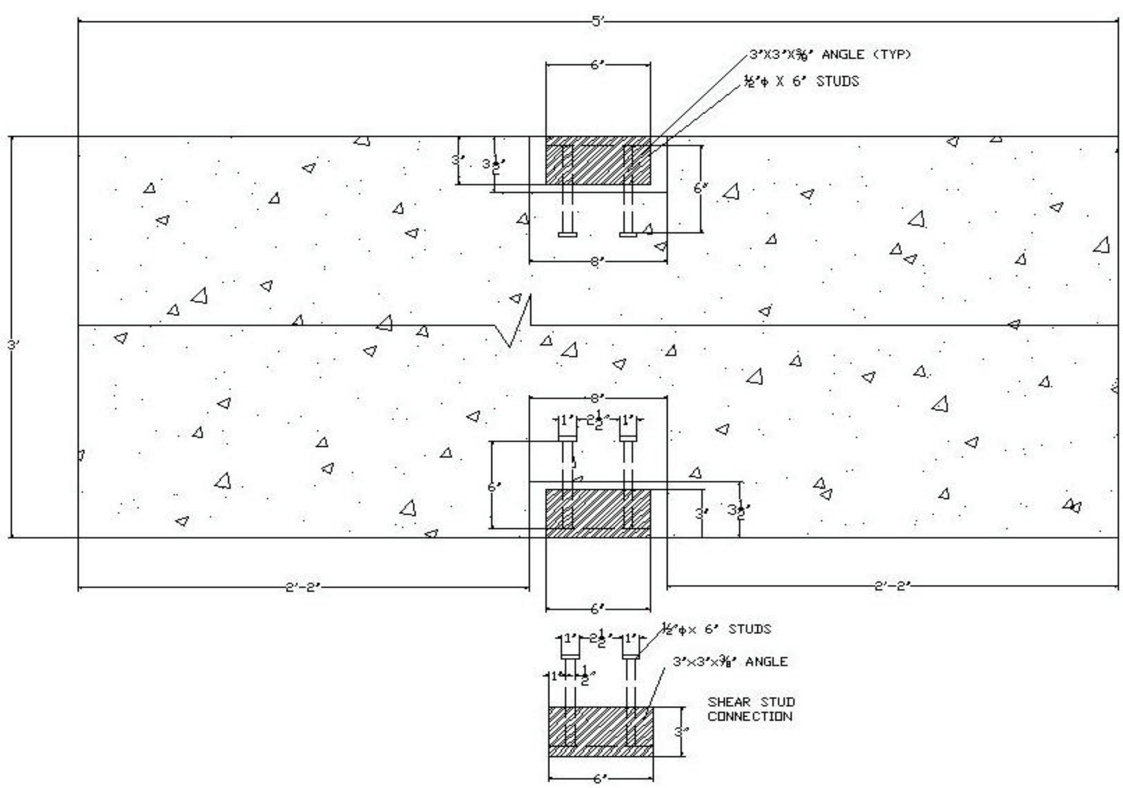

Figure 4-5. Test Specimen Plan View

Figure 4-6. Rebar Assembly in Formwork

The specimens and test setups were designed in order to determine the ultimate capacities of the flange connection in tension and longitudinal shear, approximately following the testing protocol (specimen setup and loading application) developed by Anderson and Meinheit (2005). The tension specimens were fixed to the load frame to prevent translation and rotation of the specimens (Figure 4-7). Furthermore, displacement transducers were attached to both the concrete slab and the connections in two orthogonal directions, allowing the measurement of net specimen deformations.

The load was measured through a load cell, and a pressure transducer attached to the hydraulic pump, and was applied to the specimen through a steel plate connected to a hydraulic jack. Strain gages were attached to the plate connection, and to both headed studs embedded in concrete.

Each test began with a diagnostics check with the data acquisition device (DAQ) to ensure accuracy and quality. As loading began in the beta models (first shear specimen, and first tension specimen) load was applied at a very slow rate so that failure would be noted very precisely. In the proceeding tests, load was allowed to climb at a much higher rate in the beginning of the test, and then decreased as the load reached the point of failure that had been observed in previous tests. This was decided because the first tension and shear tests approached one hour in duration. By the end of the laboratory testing, the research team had cut the time in half, which shows that further study of studded specimens can be completed in a timely fashion.

4.3 Experimental Results

The following are the shear and tensile loads that were applied to specimens to the point of ultimate failure. The load versus displacement curves, and ultimate results accurately show the uniformity within the tests as well as the specimen construction. Table 4-1 is the ultimate log for connection tests.

Table 4-1. Experimental Results – Ultimate Values

Tension Tests	Test #1	Test #2	Test #3	Test #4	Average
Ultimate Failure Load (lbs)	13,150	12,700	13,160	12,100	12,778

Shear Tests	Test #1	Test #2	Test #3	Test #4	Average
Ultimate Failure Load (lbs)	26,970	31,470*	23,940	23,030	24,646

* Excluded from analysis

The average load versus displacement graphs for the four tensile test specimens are shown in Figure 4-8. Figure 4-9 is a picture of the connection failure with a tensile load. It is clear from these curves that the angle yielded (adjacent to the welded shear studs – the location of peak bending moment from eccentric loading) and the largest deformation occurred at an approximate load of 5,000 lbs, transferring the force mostly through tension to the embedded studs. An average capacity of 12,778 lbs capacity was reached, followed by large deformations, and finally, a failure due to stud/angle connection fracture.

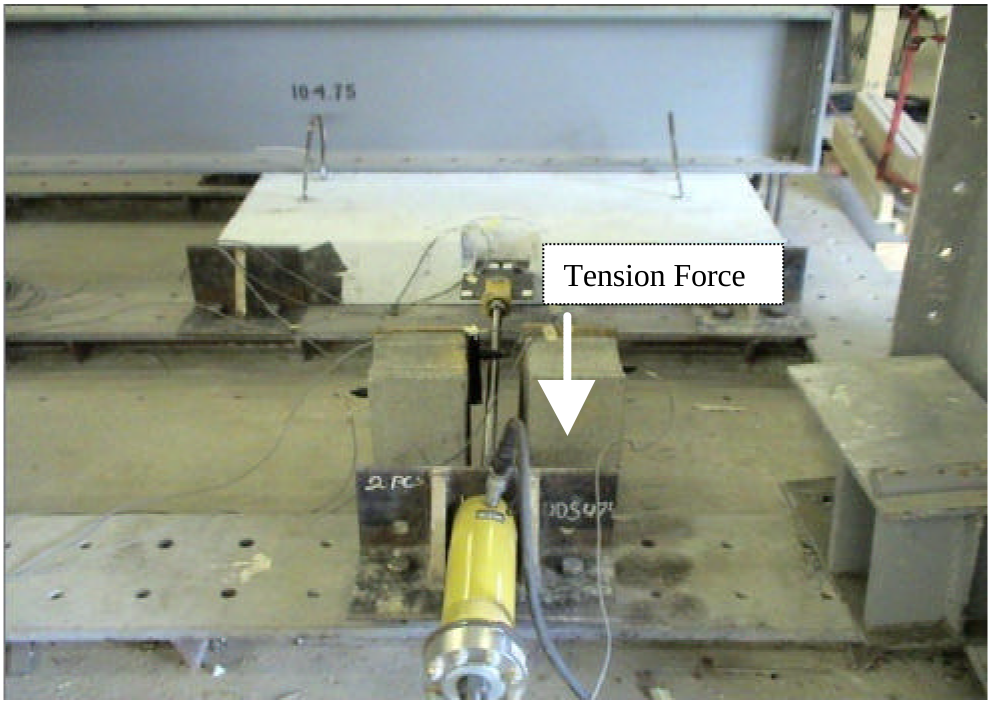

Figure 4-7. Tension Connection Test

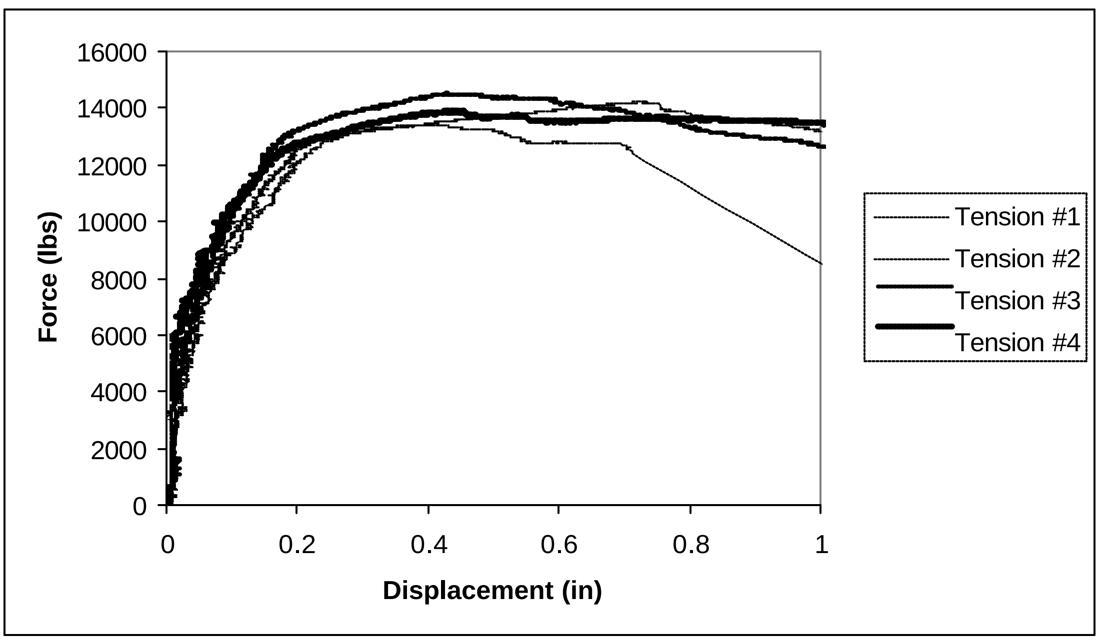

Figure 4-8. Load vs. Displacement for Tension Tests

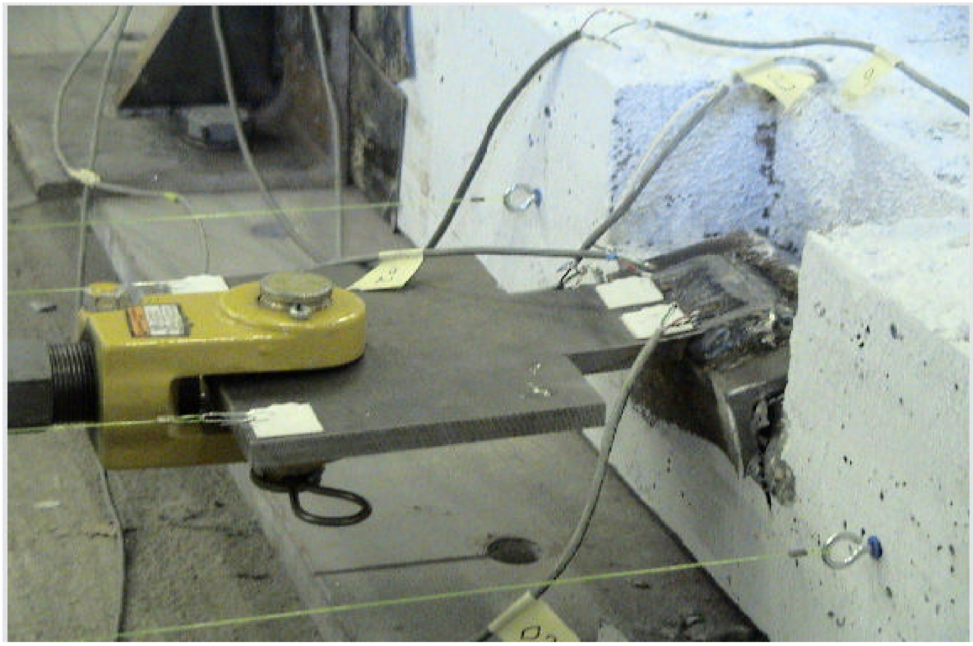

Figure 4-9. Tensile Connection Failure

The longitudinal shear test setup had the same specimen details used in the tension testing; however, the specimens were rotated 90 degrees, and the shear force was applied through a steel plate/channel configuration (shown in Figure 4-10). This allowed testing of the connection with minimal eccentricity, similarly to the actual bridge details. Similar restraints and instrumentation was applied to the shear specimens, as the ones applied to the tensile tests.

Even though four shear tests were performed, the results of only three tests are included in Figure 4-11. Figure 4-12 is the deformed shape of the connection after being subjected to ultimate shear loading. One of the specimens did not produce reliable research data, and was omitted from further common analysis. During the testing of specimen #2, the research team noticed that all initial cracking and yielding took place similarly to the other specimens. In researching why Test #2 had a much higher ultimate capacity than the other specimens, primarily pointed at the construction process (in all probability during the placement of the concrete) the rebar cage slipped under one or both of the studs. This steel-to-steel connection would appear to cause a higher ultimate load than the concrete to steel interface that the research team usually witnessed throughout testing.

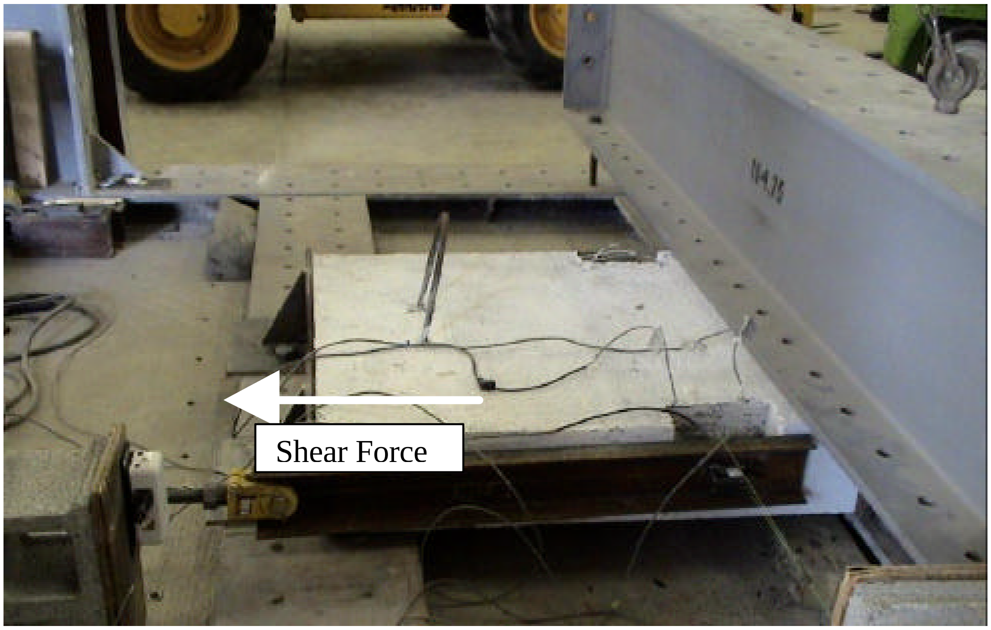

Figure 4-10. Shear Connection Test

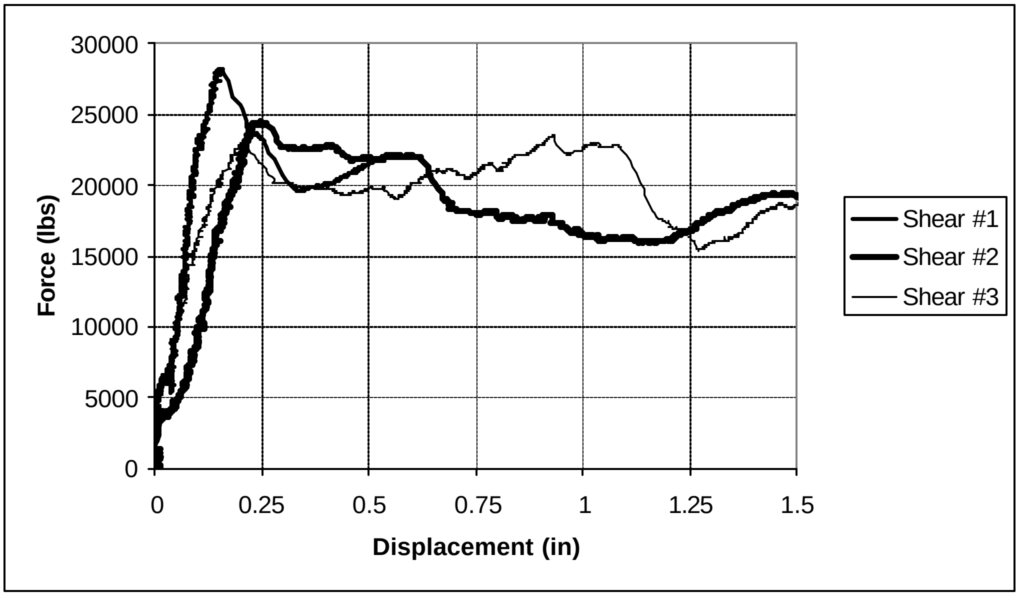

Figure 4-11. Load vs. Displacement for Shear Tests

Figure 4-12. Shear Connection Failure

At approximately 5,000 lbs in Figure 4-11, shifts in the graphs indicate that some of the connection steel members yielded. After this initial steel yielding, load redistribution occurred, which was followed by significant rotation of the connection angle, resulting in a failure governed by stud-to-angle connection capacity. The average ultimate value for the shear tests was 24,646 lbs.

4.4 PCI Calculations vs. Experimental Results

In trying to analyze the loads that were predicted versus the loads achieved in testing the connection, the research team began by reviewing “Chapter 6 Design of Connections” in the PCI Design Handbook 6th Edition and various formulas in the AISC steel manual. First, the steel was analyzed and ultimate values were calculated regarding capacities of the steel plate, welds, and studded connections. The next step was to review all types of concrete analyses provided by PCI for both the tension and shear testing procedures.

A. Tensile Capacity of Steel

Section 6.5.2 of the PCI 6th Edition addresses the capacity of steel within studded connections. See Equation 4-1:

$$f V_s = f N_s = f(n)(A_{se} f_{ut}) \qquad (4\text{-}1)$$

- f = steel strength reduction factor
  = 0.65 (shear)
  = 0.75 (tension)
- V_s = nominal shear strength of an anchorage based on steel capacity
- N_s = nominal tensile strength of an anchorage based on steel capacity
- n = number of headed studs in the anchorage assembly
- A_{se} = nominal area of the headed stud shank

- f_{ut} = specified tensile strength of the stud steel
  65 ksi for Type B headed studs normally used in precast anchorages
  (see Table 6.5.1.1)

Since the research team was interested in the ultimate capacity and not the design calculations, the "f " values were omitted in the calculations. Due to the fact that the strength reduction factors were omitted in these calculations, the ultimate capacities for tension and shear are the same. This value was calculated as follows:

$$V_s = (n)(A_{se} f_{ut}) = (2)(0.20\text{in}^2)(65\text{ ksi}) = \underline{26\text{ kips}}$$

The analysis of the steel connection was completed to check the ultimate strength of the plate and welds to verify that both surpassed the strength of the studded anchorage connection. The steel plate was a 4" x 3" x ½" plate of grade 36 steel (same material specifications as actual bridge detail). A simple calculation of multiplying the area of the plate oriented in the transverse direction by the strength of the steel resulted in the plate tensile capacity (Equation 4-2).

$$V_s = (A)(f_{ut}) = (1.50in^2)(58\ ksi) = 87\ kips \qquad (4\text{-}2)$$

This calculation shows that failure will likely occur somewhere else than in the welded plate.

B. Weld Capacity

The weld between the angle and the steel plate were also evaluated. The research team used the LRFD method to calculate the strength of the weld. This calculation was based on the smaller yield of the plate and the ultimate strength of the other steel members. The first step in this process is to calculate the gross cross section yield (Equation 4-3). Please note that since the research team was once again looking for the ultimate strength calculations, the f factor (steel strength reduction factor) was ignored.

$$f_t P_n = f_t F_y A_g = (58\ ksi)\ (3\text{''} \times ½\text{''}) = 87\ kips \qquad (4\text{-}3)$$

The net-section fracture can be calculated using Equation 4-4:

$$A = A_e = 3\text{''} \times ½\text{''} = 1.5in^2 \qquad (4\text{-}4)$$

The U factor is the next analysis in the steel weld calculations. The U factor is a variable which takes into account the non-uniform stress distribution in a simple manner. For welded sections the acceptable U is characterized by LRFD Specification B3.2 (d).

When $l = 2w$	U = 1.0
When $2w > l = 1.5w$	U = 0.87
When $1.5w > l = w$	U = 0.75

In the case of the studded angle connection, the plate that was welded to the angle had dimensions of w = 1.75in. and l = 3.0in. Therefore, $2w$ = 3.5in., and $1.5w$ = 2.625in. The computations were then substituted back into LRFD Specification B3.2(d) in order to determine the correct U factor. Looking at the second case reveals the following:

$$2w > l = 1.5w \;=\; 3.5\text{in.} > 3.0\text{in.} = 2.625\text{in.} \qquad U = 0.87$$

In further calculation of the net-section fracture, an effective area (A_e) must now be derived. This is done by taking the gross section area and multiplying it by the U factor that was previously computed (Equation 4-5).

$$A_e = AU = (1.5\text{in.}^2)(0.87) = 1.305\text{in}^2 \qquad (4\text{-}5)$$

This area will now provide all of the information needed to calculate the net-section fracture of the weld holding the plate to the angle on the studded connection. This can be obtained from the equation $f\,_tP_n = f\,_tF_yA_g$, while disregarding the "f " factor for steel strength reduction (Equation 4-6).

$$P_n = F_uA_e = (58\text{ksi})(1.305\text{in}^2) = \underline{75.69 \text{ kips}} \qquad (4\text{-}6)$$

This value, being lower than the gross-section yield, will control and be the expected ultimate value for failure in the weld.

C. Concrete Tensile Strength

After all of the values for steel strength were calculated, computations regarding the ultimate capacity for concrete were then analyzed. The calculations follow the guidelines from Chapter 6 of the PCI Design Handbook 6th Edition, "Design of Connections". Section 6.5.3 addressed many of the situations that arose within the experimental testing of the flange connection. These areas of ultimate tensile capacity included breakout strength, pullout strength, and side-face blowout capacity of the high performance concrete members. As Section 6.5.4 addressed the concrete capacity in tension, Section 6.5.5 evaluates the concrete shear strength. In this section the basic strength, single anchor strength was calculated with X-spacing, thickness, eccentricity, and cracking factors to provide more precise predictions.

The first concrete tensile strength calculation was the breakout strength computation. The breakout strength formula for concentrically loaded studded connections is PCI Equation 6.5.4.1 (Equation 4-7):

$$N_{cb} = N_{cbg} = C_{bs}A_NC_{crb}?_{ec,N} \qquad (4\text{-}7)$$

where:

h_{ef} = effective embedment length (in.). For headed studs welded to a plate flush with the surface, it is the nominal length less the head thickness, plus the plate thickness, deducting the stud burn off lost during the welding process (Equation 4-8)

$h_{ef} = l_e + t_p - t_{hs} - 1/8\text{in} = 6\text{in.} + 3/8\text{in.} - 5/16\text{in.} - 1/8\text{in.} = 5.9375\text{in.}$ (4-8)

C_{bs} = breakout strength coefficient (Equation 4-9)

$$C_{bs} = 3.33\,l\sqrt{\frac{f'_c}{h_{ef}}} = 3.33(1.0)\sqrt{\frac{9000}{8''}} = 128.48 \qquad (4\text{-}9)$$

A_N = projected surface area for a stud or group of studs in square inches

$A_N = A_{1+2+3+4}$ (see Figure 4-13)

$A_{1,2,3,4} = ½(h)(L_1+L_2)$

$A_1 = ½(10.404)(½+10.41) = 56.75\text{in}^2$

$A_2 = ½(10.404)(½+10.41) = 56.75\text{in}^2$

$A_3 = ½(4.65)(4+21.05) = 58.24\text{in}^2$

$A_4 = ½(5.76)(4+21.05) = 72.14\text{in}^2$

$A_N = A_{1+2+3+4} = 56.75\text{in.} + 56.75\text{in.} + 58.24\text{in.} + 72.14\text{in.} = 243.88\text{in}^2$

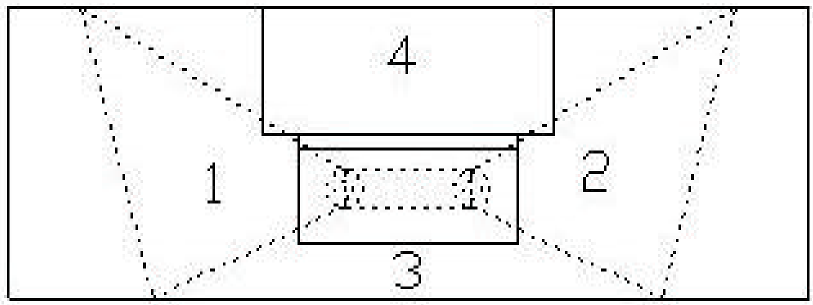

Figure 4-13. Trapezoidal Areas

C_{crb} = 1.0 for concrete assumed un-cracked

= 0.8 for locations likely to become cracked

(*please note that some specimens cracked and some did not)

? $_{ec,N}$ = edge modification factor (Equation 4-10)

$$y_{ec,N} = \left(\frac{1}{\left(1 + \frac{2e'_N}{3h_{EF}}\right)} \right) = y_{ec,N} = \left(\frac{1}{\left(1 + \frac{2(1.75")}{3(5.9375")}\right)} \right) = 0.8358 \qquad (4\text{-}10)$$

With all of the coefficients calculated the research team was now able to calculate the breakout strength (Equation 4-11):

$N_{cb} = N_{cbg} = C_{bs}A_N C_{crb}$? $_{ec,N}$ = (128.48)(243.88)(1.0)(0.8358) = <u>26.188 kips</u> (4-11)

$N_{cb} = N_{cbg} = C_{bs}A_N C_{crb}$? $_{ec,N}$ = (128.48)(243.88)(0.80)(0.8358) = 20.951 kips

The pullout tensile strength calculation or the bearing capacity of the stud against the concrete is as follows (Equation 4-12):

$$N_{pn} = 11.2A_{brg}f'_c C_{crp} \qquad (4\text{-}12)$$

where:

A_{brg} = bearing area of the stud head in tension (sq. in.)

= area of the head – the area of the shank

C_{crp} = cracking coefficient (pullout)

= 1.0 for concrete assumed uncracked (most common)

= 0.7 for locations likely to become cracked

$N_{pn} = 11.2A_{brg}f'_cC_{crp}$ = (11.2)(1.18)(9000)(1.0) = <u>118.9 kips</u> (no cracking)

$N_{pn} = 11.2A_{brg}f'_cC_{crp}$ = (11.2)(1.18)(9000)(0.70) = 83.3 kips (cracking)

The last of the concrete tension calculations was the side-face blowout computation. For additional explanation of how dimensions were derived please see Figure 4-14. The studs analyzed were located at a perpendicular distance, d_{e2}, less than $3d_{e1}$, which allows for the side-face blowout calculation to contain a multiplier as opposed to studded heads located closer to edges. The basic equation for side-face blowout is as follows (Equation 4-13):

$$N_{sb} = 160d_{e1}\sqrt{A_{brg}}\sqrt{f'c} = 160(3)\sqrt{1.18}\sqrt{9000} = 49.47 \text{ kips} \qquad (4\text{-}13)$$

The strength reduction coefficient due to the location of the studded connection positioned away from an edge (dimensions for this equation can be seen in Figure 4-10) is obtained by (Equation 4-14):

$$\text{Strength reduction coefficient} = \frac{\left(1+\frac{d_{e2}}{d_{e1}}\right)}{4} = \frac{\left(1+\frac{5''}{3''}\right)}{4} = 0.666 \qquad (4\text{-}14)$$

It was now possible to compute the most accurate side-face blowout capacity by multiplying the reduction factor by the side-face blowout capacity (Equation 4-15).

$$N_{sb} = N_{sb}(\text{reduction factor}) = (49.47 \text{ kips})(0.666) = \underline{32.98 \text{ kips}} \qquad (4\text{-}15)$$

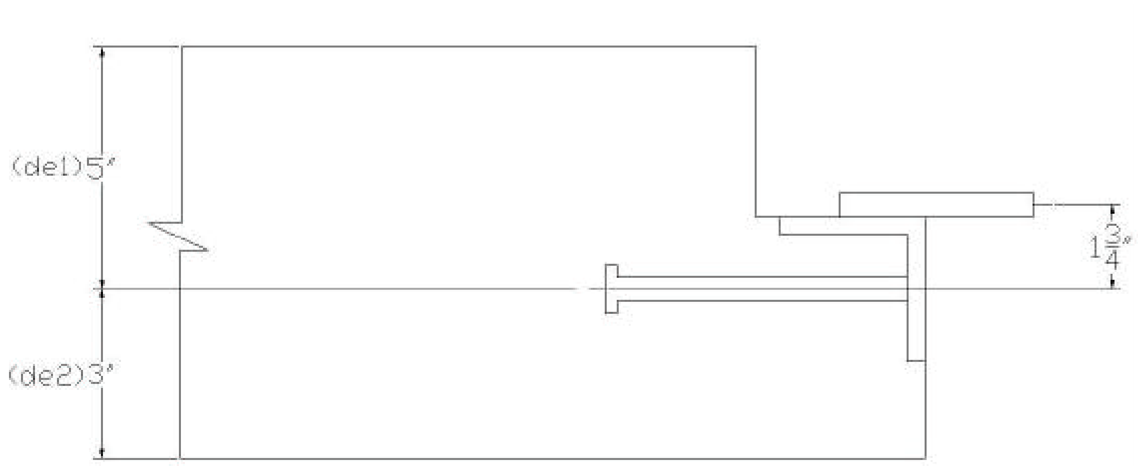

Figure 4-14. Distance Explanation for Specimen

D. Concrete Shear Strength

The next series of calculations were from 6.5.5 of the 6th Edition of the PCI Design Handbook. This particular section deals strictly with shear strength governed by concrete failure. The basic strength is the primary equation used to calculate the ultimate capacity, but is comprised of many different factors. These factors include spacing, thickness, eccentricity, and cracking. All of the factors had to be calculated along with the single anchor strength before the basic strength could be found. The actual basic strength equation is as follows (Equation 4-16):

$$f\ V_{cb} = f\ V_{co3}(C_{x3})(C_{h3})(C_{ev3})(C_{vcr}) \qquad (4\text{-}16)$$

where:

f = concrete strength reduction factor (please note that since the research team was analyzing ultimate capacities, this was neglected)

V_{c3} = nominal concrete breakout strength for a single or multiple stud connection accounting for member and connection geometry (lbs)

V_{co3} = concrete breakout strength for a single stud connection unaffected by connection or member geometry (lbs)

C_{x3} = coefficient for overall X spacing of a connection with two or more X rows for a d_{e3} type anchorage

C_{h3} = coefficient for member thickness (h) for a d_{e3} type anchorage

C_{ev3} = coefficient for eccentric shear force influences for a d_{e3} type anchorage

C_{vcr} = coefficient for cracking in a member, loaded in shear

- Single Anchor Strength

$$V_{co3} = 16.5 l \sqrt{f'_c}\left(BED\right)^{1.33} \tag{4-17}$$

BED = d_{e3} + Y = 6 + 3.5 = 9.5in. (4-18)

? = 1.0 because normal weight concrete was used

$$V_{co3} = 16.5(1.0)\sqrt{9000}(9.5)^{1.33} = 31.26 \text{ kips}$$

- X Spacing Factor

C_{x3} = 1.0 when X = 0

- Thickness Factor

$$C_{h3} = = 0.75\sqrt{\frac{h}{BED}} \text{ for } h \le 1.75BED \tag{4-19}$$

h = member thickness (in.)

C_{h3} = = $0.75\sqrt{\frac{8}{9.5}}$ = 0.6882

- Eccentricity Factor

$$for \quad e'_v \le \frac{x}{2} = 1.75 \le \frac{3.5}{2} = 1.75 \le 1.75$$

$$C_{ev3} = \frac{1}{1+0.67\left(\frac{e'_v}{BED}\right)} \le 1.0 = \frac{1}{1+0.67\left(\frac{1.75}{9.5}\right)} \le 1.0 = 0.89 \le 1.0 \qquad (4\text{-}20)$$

where:

e'_v = eccentricity of shear force on a group of anchors; distance between point of shear force application and geometric centroid of group of anchors resisting shear in direction of applied shear (in.).

- Cracking Factor

C_{vcr} = 0.85 edge reinforcement = No. 4 bar

The research team could now revert back to PCI Eq. 6.5.5.1 in order to determine the basic strength of the studded connection in shear (Equation 4-16):

$V_{cb} = (V_{co3})(C_{x3})(C_{h3})(C_{ev3})(C_{vcr})$ = (31.26)(1.0)(0.6882)(0.89)(0.85) = <u>16.47 kips</u> (4-16)

Experimental results were then compared against the PCI calculations, there were some variances in the ultimate values. However, the value that was most notable was the tensile strength comparisons that were observed in the laboratory testing. The problem was approached using basic mechanics to determine why and where failure occurred.

Failure had been noted in all tensile specimens at the location where the stud shanks connected to the angle. Initially, all stress, force, and basic moment calculations proved ineffective until they were considered about the angle cross section. Therefore, the first step was to determine the section modulus for this particular angle (Equation 4-21).

$$Z = \frac{(bh^2)}{6} = \frac{((6'')(0.375)^2)}{6} = 0.140625\text{in}^3 \qquad (4\text{-}21)$$

Then multiplying the ultimate failure load average from all four of the tensile tests by the most exact moment arm, in this case from the top of the shank weld to the bottom of the angle, the moment applied to the connection calculated (Equation 4-22) as :

$$M = (P)(e) = (12780 \text{ lbs})(1.5 \text{ in}) = 19170 \text{ lb-in} \qquad (4\text{-}22)$$

Taking the ultimate moment applied to the test specimens before failure was noted and then dividing by two in order to equate the load per shear stud, the ultimate moment load per shear stud could be computed (Equation 4-23).

$$M = \frac{19170 lb - in}{2} = 9585 \text{ lb-in per shear stud} \qquad (4\text{-}23)$$

Finally, applying the bending stress formula of $\frac{M}{Z}$ = s (Equation 4-24) it became clear why failure occurred.

$$s = \frac{M}{Z} = \frac{9585 lb - in}{0.140625 in^3} = \underline{68.1 \text{ ksi}} \qquad (4\text{-}24)$$

4.5 Connection Conclusions

In analyzing the flange connection, a comparison between the PCI design handbook and experimental results showed how unpredictable this particular connection was. The design values for the steel capacity were 26 kips in tension as well as shear. The weld capacity for this particular section was roughly 76 kips. The predicted value for concrete strength in tension was governed by the concrete breakout strength which was 26.19 kips. Finally, the basic concrete strength for members in shear was nearly 16.5 kips.

Analysis of the experimental data resulted in the average ultimate values in tension and shear of 12.8 kips and 24.6 kips, respectively. In both test setups, failure always occurred in the steel members of the connection, and not in the concrete, as the capacity calculations indicated, suggesting that in order to evaluate connection details not found in current design guidelines, experimental investigation is recommended. Furthermore, although not part of the objectives of the present report, long-term performance of these connections must also be evaluated, focusing on fatigue, section corrosion/durability, torsion, etc...

5 Deck Girder Fabrication

The steps used in the fabrication of the girders could be divided into two stages. The initial stage involved the fabrication of the Type III AASHTO girder without the deck. This was followed by the second stage, which consisted of the fabrication of the deck portion using same concrete mix as specified for the girder, and the prestress tendon release.

5.1 Deck Formwork

New formwork had to be designed for the fabrication of these girders because they were the first of their kind. The special formwork for the deck was designed and fabricated by Standard Concrete Products of Savannah, GA. The deck formwork was constructed using a space truss support system consisting of numerous steel angles (see Figure 5-1). The trusses were anchored down to the bed with the use of bolts. The exterior truss supporting the formwork was constructed so that the horizontal formwork was tilted inward. This allowed for the correct slope at the bottom of each flange.

Figure 5-1. Space Truss Used for Support in Deck Form Work

The new formwork was placed on the girder bed and attached to the existing steel tubing spaced transversely along the entire length of the bed. The inner truss of the formwork was attached to these steel tubes using a steel collar and bolt system (see Figure 5-2). The steel collar fit around the steel tube, while the bolt was tightened at the top of the collar to ensure a snug fit. This system allowed the deck formwork to slide out to provide space for the girder formwork, and then returned to its original position for the pouring of the next deck section (see Figure 5-3).

Figure 5-2. Bolt and Collar System for Inside Truss in Deck Formwork

Figure 5-3. Deck Form Work Slid Back for the Girder Fabrication

5.2 AASHTO Girder Fabrication

This phase of the deck girder fabrication is identical to the traditional Type III fabrication process. Initially, the strands were placed in the bed. The end plate of the girder formwork was used as a template for the layout of the strands through the bed (see Figure 5-4). Each end of the strands were then anchored into the ends of the bed using a jacking device that pulls on each strand while an end cap, shown in Figure 5-5, was used to react the tensioning force in the strand. The strands were then checked carefully to ensure that none were damaged in the tensioning process.

All of the transverse reinforcement for the girder was then tied. The PVC inserts for the diaphragms were also tied to the rebar before the placement of the girder formwork (see Figure 5-6), securing them in the right position. The reinforcement was then checked by NCDOT representatives, before the girder formwork was put into place.

Figure 5-4. End Plate of the Formwork for the Girder

Figure 5-5. End Anchorage for the Strands

Figure 5-6. PVC Inserts for the Diaphragms

The girder formwork was then positioned into place by using a crane with two lifting devices that picked up on the formwork at both ends. The forms were connected together to ensure a tight fit to the two end plates (see Figure 5-7). The concrete was batched and tested on-site. The concrete was tested for slump, air content, temperature, and cylinders were made for compressive strength tests. The concrete contained a corrosion inhibitor to help protect the reinforcement. Each batch was tested to ensure that the corrosion inhibitor was added.

Once the batch was approved, the concrete was placed using a small all-terrain vehicle with a bed and chute (see Figure 5-8). The concrete was poured in three different layers in the girder. A vibration device that was attached to the formwork was used for the first two layers so that the rebar would not be damaged. A square head internal vibrator system was used to vibrate the final top layer of concrete. The girder formwork was completely filled with concrete and then raked, so that sufficient bonding with the deck would be achieved when later poured.

The connector ties that would connect the girder with the deck were then brushed clean of concrete to ensure proper bonding. The concrete was left to cure for 17 to 18 hours, so that the girder formwork could be removed. During the curing process, burlap cloth and tarps were used to cover the concrete. A water system, which ran underneath the tarps and burlap cloth, provided a steady mist for the duration of the curing time. The concrete strength when the girder formwork was removed varied between 5,500psi and 8,000 psi.

Figure 5-7. Final Placement of Girder Formwork with Connectors

Figure 5-8. Vehicle Used to Place the Concrete into the Formwork

5.3 Deck Fabrication

The next stage of the fabrication process started with the removal of the girder formwork. The come–alongs were then released so that the deck formwork could be bolted into place. Steel channels were then welded to the top of the form work to support the longitudinal sides of the deck (see Figure 5-9). Number six rebar lengths were also used to help laterally support the channel on the form work. A small triangular piece of steel was used for the chamfer on the inside of the channel. This steel strip was welded to the formwork, before the channel was secured.

Figure 5-9. Channel Welded to the Deck Formwork

The shear keys were formed by using steel angles welded to the inside of the channel (see Figure 5-10). Then longitudinal and transverse rebars were tied and inspected before the concrete was poured. PVC pipe inserts were also placed according to the specifications for the breathing of the concrete in the end walls. Similarly, special inserts were also positioned and secured to the reinforcement, which were intended to be used during the jacking procedure (see Figure 5-11).

The embedded angle connectors were placed according to the specifications, and tied to the longitudinal rebars (see Figure 5-12). The block-outs for the embedded angles were made using a piece of wood wrapped in duct tape to prevent the bonding to the concrete (see Figure 5-13). A thin strip of liquid silicon was applied to the wood and steel channel to prevent the wood block-out from floating when the concrete was poured. The concrete was poured continually in one layer along the entire length, properly vibrated, broom finished, and allowed to cure to the appropriate strength (minimum 5,500psi) before cutting the strands. The concrete was then covered again with the burlap cloth and tarps. A steady mist was also applied during the curing process of the deck.

Figure 5-10. Steel Angles Welded to Formwork to Form the Shear Key

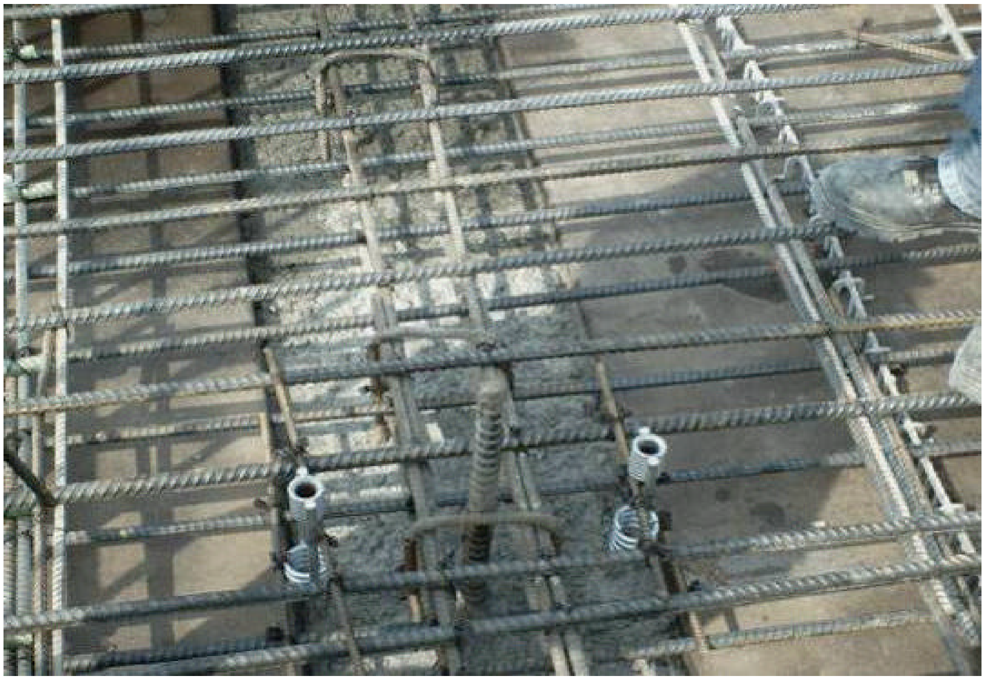

Figure 5-11. Inserts in Deck for Jacking

Figure 5-12. Embedded Angle Installation Before Placing the Concrete

Figure 5-13. Block-out for Embedded Angle Connection

Once the concrete reached a compressive strength of 5,500psi, the strands were released. The deck formwork was then shifted back away from the girder and the deck girder was lifted out of the bed using two 80-ton cranes. The deck girder was then moved to the storage area in the yard, and placed on timber supports. Each deck girder was fabricated using the same process. The two exterior deck girders were fabricated first, then the three interior deck girders. Once all of the deck girders were fabricated and moved to the storage area, a dry assembly (see Figures 5-14 and 5-15) was completed. The dry assembly was done to provide the contractor with the order of placement to ensure the most efficient and correct layout.

Figure 5-14. Dry Assembly – Lateral View

Figure 5-15. Dry Assembly – Top View

5.4 Formwork Critique

The formwork was measured in the yard for both the deck and AASHTO girder. The measurements were made with a standard tape measure and recorded. The measurements were used to produce AutoCAD™ drawings of each formwork, which are shown in Figure 5-16 through 5-18.

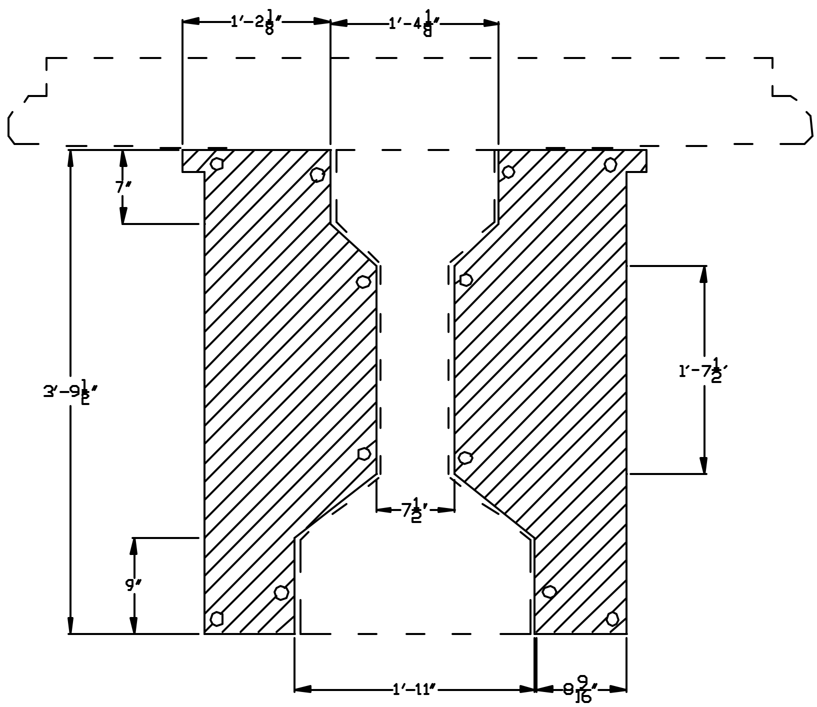

Figure 5-16. AASHTO Girder Formwork

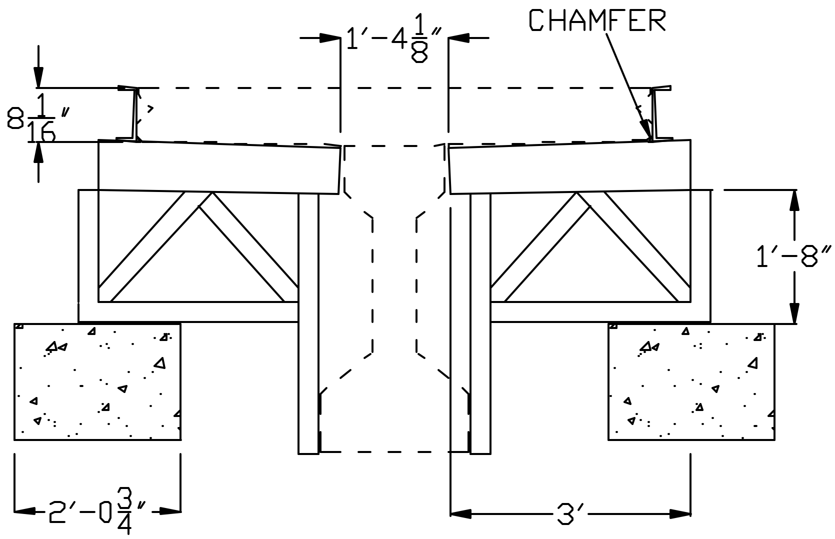

Figure 5-17. Section of Deck Formwork

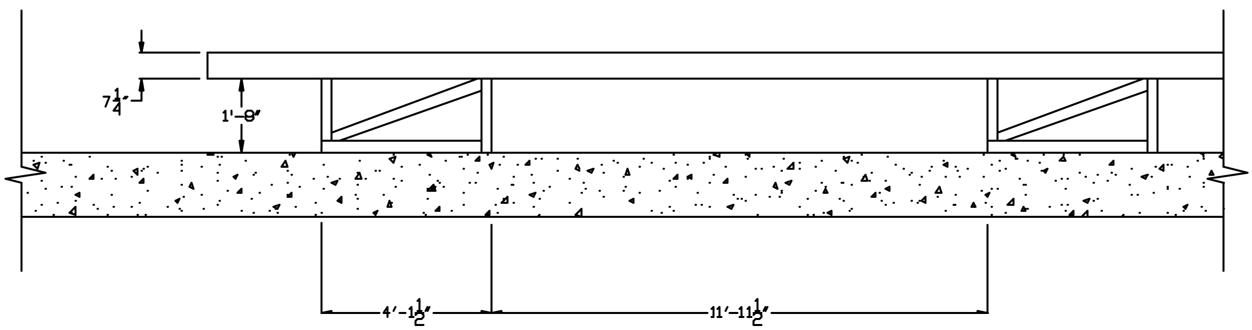

Figure 5-18. Side View of Deck Formwork

The formwork for the deck was designed efficiently and was easy to slide in and out as needed. The only concern that was found was with the embedded plates and block-outs. The block-outs were fabricated using a piece of wood placed on top of the embedded angles, which were tied to the rebar. When the concrete was placed, the wood and angles both started to float and move out of position. This caused concrete to cover the plates as well as let the plates move out of alignment. This initial problem was quickly resolved by using liquid silicon adhesive to keep the piece of wood in place. The embedded angles and studs were tied onto the deck reinforcement more efficiently as well.

The formwork also required the girders to be poured in two separate parts. For future use, it is suggested to allow the deck formwork to attach directly to the existing AASHTO girder formwork. This would allow the deck girders to be poured in one day instead of two. On the other hand, this will only make economic sense when these types of deck girders are fabricated in larger quantities. Several ideas were considered, but only one is presented here at a rough sketch level. No attempt was made to fully design these possible modifications. First, two longitudinal steel plates are fabricated that are fastened together at an angle of 90 degrees on the edge (see Figure 5-19). These two pieces would then hook into the top outside edge of the existing Type III girder formwork. These hooks would slide into slots on the existing formwork and hook into place.

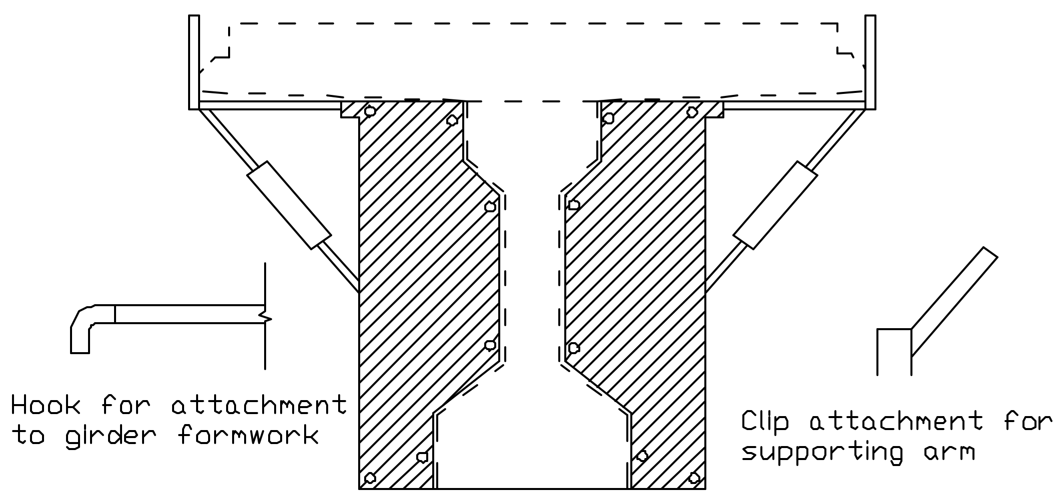

Figure 5-19. Formwork with Turn Buckles

The new attachment would be supported by angled arms spaced out through the entire length of the girder. These arms would consist of two rods that are attached by a turn buckle. The turn buckle could be used to lower or raise the attaching formwork. This can be used to produce the designed slope for the flanges, as well as to allow for flange vertical alignment. The bottom rod in the supporting arm system would have a clip that would slide onto the side of the girder formwork.

As an alternative, the flange support could also be accomplished by the use of vertical jacks placed along the entire length of the deck girder. These jacks, similarly to the turn buckles, would provide support for the flange. The advantage of this system would be quick formwork assembly, and one-step concrete placement.

5.5 Release Camber and Stress Comparison

The measurement of the camber in the deck girders was completed using two different methods. The first method was an actual survey of the girder, and the second method was done using a taut string.

The first camber measurement method required the use of a total station. The total station was set up parallel to the girder being measured and then leveled off. It was decided to measure the camber at every tenth point on the girder, so a measurement of these points was done using a tape measure and red permanent marker. The ground was then surveyed at the same points. Once the elevations were recorded, a simple mathematical equation was used to find the slope of the ground between each point. The next step in the process was to measure the distance between the bottom of the girder to the ground. This was done using a tape measure. The camber was then found through simple calculations.

The second method used to measure the camber was performed using a string and tape measure. The string was tied to the tendons at one end of the girder and then stretched extremely tight along the entire length of the girder, from girder corner to corner. Once the string was tightened properly, a tape measure was used to measure the distance between the bottom of the girder to the top of the string. These measurements were recorded and compared to the camber which was calculated using the previous method. It was found that the difference in the camber values from these two methods was very small.

5.6 Actual vs. Design Camber

The measured camber from the two methods was then compared with both the design values and the values from the Larsa™ model (see Table 5-1). The predicted camber values, obtained from hand calculations, were updated to reflect the actual concrete compressive strength of approximately 9,000 psi at prestress tendon release.

Furthermore, the Larsa™ camber values were recorded at slightly different positions from the end of the deck girder; these positions, as opposed to the 10^{th} points, matched the location of member type changes along the length of the bridge. The results showed that the designed/predicted and actual camber values were close. The discrepancy shown in Figure 5-20 could be a result of differences between actual versus design concrete strength (8,000-9,000psi as compared to the specified 5,500psi) and prestress losses, slight deviations from prestress stress, actual versus specified tendon locations, etc... However, the overall comparison is satisfactory.

Table 5-1. Comparison of Camber Values

Position	Distance from End (ft)	Predicted Camber (in.)	Actual Camber (in.)	LARSA Distance (ft)	LARSA Camber (in.)
A	0.00	0.000	0.000	0.00	0.000
B	10.77	1.475	1.578	10.67	1.040
C	21.54	2.625	2.052	20.75	1.730
D	32.30	3.441	2.634	30.75	2.200
E	43.07	3.933	2.772	40.75	2.490
F	53.84	4.100	2.892	50.75	2.600
G	64.61	3.933	2.592	65.25	2.490
H	75.38	3.441	2.544	75.25	2.200
I	86.14	2.625	2.076	85.25	1.730
J	96.91	1.475	1.260	95.33	1.040
K	107.68	0.000	0.000	106.00	0.000

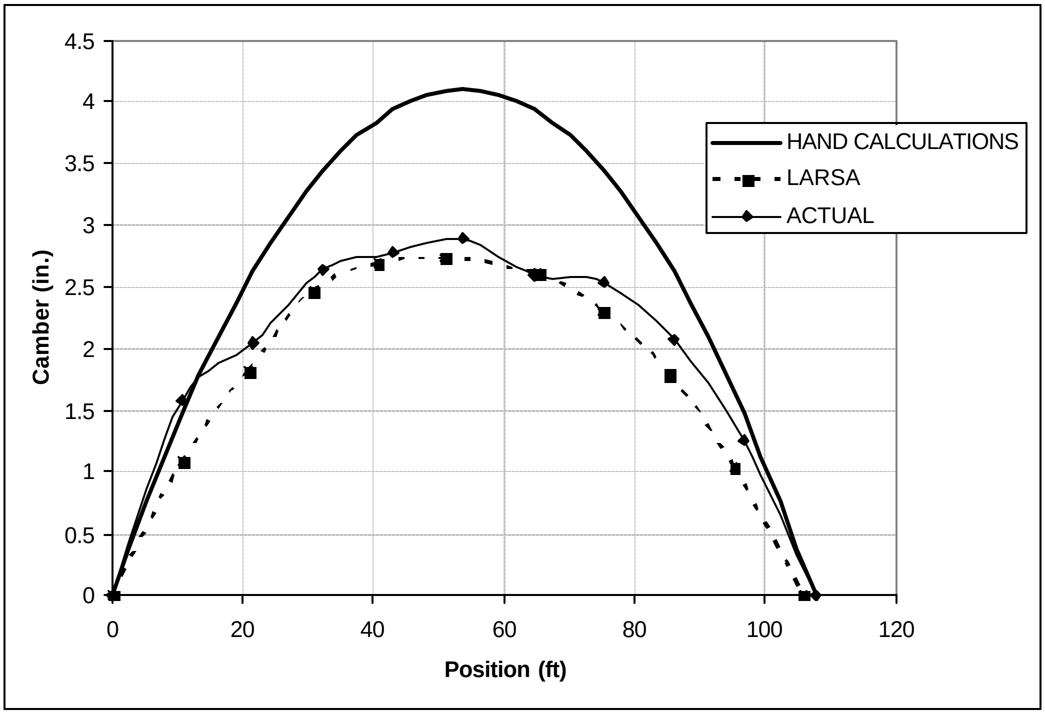

Figure 5-20. Predicted vs. Actual Camber Measurements

5.7 Strain Measurements

Strain measurements were made before and after the strand release, measured on the last girder being fabricated. Mechanical strain gages were used to measure strain, and to calculate stresses at certain points on the deck girder. The points of interest were the quarter and center points of the deck girder. There were four holes drilled using a hammer drill at each of these points on the deck girder. There were two holes drilled at 14” from the top of the AASHTO girder section, and two holes drilled 3” from the bottom of the girder section (see Figure 5-21 and 5-22).

Each set of holes were spaced 8 inches on center. The mechanical strain gage required special brass inserts to be secured into these holes, so that measurements of strain could be made using tabs screwed into these inserts. A template was made for the installation of the inserts, allowing for a better insert positioning while the fast curing epoxy hardened. A two-part epoxy was used to glue the inserts into place. Once the epoxy was set, the template was removed from the tabs.

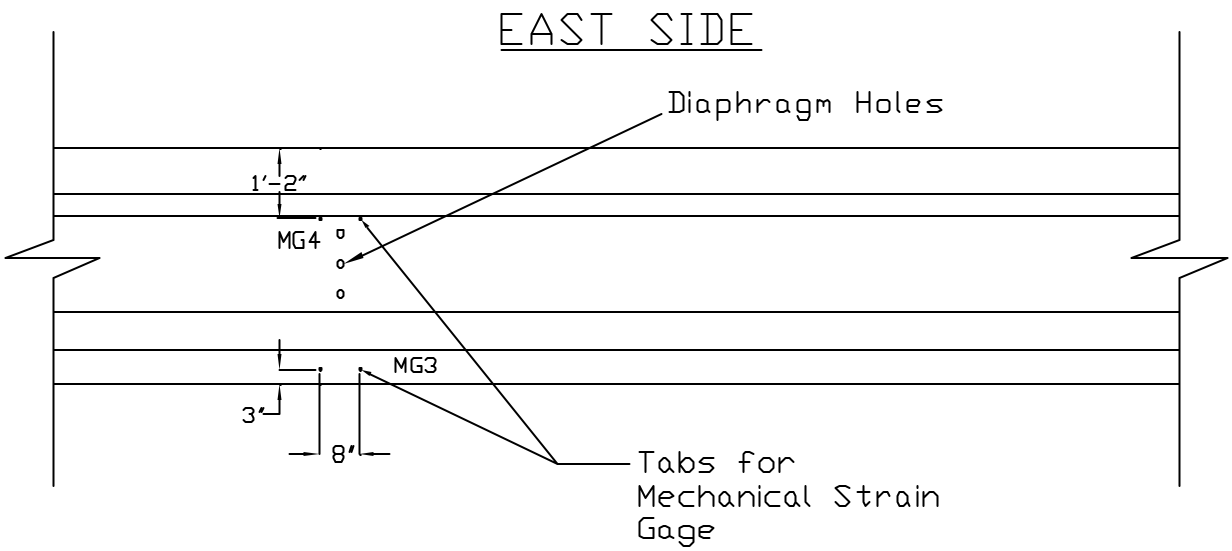

Figure 5-21. Location of Tab Inserts at Quarter Point on the Girder

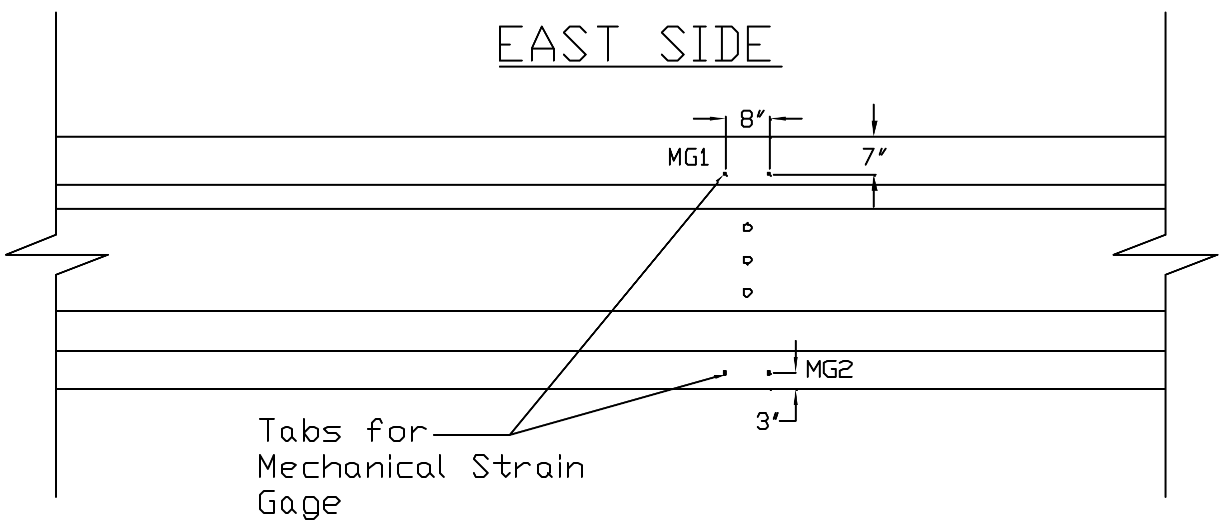

Figure 5-22. Location of Tab Inserts at Mid-Span of the Girder

The mechanical strain gage utilizes a high-precision electronic caliper that measured the change in spacing between the tabs secured to the brass inserts. An initial measurement was made and recorded before the strands were cut in the deck girder. Once the strands were cut, another measurement was made and recorded. These measurements were then used to find the strains associated with stress release, which was then converted into stress. These values are provided in Table 5-2.

The design stress values (Hanks, 2005) shown in Table 5-3 were computed with an assumed concrete compressive strength of 5,500 psi at release. However, the actual strength at release was around 9,000 psi, so the design values were recalculated using the actual compressive strength. The design stress values were approximately 500 psi lower than the actual values, possibly a result of a slightly different camber than anticipated. The stress values at the mechanical strain gage locations were also found using the previously developed Larsa™ model (see Table 5-4). It is clear that there are some differences, but for the most part, the predicted values are fairly close to the measured values. This comparison is also given in Figure 5-23, from which, the values of MG3 and MG6 were omitted due to apparent erroneous measurements.

Table 5-2. Measured Strain Values After Release of Strands*

Gage Number	Readings Before Release (in.)	Readings After Release (in.)	Difference ? (in.)	Actual Strain (e = ? / 8”)	Actual Stress (psi)
MG1	0.0373	0.0385	0.0012	1.500E-04	819
MG2	0.0129	0.0178	0.0049	6.125E-04	3347
MG3	-0.0062	-0.0065	0.0003	3.750E-05**	204**
MG4	0.0123	0.0156	0.0033	4.125E-04	2254
MG6	-0.0268	-0.0051	0.0217	2.713E-03**	**
MG7	0.0144	0.0175	0.0031	3.875E-04	2118
MG8	0.0200	0.0233	0.0033	4.125E-04	2254

Note: * Positive values for compression
** Erroneous values excluded from comparisons

Table 5-3. Comparison of Design Values and Actual Values of Stress

Gage Number	Predicted Stress by Hand Calculations (psi)	Actual Stress (psi)
MG1	176	819
MG2	2817	3347

Table 5-4. Stress Values From Larsa™ Model

Gage Number	Location From Bottom of Girder (in.)	Larsa Stress @ Top of Girder (ksi)	Larsa Stress @ Bottom of Girder (ksi)	Larsa Stress @ Instrumented Locations (psi)	Corresponding Larsa Strain
MG1	40.0	0.165	2.788	914	1.673E-04
MG2	3.0	0.165	2.788	2647	4.843E-04
MG3	3.0	-0.091	3.322	3091	5.655E-04
MG4	33.0	-0.091	3.322	1301	2.382E-04
MG6	3.0	0.165	2.788	2647	4.843E-04
MG7	33.0	-0.091	3.323	1301	2.382E-04
MG8	3.0	-0.091	3.323	3091	5.655E-04

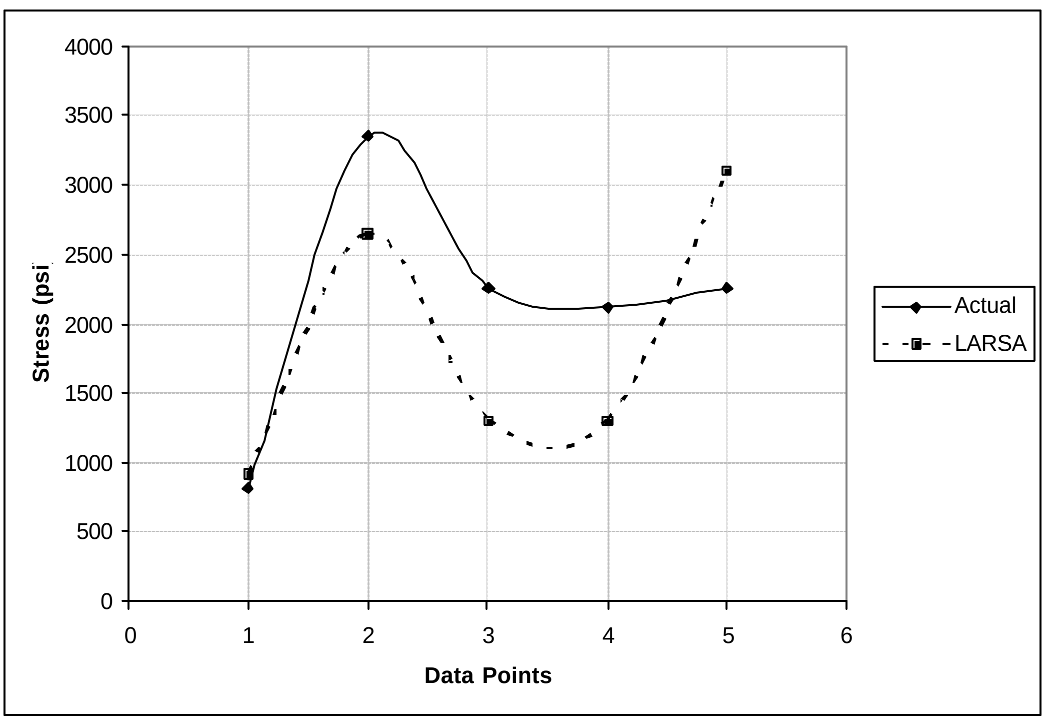

Figure 5-23. Actual vs. Predicted Stress Levels at Selected Points

5.8 Transportation

Once the fabrication of the girders was completed, a compressive strength of at least 9,000psi was reached, they were prepared to be transported from Savannah, GA to Stanly County, NC. A total of five trucks were used to transport the girders. Before the girders were loaded onto the truck an anchor bolt was slid through inserts at opposite ends of the girders (see Figure 5-24). A hook was then tightened onto this bolt on either side of the girder with a nut. This device was used in route to help chain down the girders while transporting them. Timbers were then stacked on each end of the girders to help protect the top surface of the girders from the chains (see Figure 5-25). The girder(s) were raised by two cranes in operation at the fabrication plant.

Figure 5-24. Hook Attached to Girder for Securing Down

Figure 5-25. Timbers Used for Protection of the Top Surface from the Chains

Each truck consisted of a semi-truck with a 6-axle trailer (see Figure 5-26). One end of the girder was placed on the back of the semi itself and the other end located on the trailer. The end of the girder would be positioned in a slot shown in Figure 5-27 to secure the girder from sliding in transit. Once the girder was secure in the slot, the crane was detached from the girder. The girder was then secured down by chains. Chains were placed over the top of the girder and tightened by the use of a lever load binder (see Figure 5-28). Plastic corner covers were used on the edges in contact with the chain to protect the girder from rubbing and grooving damage.

Chains were also inserted through the hook that was attached to the side of the girder to help with lateral stability. The chains were used to keep the girders from overturning while transporting them. The center of gravity and weight of each girder were two issues that had to be addressed when transporting the girders. The center of gravity of the girder was in the top third of the girder x-section which made it very top heavy. This was the reason for multiple chains at each end of the girder. The weight of the girder(s) demanded the use of specialized 13 axle vehicles.

Figure 5-26. Truck Used for Transporting Girders

Figure 5-27. Slot for Placement of the End of a Girder

Figure 5-28. Chain Assembly for Securing the Girders

The only permit needed for hauling the girders was an oversize length permit. Each truck also required two escorts, one in the front and one in the rear. The route taken by the trucks required that they stay on primarily four lane or larger highways. The route taken leaving the plant stared with I-95 North to I-26 West. Then the fleet proceeded to I-77 North to I-85 North. Then they merged onto I-485 to Hwy 49 towards Albemarle. Then they exited Hwy 49 to Hwy 73. The final destination at Austin Rd., the location of the site, was then reached. The drivers were limited to a speed limit of 65 mph, but no problems occurred during the transporting process and the girders arrived on schedule.

One issue that occurred was a request by the drivers of the trucks. They requested that an extra set of holes be drilled into the flanges to help with the stability of the deck girders while hauling. The request was not granted because of the reinforcement layout in the flange did not allow it. In future projects, this option could possibly be taken into consideration during the fabrication process by the use of PVC inserts into the flanges.

5.9 Construction

The construction process is described in the construction report located in Appendix A. A few issues and recommendations can be discussed about the construction process. The washers on the diaphragms began to push through the holes when the nuts were being tightened in the field. The holes in the diaphragm appeared to be too large to prevent this from happening. A smaller hole for the bolts in the connections would be a solution for this problem. In future projects, the use of concrete diaphragms could be another option for this type of bridge.

Another issue brought up in many meetings had to deal with the riding surface of the actual girders. The location of the bridge required an average of 4" of asphalt to be added to the top of the bridge (bridge is located at the bottom of a sag curve). A surveying study was done to address this issue. The entire bridge deck surface was surveyed using a total station and the coordinates and elevations were recorded. A mapping program was then used to plot these points to verify the quality of the concrete surface. The program used was Arcview GIS 3.3®, which allows the user to import an Excel spreadsheet with geographical data and create numerous types of maps. The type of map created for the assessment of the riding surface was a 3-D surface map (see Figure 5-29). This map shows how the surface changes along the bridge according to the locations and elevations of the geographical points used. The different colors represented ranges of elevations. The map shows that the deck girders on the west side of the bridge are slightly higher than the ones on the east, as expected, since the bridge was sloping in that direction.

Furthermore, when asphalt is not needed, if an extra inch of concrete would be placed on the deck surface during fabrication, this layer can be removed by surface grinding after the members are installed, allowing for a smoother riding surface. Finally, the use of lightweight concrete could reduce the gross weight by 20% (and would present a few design challenges to be considered), which would reduce the demand for both hauling and lifting equipment, as well as the demand on the gravity load supporting system.

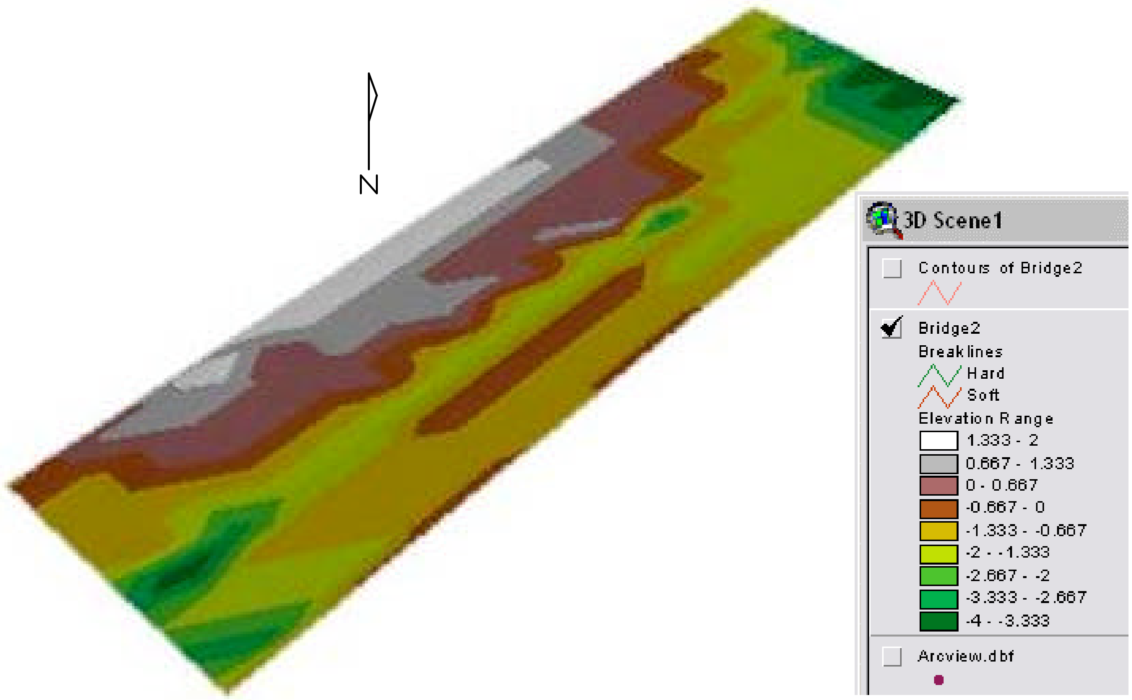

Figure 5-29. Arcview GIS 3.3® Image of Riding Surface Without Wearing Surface

6 Bridge Load Test

6.1 Instrumentation

The bridge was monitored during testing using three instruments: displacement transducers, strain transducers, and strain gages. Displacement transducers, shown in Figure 6-1, were used to measure vertical displacement in the bridge girders. The strain gages were used to measure strain on the diaphragms between the girders, and the connection plates in the deck (see Figure 6-2). The strain transducers were used to measure strain at the bottom and top of the deck girders themselves (see Figure 6-3). Once all of the instruments were in place, cables were attached to each device. The cables were then attached to the Data Acquisition System (DAQ) so that the strains and displacement could be recorded into spreadsheets during the testing. The layout of the instruments was designed to allow the determination of distribution factors, impact factors, strain levels, and displacements of each girder due to the different loading conditions (see Appendix C).

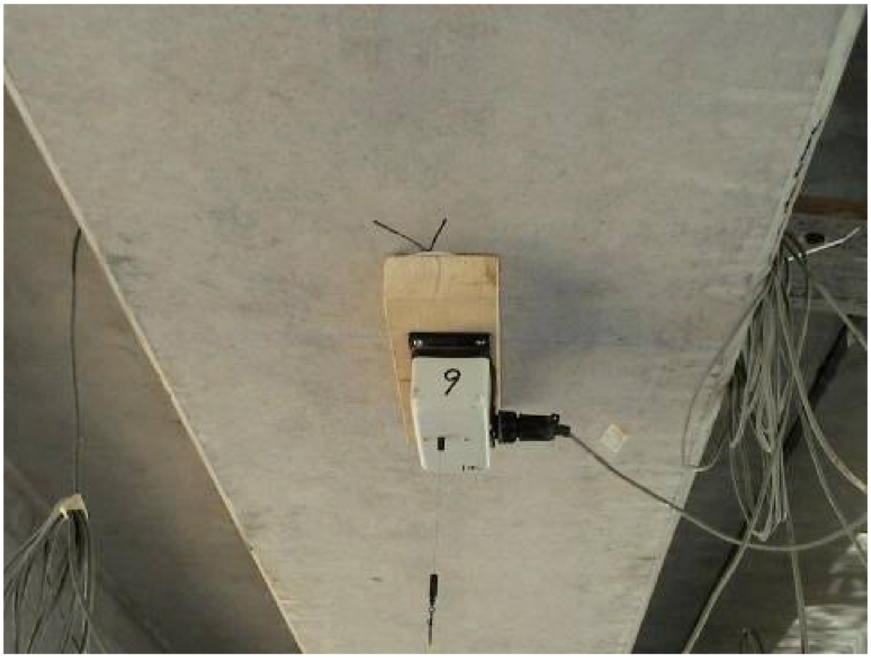

Figure 6-1. Displacement Transducer Attached to the Bottom of Deck Girder

Figure 6-2. Strain Gages Applied to Plate Connection

Figure 6-3. Strain Transducer Attached to the Bottom of Deck Girder

6.2 Load Test

In this project, two types of truck loads were applied: quasi-static (slow moving) and dynamic. The loading vehicle for the testing was determined through the use of a SAP2000™ model. A simply supported beam was used to model the deck girder (see Figure 6-4). An arbitrary weight was chosen for the trucks first, and then each axle weight was determined. Each axle weight was then divided in half for one wheel line and placed on the simply supported beam. The axles were spaced five feet apart on the beam. The axles were then moved at one foot increments along the beam until the maximum moment was achieved. The weights of the trucks were then adjusted to achieve a moment that was approximately 70% of the design moment of 1,632 k-ft. The total weight of the two trucks selected was found to be approximately 100,000 lbs.

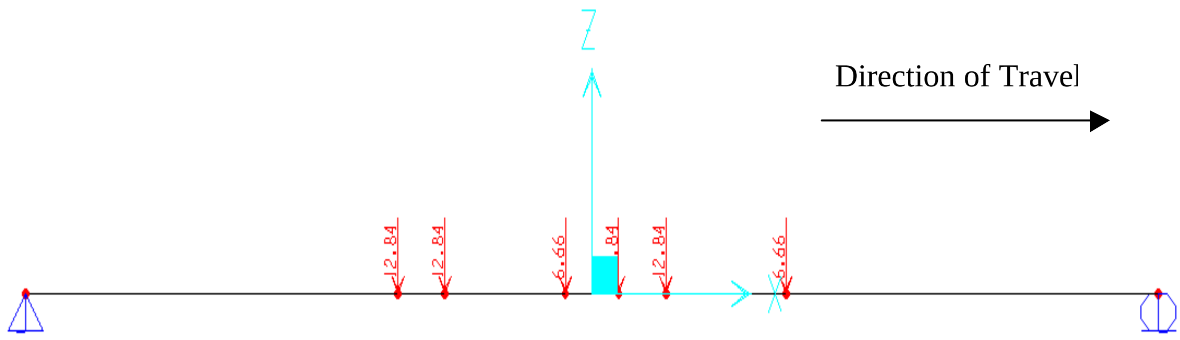

Figure 6-4. SAP2000™ Model

The NCDOT Division 10 provided two tandem trucks (see Figure 6-5) that were loaded with coarse aggregate. The trucks were weighed on the day prior to the test. Each axle was weighed separately and recorded (see Table 6-1). The quasi - static loading required the two trucks to be positioned one behind the other as close as possible. The trucks were then driven across the bridge at 5 mph in both directions (EW then WE), twice for each load path. There were five different load paths used, shown in Figure 6-6. These load paths were chosen in order to achieve maximum stress in each girder. These paths were also selected to investigate how each girder reacts to loading at different points in the transverse direction of the bridge.

The dynamic testing only allowed the use of one truck. The selected truck was first driven at 5 mph to establish a baseline reference, and then allowed to drive at the normal speed limit across the bridge. An AutoCAD™ drawing of the North direction used for testing is shown in Figure 6-7.

Table 6-1. Measured Weight of NCDOT Tandem Trucks

Truck	Front Axle Weight (lbs.)	Middle Axle Weight (lbs.)	Back Axle Weight (lbs.)	Total Weight (lbs.)
1	12,640	18,380	17,680	48,700
2	14,120	17,140	16,660	47,920
Total Wt.				**96,620**

Figure 6-5. Testing Vehicles Provided by NCDOT

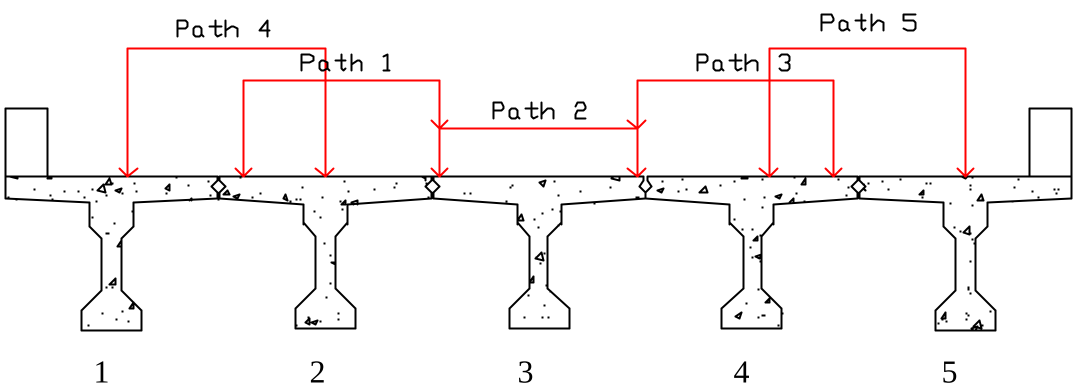

Figure 6-6. Loading Paths for Testing

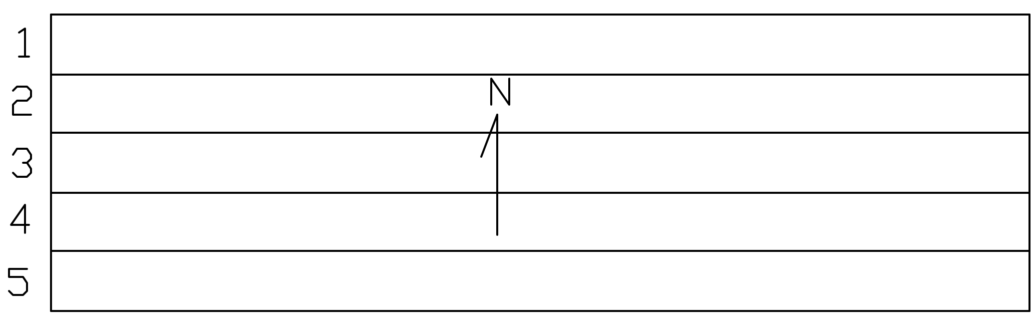

Figure 6-7. Top View of Deck Girder Bridge

6.3 Test Results

The bridge testing resulted in the generation of hundreds of data points that were analyzed. Each load path was analyzed and the non-erroneous data was used. Once the deck girder strains were graphed for each load path, the peak values for each instrument were recorded (see Table 6-2.) The strains were then used to calculate the stress values in the girder. The stress values were later used to compare with the results of the FE model.

The stresses were also used to calculate moments in girder 1 and girder 2. The strain values along deck girders 1 and 2 are shown in Figures 6-8, 6-9, and 6-10. A negative (or compression) strain was present in one of the instruments on each deck girder. The two instruments which contained negative strain were located on the bottom of the deck girders which, on a simple span, should show positive strain. On these graphs, the horizontal axis, unless labeled otherwise, represent a simple scan number assigned by the DAQ system, and does not represent a real physical variable, unless one considers that readings were taken every other second during slow testing.

Table 6-3 shows the calculated moments for mid-span and end of both deck girders 1 and 2. These moments were checked with an equivalent SAP2000™ model that was created to check the amount of fixity at the integral end bents. The model results are discussed later in this chapter. The data in Table 6-3 shows that there was some fixity in the deck girders, as the end of each deck girder contains negative moment proved by the presence of tensile strain values at the top of the deck girder. This demonstrates that the integral end bent does provide the deck girders with some end fixity. Paths 1 and 4 were the only paths that showed significant fixity, since they were positioned directly over girders 1 and 2. The strain values were also used to determine the actual distribution factors for the interior and exterior deck girders.

Table 6-2. Maximum Deck Girder Strain (μe) for Load Paths (Both Directions)

Instrument*	Load Path									
ST	1E	1W	2E	2W	3E	3W	4E	4W	5E	5W
1	5.9	5.5	4.9	4.0	2.2	1.5	4.8	5.2	1.8	0.5
2	-21.4	-14.1	24.8	26.4	25.3	22.4	-54.3	-47.3	22.4	19.0
3	-38.1	-33.5	9.4	14.3	22.5	23.0	-49.0	-45.2	22.7	21.4
4	61.2	5.91	7.0	6.9	4.56	4.1	3.9	4.0	3.6	2.6
5	-5.2	-4.4	5.7	4.1	4.8	3.0	-10.4	-8.6	4.7	2.5
6	-6.2	-7.7	-4.2	-4.3	2.6	2.3	9.8	11.2	3.6	2.3
7	28.3	23.0	8.5	6.1	3.9	1.2	32.7	33.4	2.3	0.4
8	19.4	22.2	19.8	17.4	7.2	5.7	17.3	18.8	4.5	3.4
9	13.5	16.2	25.7	25.5	25.4	23.3	10.5	12.4	18.8	16.4
10	7.5	8.3	11.3	11.9	21.4	24.4	6.0	6.6	21.3	21.8
11	5.6	7.0	10.9	11.7	12.7	16.6	2.3	7.5	20.6	18.5
12	28.6	20.9	10.7	7.7	4.7	2.3	38.1	36.9	3.2	1.3
13	20.1	18.9	13.1	11.1	6.7	5.4	18.3	18.8	5.0	4.0
14	40.7	32.2	10.5	6.6	1.2	-1.0	51.0	48.3	0.7	-1.5
15	-2.2	-2.8	-3.9	-3.7	-2.2	-2.7	-2.4	-2.1	-2.0	-2.2
16	41.0	40.3	38.1	33.7	13.2	8.3	35.6	37.0	5.5	3.9
17	-5.0	-4.7	-1.8	-1.9	-3.7	-4.6	-6.7	-5.5	-4.2	-5.0
18	20.1	22.2	40.8	40.7	45.0	41.2	19.0	19.2	35.1	30.0
19	8.5	10.4	16.3	17.8	27.5	28.6	6.9	7.3	28.5	27.4
20	6.7	7.7	8.3	12.0	21.4	16.2	2.4	3.6	21.9	26.0

(-) Compression; (+) Tension; *Refer to Figure C-1 (Appendix C) for instrument location

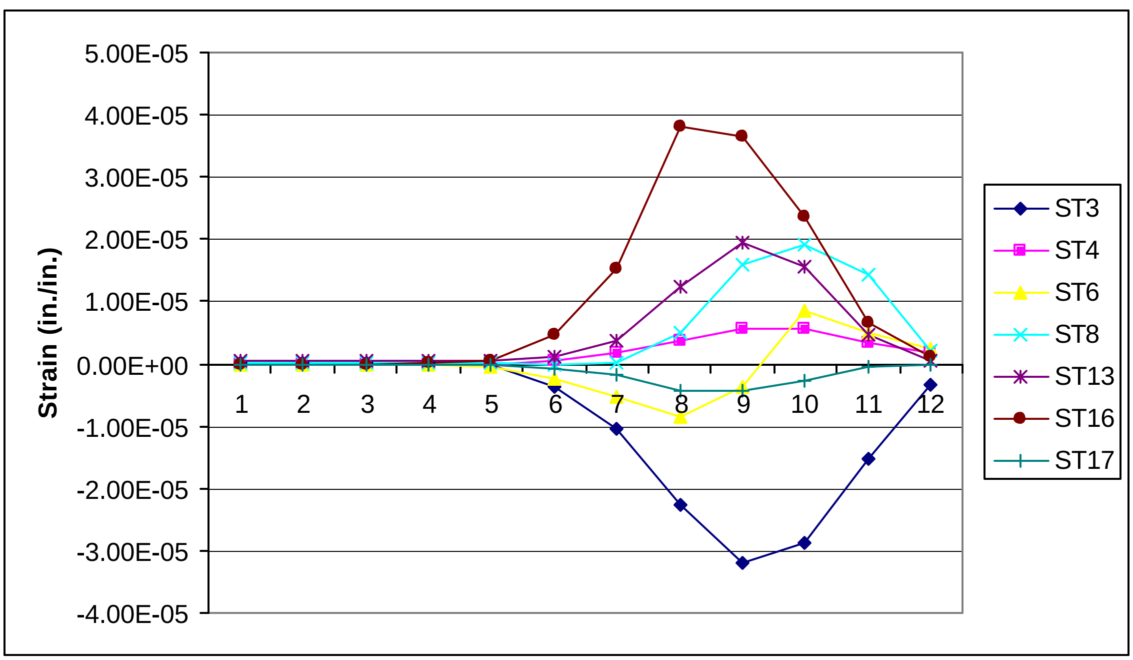

Figure 6-8. Deck Girder 1 Strain Values from Path 1W

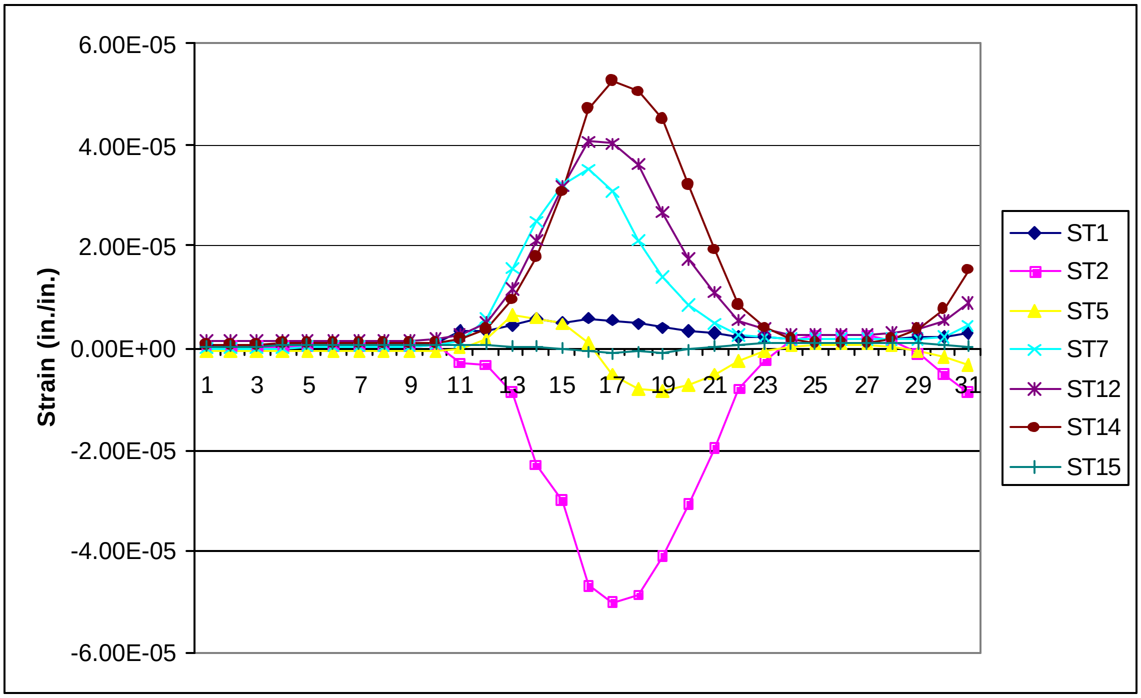

Figure 6-9. Deck Girder 1 Strain Values from Path 4E

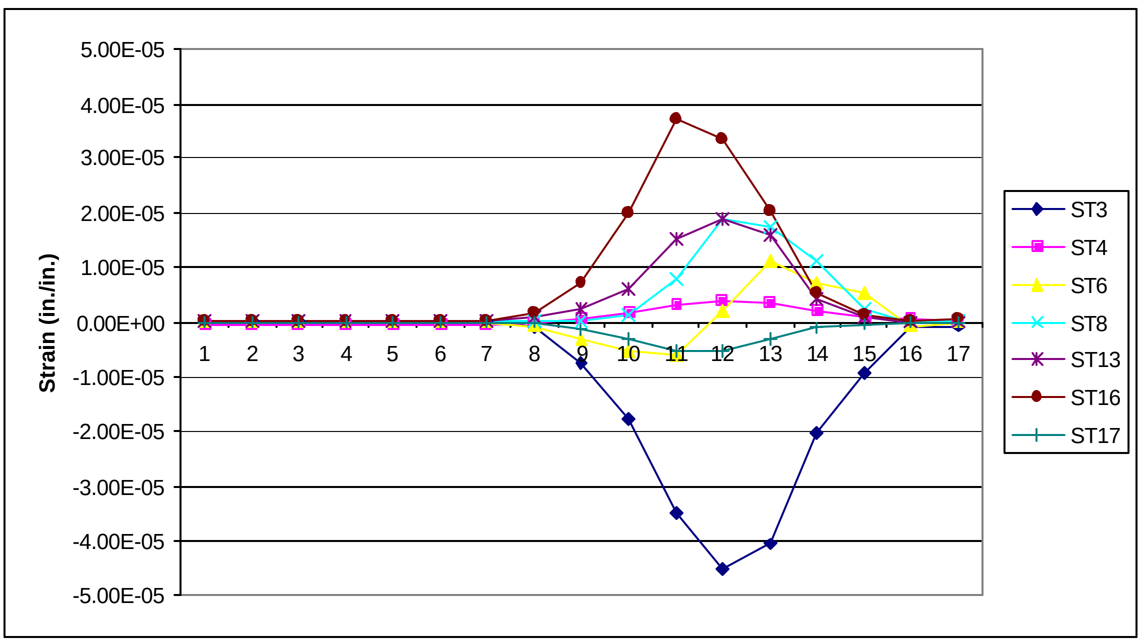

Figure 6-10. Deck Girder 2 Strain from Path 4W

Table 6-3. Moment Values (in k-ft) for Deck Girders 1 and 2

Load Path	Girder 1		Girder 2	
	End	Mid-Span	End	Mid-Span
1E	-277.47	527.71	-494.00	531.60
1W	-182.82	417.50	-434.35	522.52
4E	-704.04	661.25	-635.32	461.58
4W	-613.28	626.25	-586.05	479.73

6.4 Distribution Factors

The distribution factors of transverse load to longitudinal members are determined using the deck girder spacing and the number of design lanes loaded. The distribution factors shown in Tables 6-4 and 6-5 are the transverse distributions at the quarter point of the bridge, a location used because some of the instruments at the center line produced erroneous results for Paths 3 and 5.

The LRFD and LFD design distribution factors were calculated according to the AASHTO specifications. The distribution factors from the test data were calculated using the equation (Equation 6-1) developed by Stallings and Yoo. The values in Table 6-4 were calculated using 2 (n = 2) wheel lines (representing one truck loading the bridge), to reflect the actual loading condition during the tests.

$$DF_i = \frac{ne_i}{\sum_{j=1}^{k} e_j w_j} \qquad (6\text{-}1)$$

where:

n – number of wheel lines (1 trucks x 2 wheel lines = 2 wheel lines)
e_i – strain at the bottom of the ith girder
w_j – ratio of the section modulus ratio of the jth girder to the section modulus of typical interior girder
k – number of girders

Table 6-4. Distribution Factors at the Quarter-Line of Bridge Using 2 Wheel Lines

	Test Data		LFD		LRFD	
	Interior	Exterior	Interior	Exterior	Interior	Exterior
1E	0.52	0.77	1.08	1.16	0.70	0.65
1W	0.58	0.60				
2E	0.78	0.26				
2W	0.73	0.33				
3E	0.75	0.37				
3W	0.69	0.47				
4E	0.50	0.95				
4W	0.48	0.85				
5E	0.67	0.65				
5W	0.54	0.74				

The LRFD values are much closer to the calculated values in Table 6-4, which correlates to the LRFD method used to design this bridge, suggesting that the 2 wheel-line approach is more accurate for newly designed bridges. The predicted values of the interior deck girder compare very closely to the values for Path 2. The test data shows that Path 2 controls the design of the interior deck girder according to the LRFD method.

The predicted values of the exterior deck girder correlate well with the values from Paths 4 and 5 in Table 6-4. The test data shows that the design for the exterior deck girder is controlled by load Path 4. The graph in Figure 6-11 shows that the interior deck girder does carry a higher amount of strain (see Appendix C for instrument layout) than the interior deck girders for Path 2. Similarly, the graph in Figure 6-12 shows that the exterior deck girder does indeed receive higher strain values from Path 4.

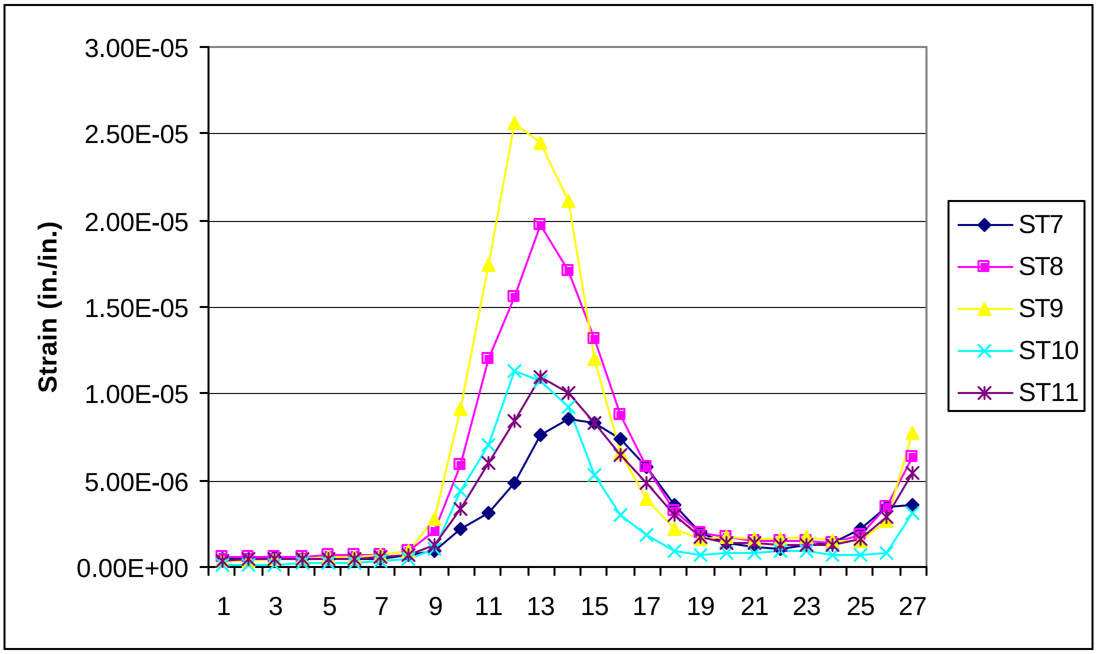

Figure 6-11. Strain Readings at the Quarter-Points on Path 2 West

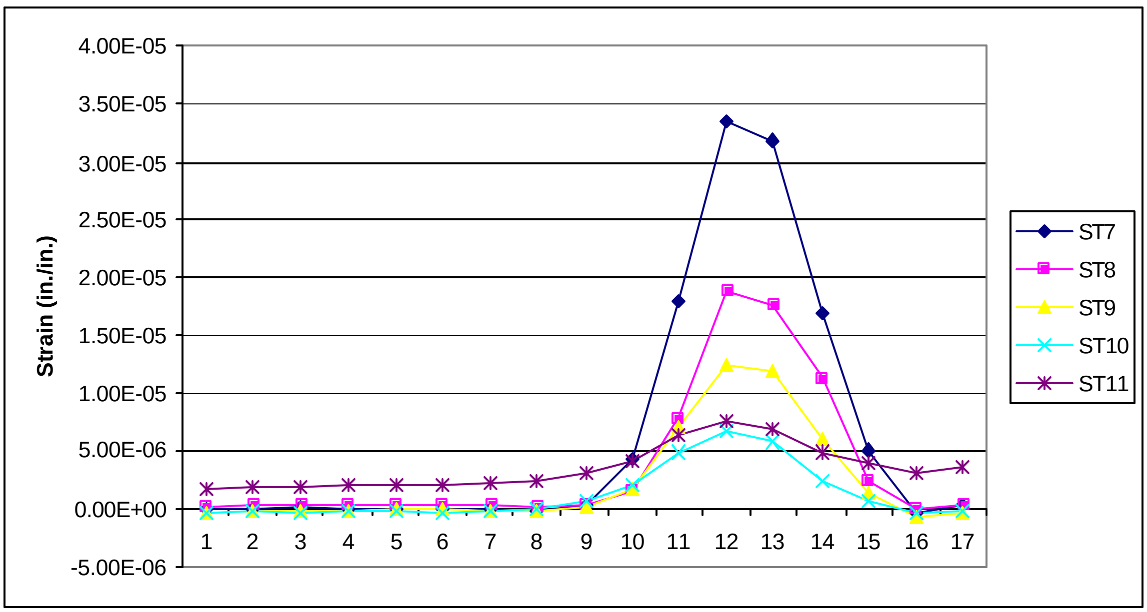

Figure 6-12. Strain Readings at the Quarter-Points on Path 4 West

6.5 End Fixity Investigation

The evidence of negative moment in the girders raised interest. This was first investigated in Chapter 3 using ANSYS. In addition, to validate this finding, SAP2000™ was used to produce a model in order to try and determine just how much fixity was present at the integral end bents. The SAP2000™ model was used to produce models with three different constraints. The types of constraints used were pinned-pinned, fixed-fixed, and the last one contained a rotational spring attached at both ends of the deck girder. The stiffness given by the integral end bent was calculated using Equation 6-2 and used for the stiffness of the rotational springs. To calculate the moment of inertia, the tributary width of one single deck girder was used for "b" and the depth parallel to the deck girder length was used for "h".

$$k = \frac{EI}{L} \qquad (6\text{-}2)$$

where:

k – spring constant (kip-ft)

L – height of the integral end bent (ft)

E – modulus of elasticity of the concrete (ksf)

I – moment of inertia calculated for integral end bent (ft.^{4}) $\left(I = \frac{bh^3}{12} \right)$

The same loading condition shown in Figure 6-4 was used for this model as well. The results at mid-span of each run are shown in Table 6-5. When comparing these results to the actual testing data, the moment values are significantly close. The SAP2000™ model does not include all five deck girders acting together; it was run using only a single representative deck girder. The deflections produced in SAP2000™ are greater than the maximum deflection created during the testing. This again could be due to the use of only a single deck girder in SAP2000™ compared to the five actual deck girders in the field. Furthermore, the SAP2000™ model did not include the diaphragms or parapet walls which contribute to the stiffness of the entire system as well. To be able to determine the stiffness of the integral end bent one would need to understand the soil interaction of the integral end bent wall. A geotechnical expert was consulted on this issue and there is not much information on this topic available to designers and researchers.

Table 6-5. Results of SAP2000™ Model with Different Constraints

Constraint Type	Pinned-Pinned	Fixed-Fixed
Shear (kips)	26.4	26.9
Moment (k-ft)	1,077.1	-653.5
Deflection (in.)	0.8	0.185

6.6 Girder Displacements, Diaphragm and Plate Connection Stresses

The layout of the instruments was designed to determine the transverse loading effects as well as the longitudinal effects along the girders. The results from the strain gages were used to calculate the stress values in the diaphragms and plates. The results of the maximum strain in each diaphragm due to each load path are shown in Table 6-6. The results show that each diaphragm carried a small amount of moment, but primarily transferred axial load (with some inconsistency). This could have been a result of the diaphragm connections not being tightened according to specifications during the construction of the bridge.

The graphs in Figures 6-13 through 6-15 show that the diaphragms contain very little moment. Table 6-6 also shows that diaphragm D3 only experienced compression during Paths 1 and 4, which may be a result of the loading being located directly above the diaphragm. The maximum strain (D6) occurred in Path 2. Path 2 also showed higher strains in other diaphragms as well. This finding suggests that Path 2 controlled the design of the diaphragms. A representation of the axial loads transferred by the diaphragms is shown in Figures 6-16 and 6-17.

Table 6-6. Maximum Diaphragm Strain (µe)

Diaphragm	SG	Load Path									
		1E	1W	2E	2W	3E	3W	4E	4W	5E	5W
D1	5	25.5	23.0	42.4	-3.7	-5.0	-4.9	13.3	13.5	-6.0	2.5
	10	22.6	35.2	-2.4	37.1	-13.6	-16.1	4.4	7.4	-18.2	21.8
D2	11	22.1	29.3	34.9	30.7	-10.1	-13.9	8.8	5.5	-14.1	-16.0
	12	36.7	28.9	37.1	33.7	-10.9	-13.7	6.8	4.3	-13.6	-15.1
	14	-18.5	22.1	31.5	33.6	40.8	37.3	-21.0	-21.8	19.7	17.7
D3	15	-18.7	-16.8	23.0	30.2	38.6	38.0	-18.6	-16.2	18.0	17.0
	16	-20.0	-17.2	24.4	31.6	43.3	41.5	-18.6	-19.1	21.7	20.6
	18	-73.0	-69.5	19.2	28.4	26.8	26.6	-53.6	-56.8	23.8	23.2
D5	25	31.6	31.0	1.3	-2.8	-5.4	-6.3	21.1	20.9	-4.9	-5.0
	27	28.9	26.7	-3.3	-6.5	-9.0	-9.5	19.3	19.5	-8.1	-7.0
	28	34.6	31.1	-3.2	-7.7	-14.0	-15.5	20.9	24.5	-11.4	-12.6
D6	29	40.3	50.6	60.1	55.7	-19.4	-28.1	8.1	12.4	-36.5	-33.5
	31	21.5	34.1	35.8	29.8	-8.5	-10.3	5.0	6.1	-14.4	-11.7
	32	46.3	61.6	76.2	71.8	-17.3	-28.6	5.9	8.9	-40.0	-38.6

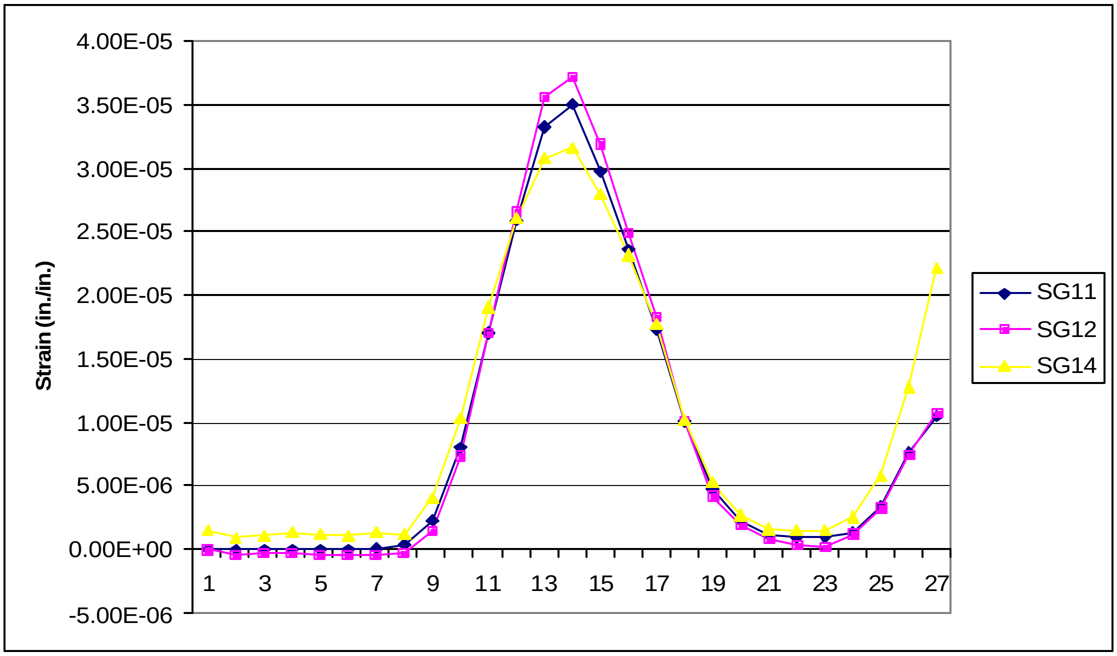

Figure 6-13. Strains in D2 for Path 2 East

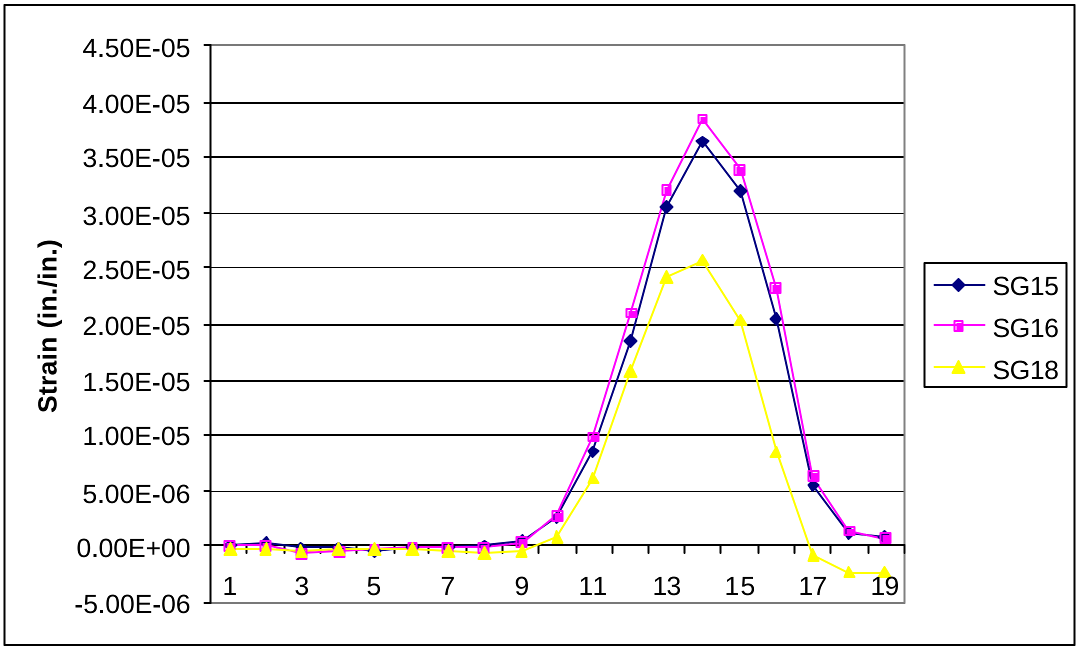

Figure 6-14. Strains in D3 for Path 3 West

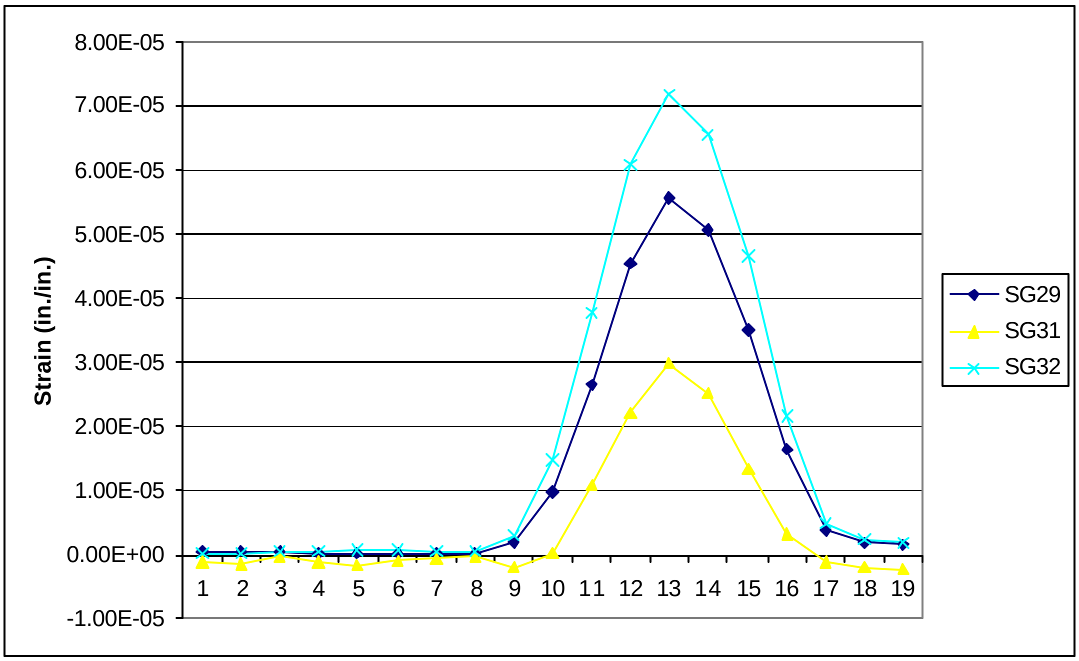

Figure 6-15. Strains in D6 for Path 2 West

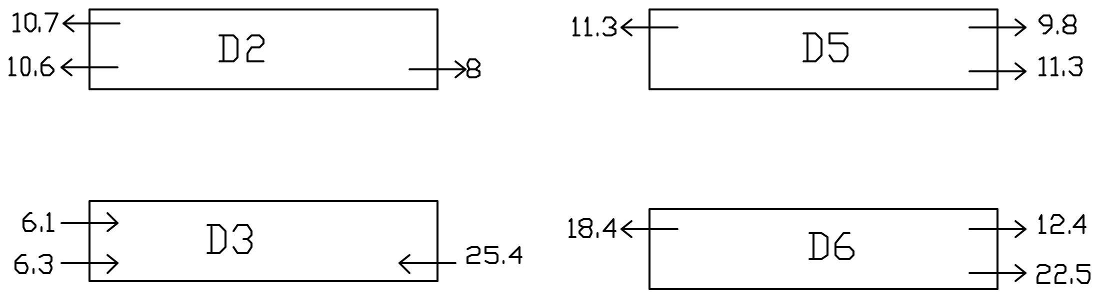

Figure 6-16. Diagram of Axial Forces in Diaphragms (kips) for Path 1 West

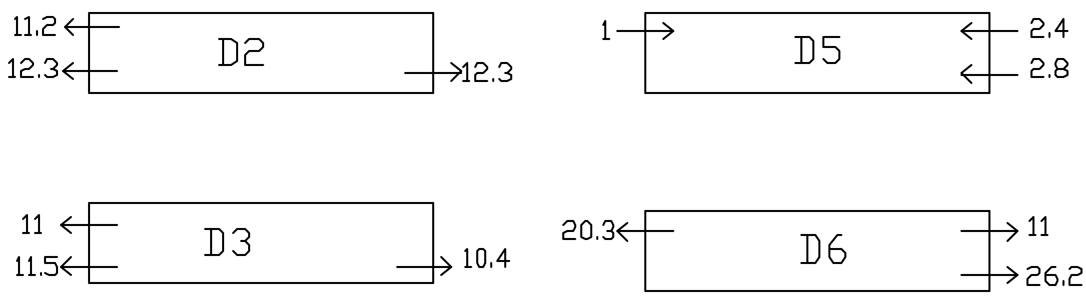

Figure 6-17. Diagram of Axial Forces in Diaphragms (kips) for Path 2 West

The plate connections were instrumented in order to measure transverse strain (see Appendix C). Each plate instrumented had two strain gages as shown in Figure 6-2. The strains due to each load path are shown in Table 6-7. The graph in Figure 6-18 shows the strain values for the two plates, P4 and P8. Values for plates P4 and P8 show that one side of the plate is in compression and the opposite side is in tension. This suggests that there was some moment occurring in the plates, in addition to an axial force.

Plate P8 experiences moment in Paths 1, 2, and 4, while plate P4 experiences moment from Paths 2, 3, and 5. Values from Path 2 produced moment throughout the load duration in the two plates in question. Path 1 generated the highest strain in Plate P4 because the wheels were located directly above this line of plates for this particular loading path. Plate P8 experienced higher strain in Path 2 because it was located closer to the wheel path for the loading configuration. The other plates listed in the table only show one reading because the other instruments that were attached to these plates did not survive the construction process.

Table 6-7. Flange Connection Plate Strains (με)

Load Path	P5	P1	P2	P3	P7	P4		P8	
	2	4	8	22	24	33	34	35	36
1E	-217.5	-41.6	32.2	-81.6	-57.3	-108.4	-163.2	17.3	-70.0
1W	-45.2	104.3	37.7	-80.0	-93.0	-96.1	-130.6	102.2	-57.5
2E	35.2	-93.5	37.3	14.8	-130.0	17.4	-95.7	98.1	-51.4
2W	74.5	-86.5	26.4	24.6	-124.2	25.5	-67.2	140.0	-41.0
3E	27.0	22.3	-107.4	24.0	-10.6	27.4	-47.6	90.5	56.3
3W	39.5	24.5	10.0	24.3	3.7	27.0	-47.0	103.0	59.4
4E	-163.6	5.9	26.2	-61.0	-11.2	-71.2	-131.0	24.7	-19.1
4W	-90.0	-2.2	-77.5	-62.8	-11.3	-75.6	-137.0	32.2	-18.7
5E	33.3	23.2	-11.8	21.6	3.5	24.2	-20.7	90.1	57.4
5W	35.2	16.2	-7.7	22.8	4.0	24.0	-14.0	91.2	52.5

(-) compression
(+) tension

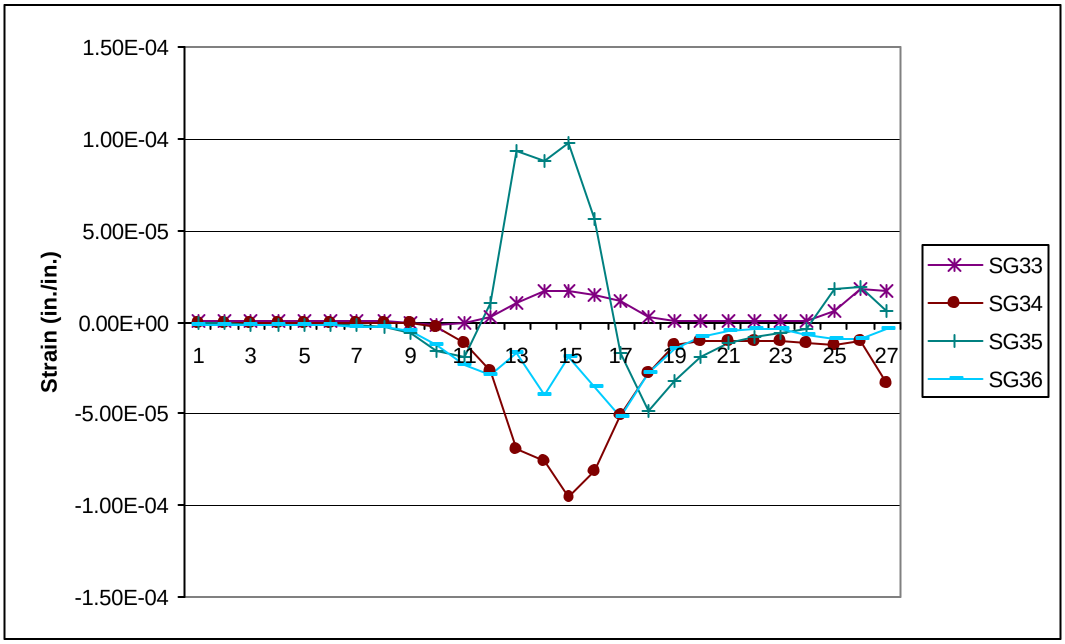

Figure 6-18. Plate Strains From Path 2 East

The maximum displacements from each load path are shown in Table 6-8. The deflections from the load testing are very small compared to the deflection limit of L/800 used in the design calculations. This could be a result of the deck girders having a higher stiffness than designed due to the integral end bent, asphalt overlay, and concrete parapet wall. The displacements at mid-span are shown in Table 6-9. The instrument for deck girder 1 was omitted because it produced erroneous data. This table shows that, as expected, each deck girder that was located beneath the corresponding load deflected more than the other girders away from the loaded area. The graph in Figure 6-19 shows the deflections along deck girder 2 for Path 1 East. The overall maximum deck girder deflection of 1/8" is well below the design limits.

Table 6-8. Deck Girder Displacements (Inches)

DT #	Path									
	1E	1W	2E	2W	3E	3W	4E	4W	5E	5W
1	0.026	0.020	0.002	0.001	0.007	0.003	0.035	0.037	0.006	0.003
3	0.060	0.060	0.014	0.006	0.002	0.001	0.094	0.098	0.002	0.002
4	0.050	0.050	0.040	0.024	0.001	0.000	0.045	0.032	0.000	0.000
5	0.040	0.050	0.073	0.078	0.057	0.057	0.029	0.030	0.040	0.039
6	0.001	0.016	0.000	0.050	0.009	0.020	0.000	0.004	0.009	0.013
7	0.007	0.010	0.002	0.024	0.012	0.021	0.024	0.001	0.049	0.041
8	0.005	0.015	0.001	0.002	0.002	0.004	0.029	0.053	0.000	0.001
9	0.080	0.090	0.066	0.067	0.004	0.005	0.080	0.083	0.005	0.002
11	0.124	0.110	0.085	0.074	0.004	0.009	0.105	0.108	0.003	0.002
12	0.033	0.040	0.050	0.050	0.040	0.039	0.004	0.007	0.009	0.033
13	0.002	0.017	0.035	0.074	0.078	0.080	0.000	0.002	0.079	0.079
14	0.000	0.002	0.000	0.053	0.006	0.019	0.000	0.006	0.033	0.027
16	0.074	0.072	0.050	0.050	0.009	0.009	0.071	0.072	0.000	0.000

Table 6-9. Displacements at Mid-Span (inches)

Girder #	Load Path					
	1E	1W	2E	2W	4E	4W
2	**0.124**	0.110	0.085	0.074	0.105	0.108
3	0.033	0.040	0.050	0.050	0.004	0.007
4	0.002	0.017	0.035	0.074	0.001	0.002
5	0.001	0.002	0.001	0.053	0.001	0.006

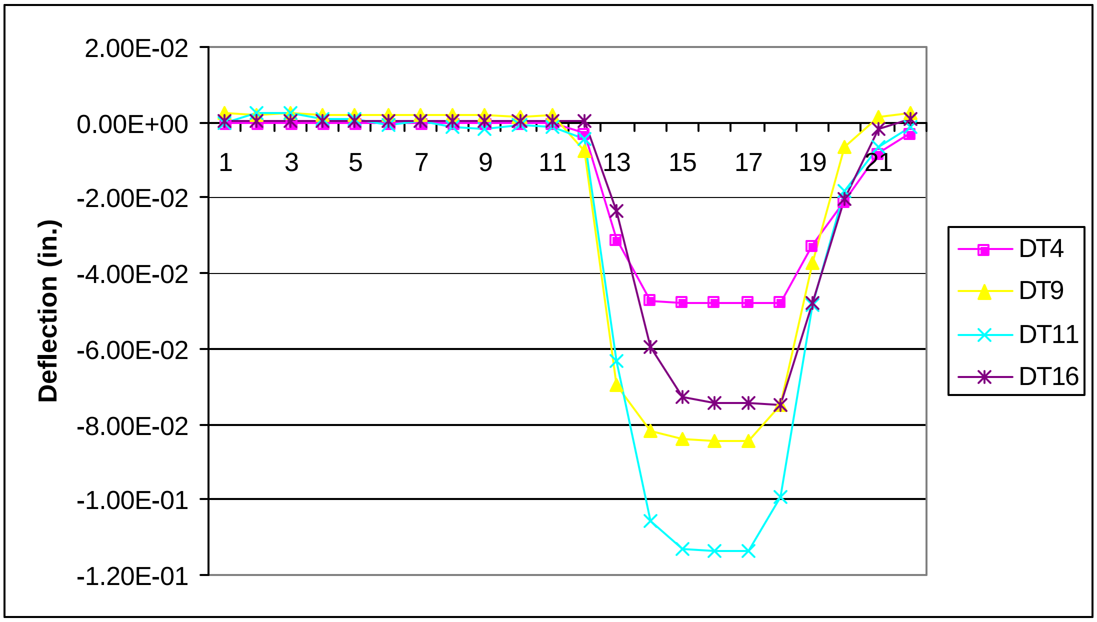

Figure 6-19. Deflections in Deck Girder 2 from Load Path 1 East

6.7 Impact Factors

For design purposes, AASHTO specifies an impact factor. This factor is applied to increase the live load effects on the bridge, by including dynamic and vibratory impact effects. In this research, the results from the dynamic loading condition produced information that was later used to calculate the impact factor for the bridge. The results summarized in Table 6-11 are the impact factors calculated from Paths 1, 2, and 3 in both directions, using a single loading vehicle. The impact factors were calculated using Equation 6-3. The table also shows that the actual impact factors are close to the calculated AASHTO values. The graphs associated with the results in Table 6-10 for the East direction are shown in Figures 6-20 through 6-25, where the horizontal axis is a DAQ generated reference number. It is clear from these figures that during the dynamic testing, a significantly larger amount of strain data was needed to capture peak strain readings.

$$\frac{\sum_{n=1}^{\infty}(e_{n_{dynamic}} \div e_{n_{slow}})}{N} \qquad (6\text{-}3)$$

where:

$e_{n_{dynamic}}$ – strain reading from the nth instrument of the dynamic loading

$e_{n_{slow}}$ – strain reading from the nth instrument of the baseline reference loading

n – instrument number

N – total number of instruments used

Table 6-10. Impact Factors for Both East and West

<table>
<tr><th>Load Path</th><th>Test Data</th><th>LRFD</th></tr>
<tr><td>1E</td><td>0.73</td><td rowspan="6">1.30</td></tr>
<tr><td>1W</td><td>1.13</td></tr>
<tr><td>2E</td><td>1.10</td></tr>
<tr><td>2W</td><td>1.03</td></tr>
<tr><td>3E</td><td>1.30</td></tr>
<tr><td>3W</td><td>1.02</td></tr>
</table>

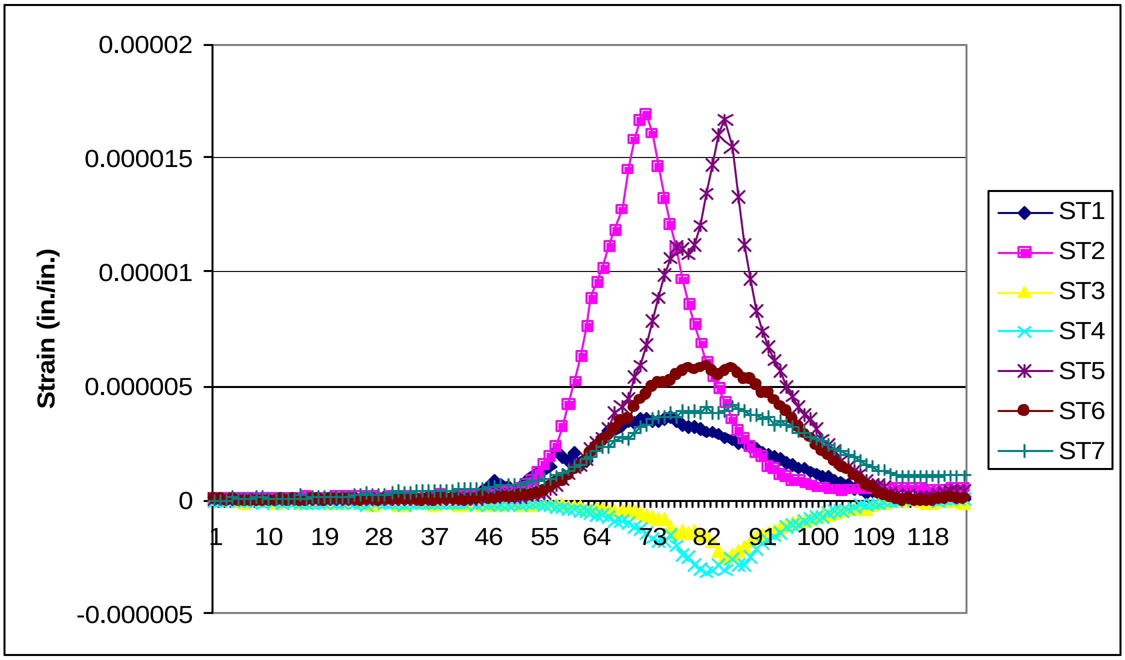

Figure 6-20. One Truck (Slow) Loading Strains for Path 1E

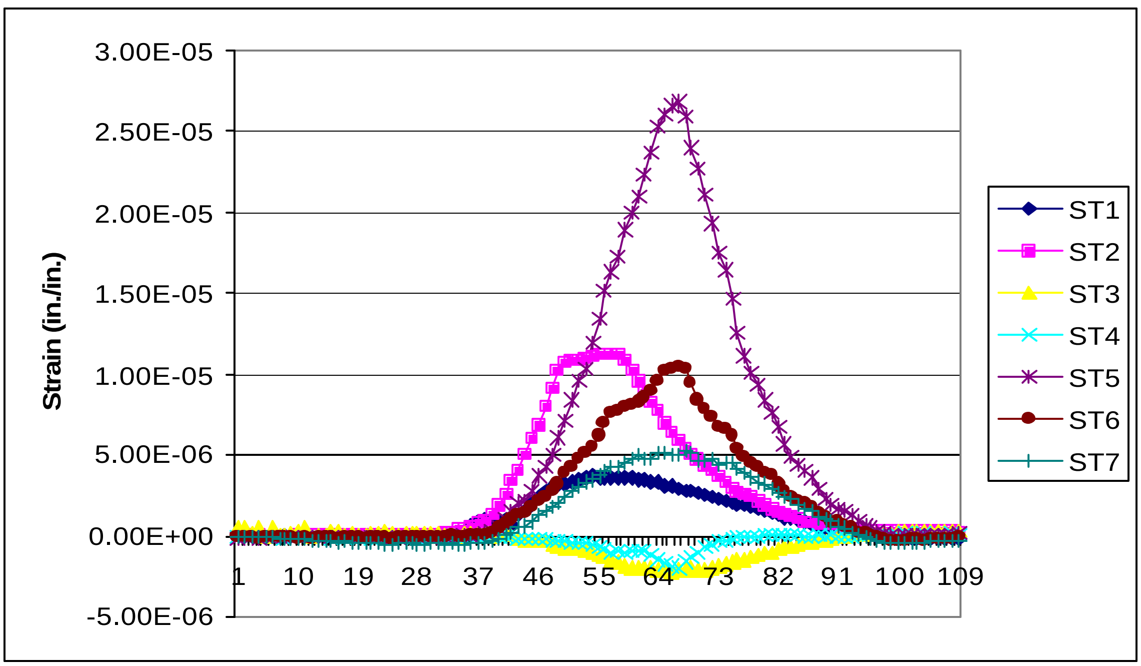

Figure 6-21. One Truck (Slow) Loading Strains for Path 2E

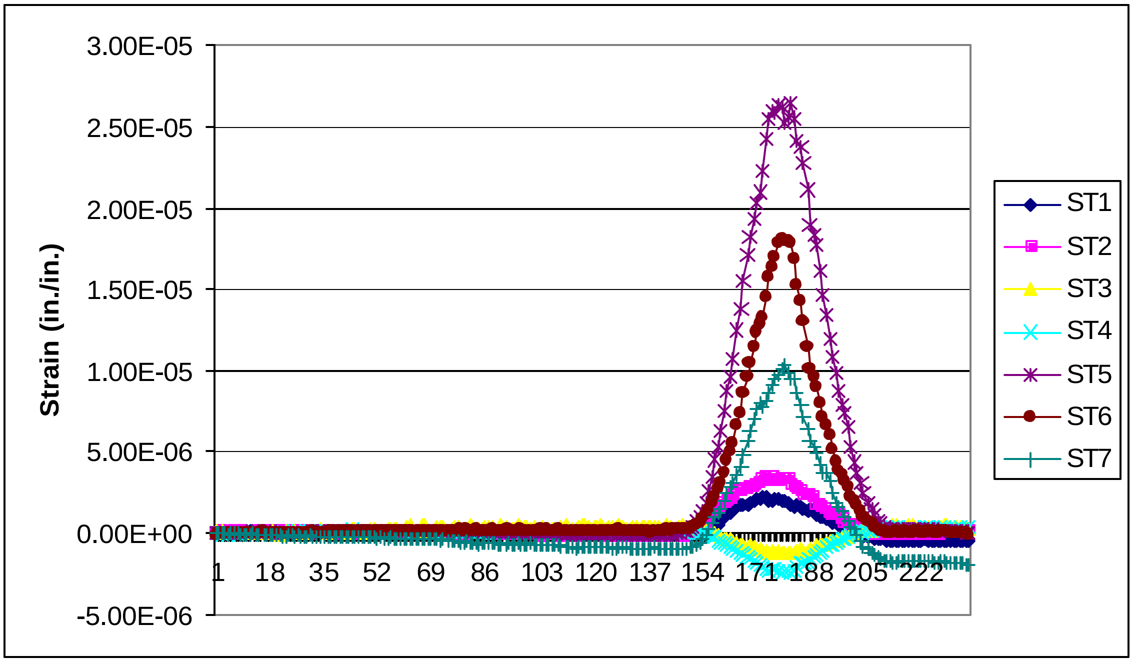

Figure 6-22. One Truck (Slow) Loading Strains for Path 3E

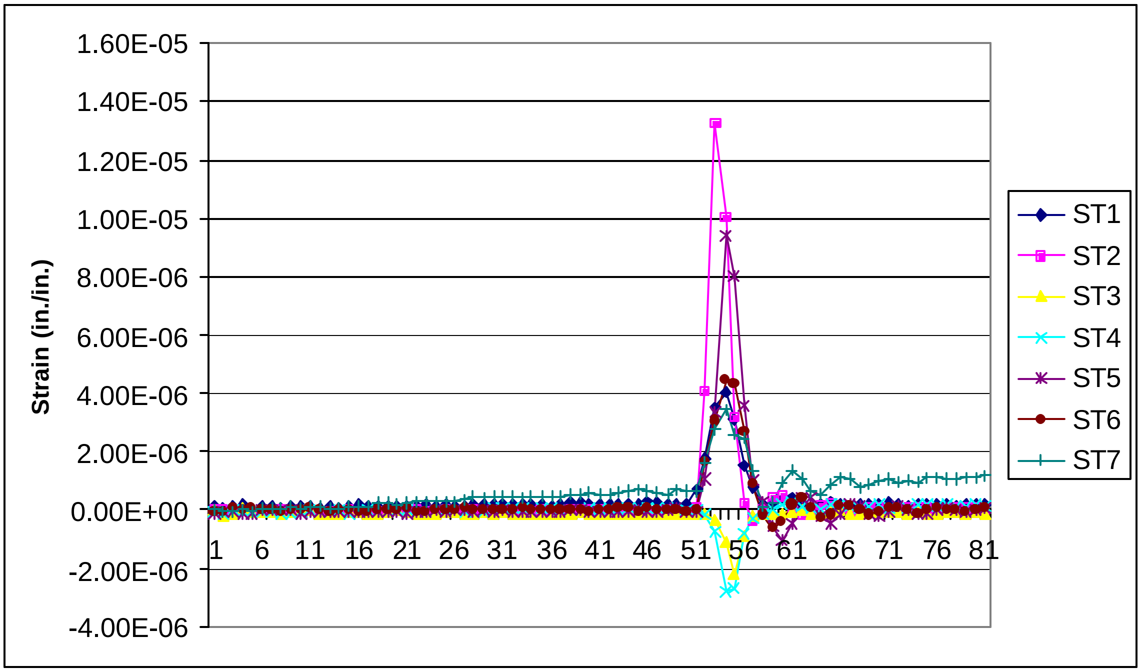

Figure 6-23. Dynamic Loading Strains for Path 1E

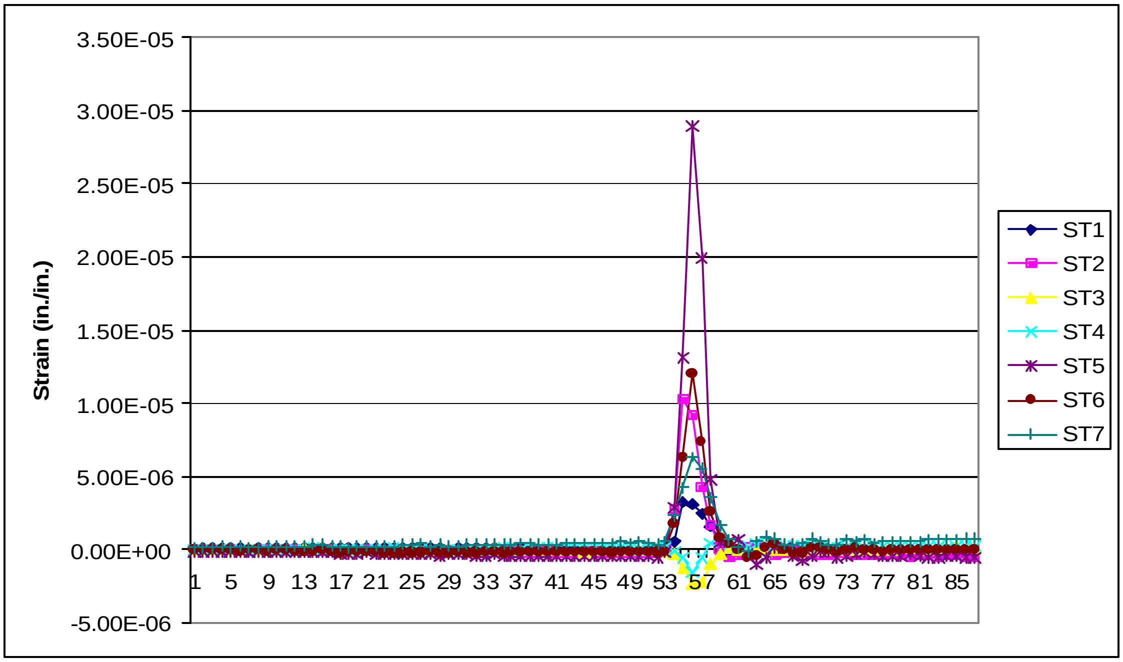

Figure 6-24. Dynamic Loading Strains for Path 2E

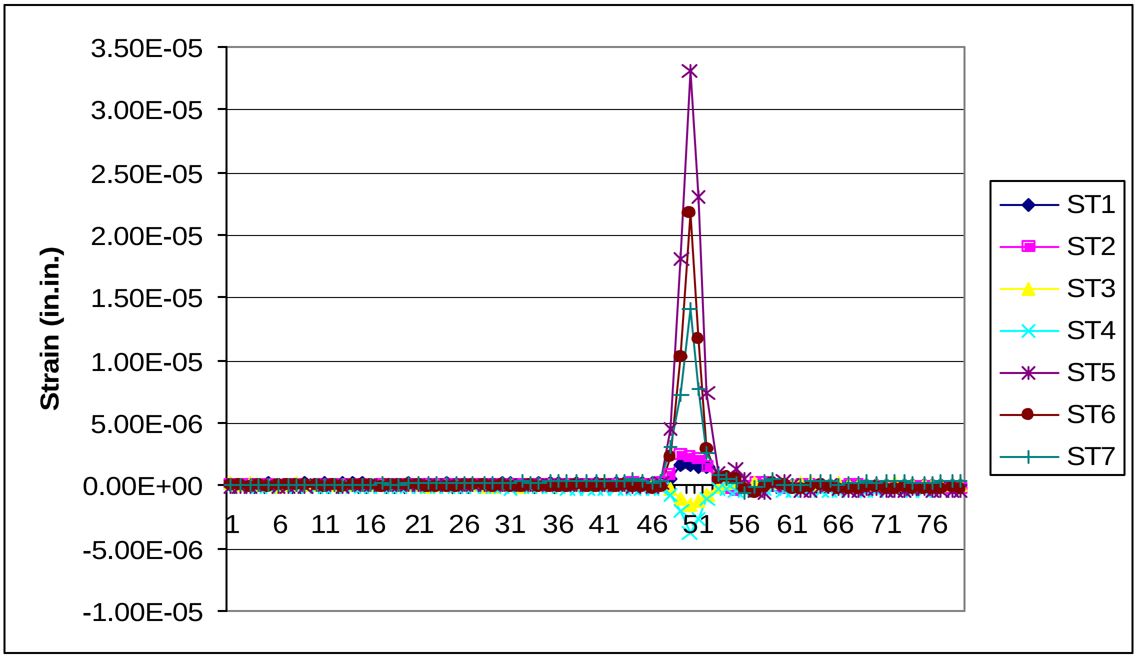

Figure 6-25. Dynamic Loading Strains for Path 3E

7 Comparison of Analytical and Experimental Studies

7.1 Girder Stresses and Deformation

The deck girder normal stress values that were recorded during the load test were compared to the values obtained from the ANSYS™ and Larsa™ models. The stress values were taken at mid-span on the bottom extreme fiber of each of the five fixed-end deck girders. These values were found to be very similar. The FE and Larsa™ models consistently predicted slightly larger stress values on all three load paths. This difference could be attributed to the parapet wall or imperfections in the path that the truck traveled as the load test was being conducted. The asphalt overlay also provides slightly more distribution of the tire load on the actual bridge surface. The comparisons from all three load paths are shown in Figures 7-1 through 7-3.

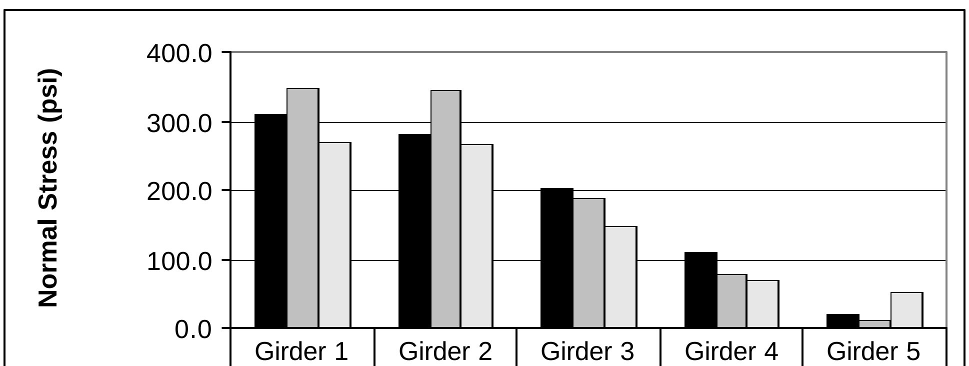

	Girder 1	Girder 2	Girder 3	Girder 4	Girder 5
LARSA™	311.0	281.0	202.0	110.0	20.0
ANSYS™	349.0	344.0	189.0	77.0	11.0
Load Test	270.0	267.0	147.0	69.0	51.0

Figure 7-1. Normal Stress at Mid-Span Path 1

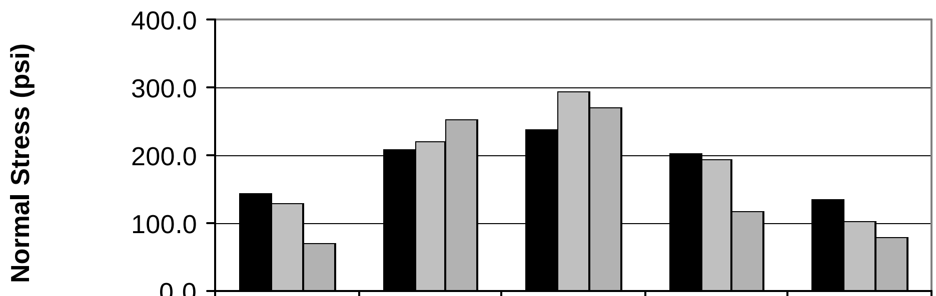

	Girder 1	Girder 2	Girder 3	Girder 4	Girder 5
LARSA™	143.0	209.0	237.0	203.0	134.0
ANSYS™	130.0	222.0	294.0	195.0	102.0
Load Test	70.0	253.0	270.0	118.0	80.0

Figure 7-2. Normal Stress at Mid-Span Path 2

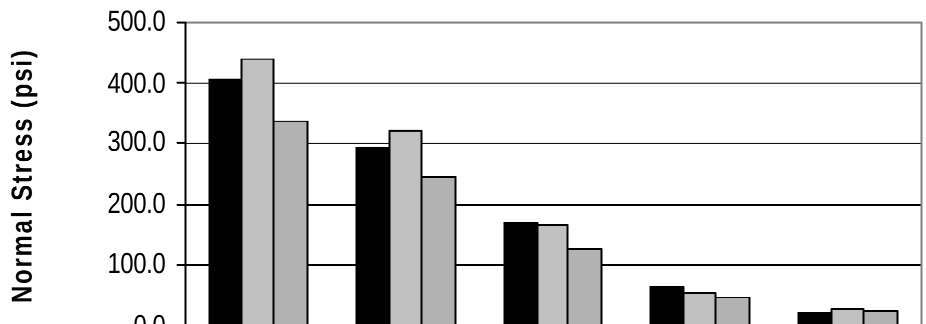

	Girder 1	Girder 2	Girder 3	Girder 4	Girder 5
LARSA™	406.0	293.0	170.0	67.0	20.0
ANSYS™	439.0	323.0	165.0	55.0	29.0
Load Test	338.0	245.0	127.0	48.0	24.0

Figure 7-3. Normal Stress at Mid-Span Path 4

The value of the vertical displacement at mid-span of the five deck girders was also compared (see Figures 7-4 to 7-6). Deck girder one is omitted due to an instrument error. The simply supported FE model resulted in very large displacements, but the fixed area ANSYS™ model and the fixed node Larsa™ model calculated the values within one tenth of an inch on average. The Larsa™ model generally predicted the displacement with a higher degree of accuracy than the ANSYS™ model. The small difference can probably be attributed to the moving load feature in the Larsa™ program. The ANSYS™ FE program does not have this feature, thus the truck can only be centered about the mid-point of the deck girder. This difference could cause a small variance in the maximum displacement at mid-span.

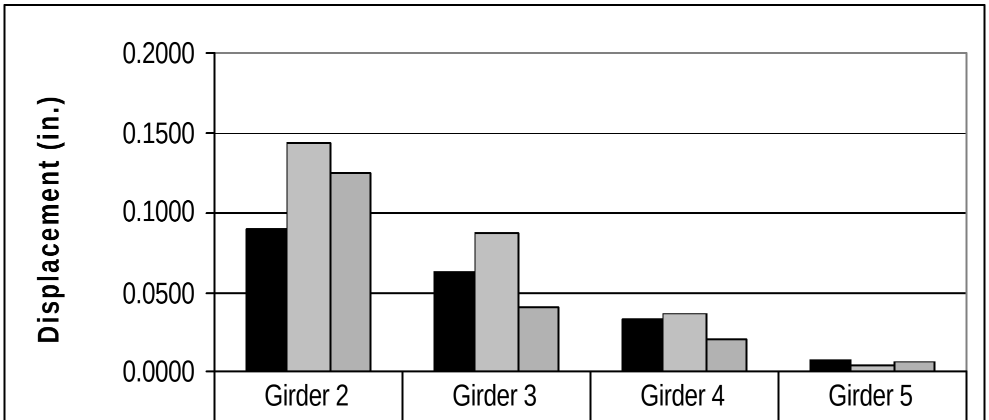

	Girder 2	Girder 3	Girder 4	Girder 5
LARSA™	0.0900	0.0630	0.0340	0.0070
ANSYS™	0.1430	0.0867	0.0360	0.0050
Load Test	0.1250	0.0400	0.0200	0.0060

Figure 7-4. Vertical Displacement at Mid-Span Path 1

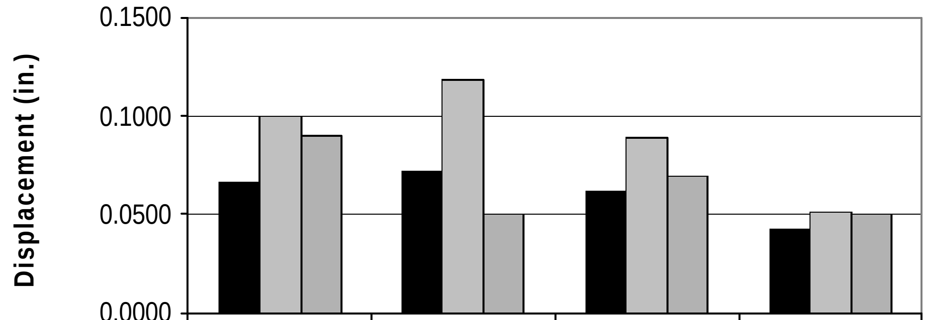

	Girder 2	Girder 3	Girder 4	Girder 5
LARSA™	0.0660	0.0720	0.0620	0.0420
ANSYS™	0.1000	0.1190	0.0890	0.0510
Load Test	0.0900	0.0500	0.0700	0.0500

Figure 7-5. Vertical Displacement at Mid-Span Path 2

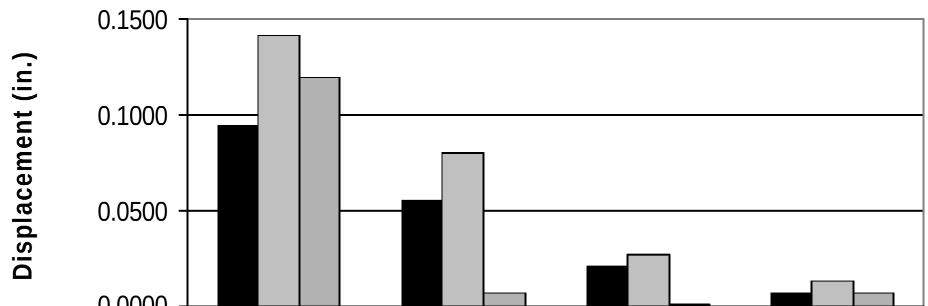

	Girder 2	Girder 3	Girder 4	Girder 5
LARSA™	0.0950	0.0550	0.0210	0.0060
ANSYS™	0.1410	0.0800	0.0270	0.0130
Load Test	0.1200	0.0070	0.0010	0.0060

Figure 7-6. Vertical Displacement at Mid-Span Path 4

The deck girder stresses were also used to find the distribution factors for the interior and exterior girders. The distribution factors from the load test portion of this paper were computed using the same truck path in two opposite directions. These two values were averaged and compared to the three ANSYS™ truck paths (see Figures 7-7 through 7-10). The ANSYS™ model distribution was found to be very similar to the actual load test when the two wheel line method was used. The four wheel line method proved to have a larger difference in distribution. The difference in distribution could be caused by the slope of the bridge or the higher stiffness that was apparent in the displacement and stress comparisons discussed earlier in this chapter.

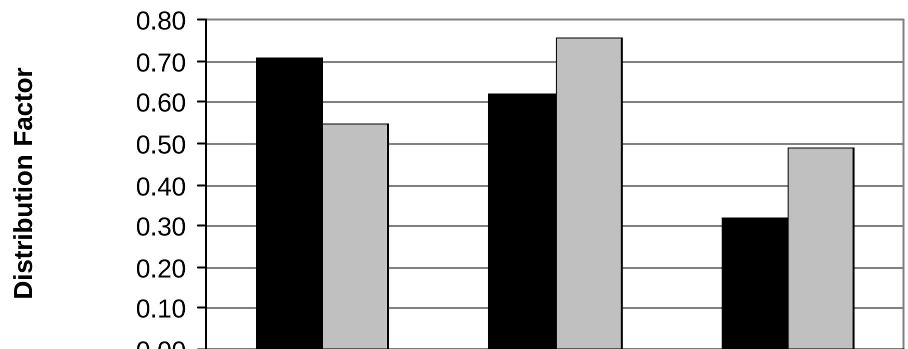

	Path 1	Path 2	Path 4
ANSYS™	0.71	0.62	0.32
Load Test	0.55	0.76	0.49

Figure 7-7. 2 –Wheel Lines Distribution Factor for Interior Deck Girder Paths

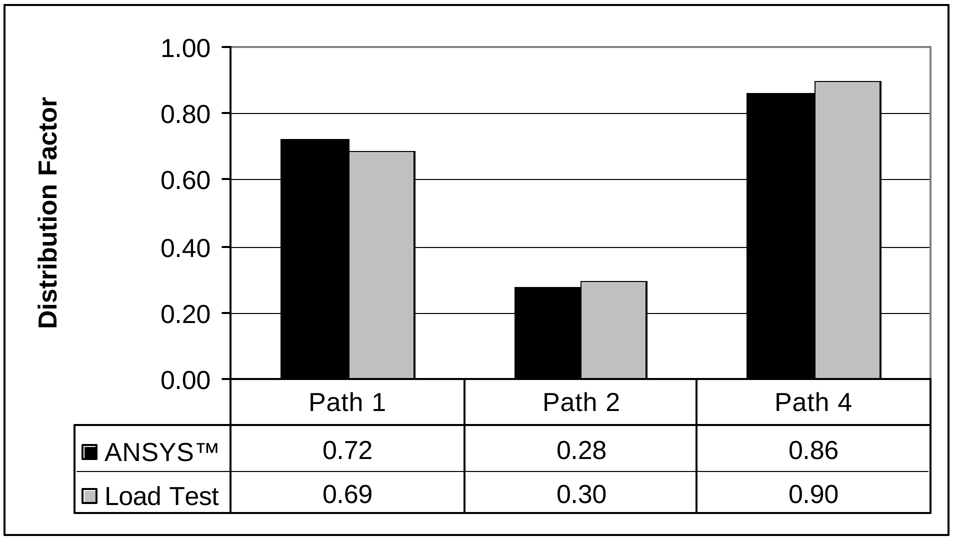

Figure 7-8. 2 –Wheel Lines Distribution Factor for Exterior Deck Girder Paths

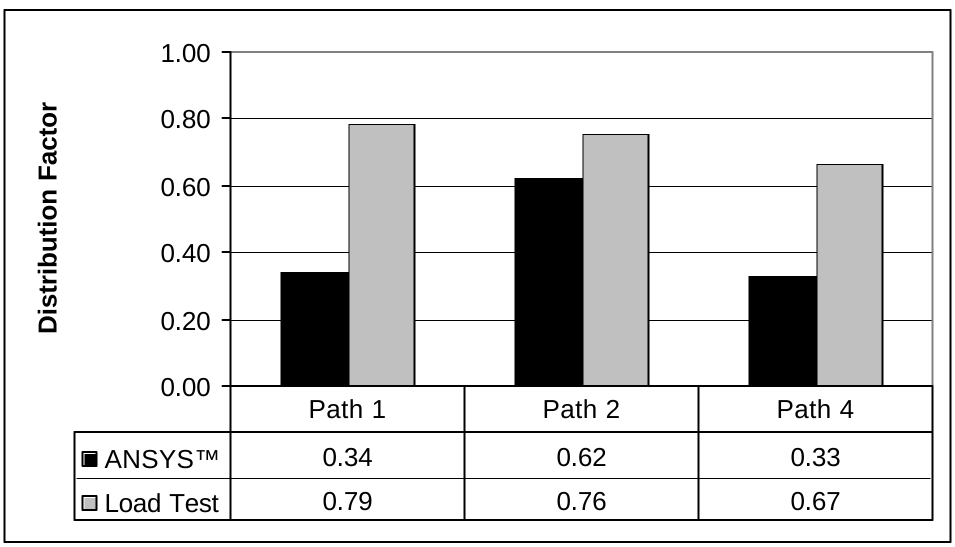

Figure 7-9. 4 –Wheel Lines Distribution Factor for Interior Deck Girder Paths

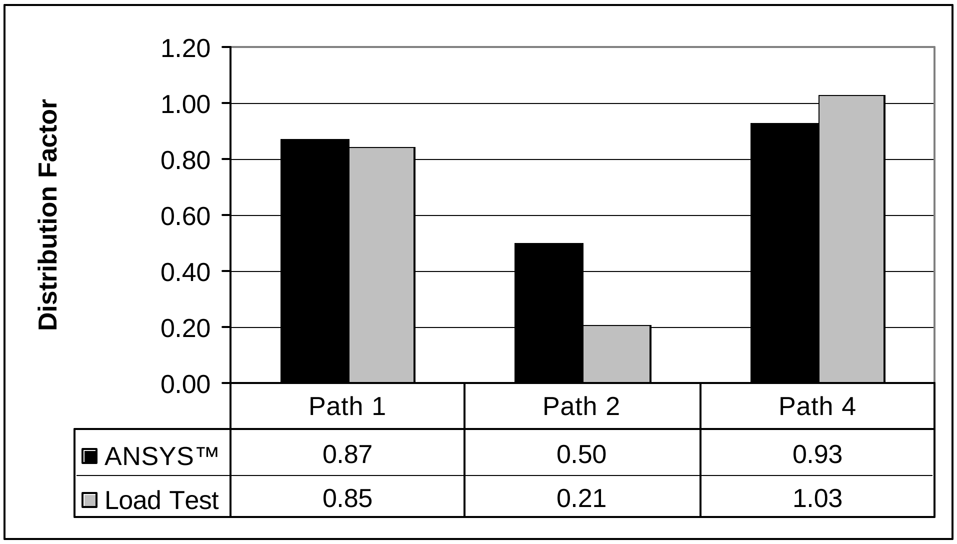

Figure 7-10. 4 –Wheel Lines Distribution Factor for Exterior Deck Girder Paths

7.2 Plate Stresses

The plates that were instrumented during the actual load test were mainly in one quadrant of the bridge. The maximum plate stresses that were obtained were the maximum transverse stress value as the truck crossed the entire bridge. The ANSYS™ model plate stress values were observed when the truck caused near maximum displacement and stress values in the deck girders. The maximum plate stress in the transverse direction (perpendicular to traffic) that was computed by ANSYS™ versus the maximum load test stress value is shown in Figures 7-11 and 7-12.

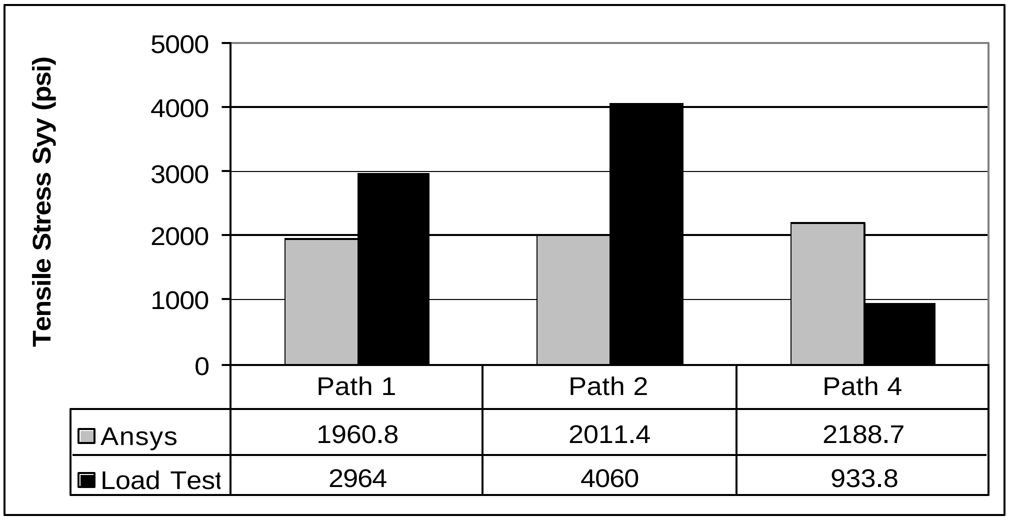

	Path 1	Path 2	Path 4
Ansys	1960.8	2011.4	2188.7
Load Test	2964	4060	933.8

Figure 7-11. Maximum Transverse Tensile Plate Stress

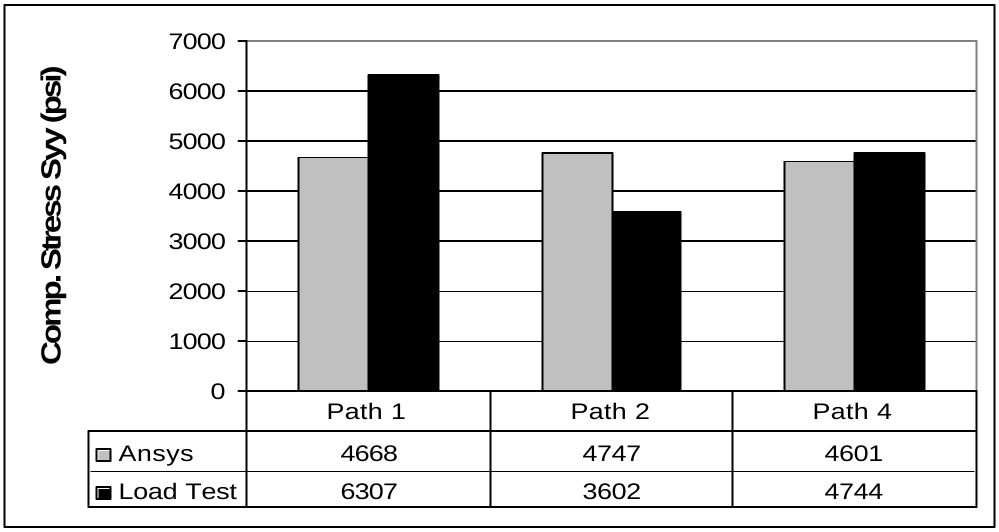

	Path 1	Path 2	Path 4
Ansys	4668	4747	4601
Load Test	6307	3602	4744

Figure 7-12. Maximum Transverse Compressive Plate Stress

The maximum principal stress that occurred in any plate, when the deck girder stress was largest, is shown in Figure 7-13. The principal stress was not measured in the actual load test but was computed in the ANSYS™ model.

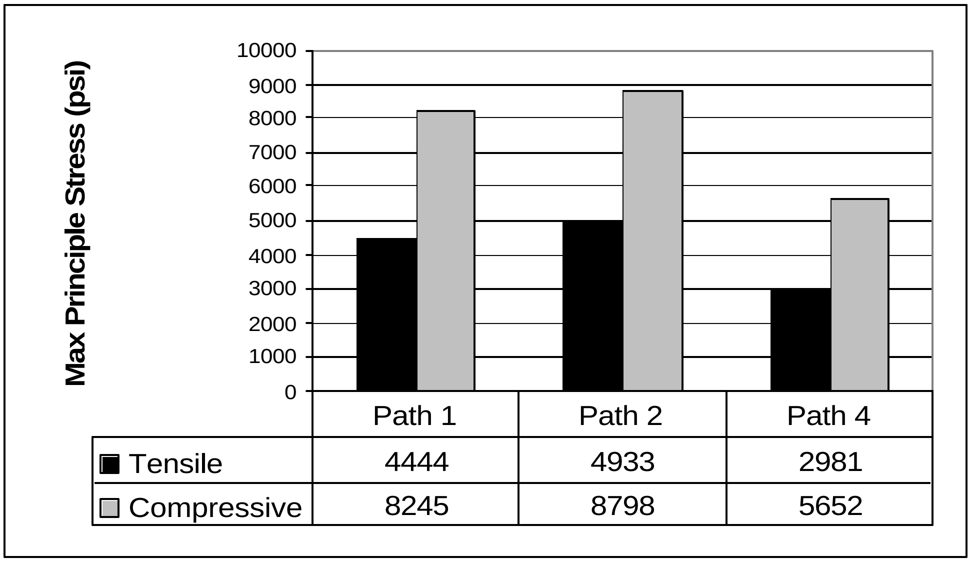

Figure 7-13. Maximum Principal Plate Stress

The load test resulted in higher transverse plate stresses than the ANSYS™ model computed. The highest tensile transverse stress observed in the load test was found to be approximately 4,000psi. The largest corresponding stress computed in ANSYS™ was approximately 3,000psi. This difference is probably attributed to the fact that the ANSYS™ model was only loaded at mid-span to maximize deck girder effects. The maximum plate stress may not occur when the truck load is at this location. The diaphragms in the ANSYS™ model were also attached to the deck girders with a rigid connection that was not entirely achieved in the actual bridge construction. This implies that the diaphragms may have transmitted more of the live load in the ANSYS™ model when the truck was in the position that caused the maximum plate stress.

The maximum transverse compressive stress was found to be larger in the actual load test. The difference in the maximum compressive stress was found to be 1,600psi. This difference could also be contributed to the position of the FE model truck load versus the moving readings that the load test recorded. The maximum plate stresses were found to be half of the ultimate stress that would cause failure in the connection. As shown in the following paragraphs, the steel plate connections were deemed adequate when compared to the ultimate values observed when the connections were tested in the laboratory.

7.3 Connection

The maximum tensile stress that occurred in a plate connector in the transverse direction in the actual load test was 4,060psi. The maximum tensile transverse stress that occurred in any plate in the ANSYS™ model was 2,189psi. According to the experimental laboratory test the maximum stress that the plate obtained at the failure of the connection was 8,533psi. This results in a safety factor of approximately 2.1.

The maximum transverse tensile stress that occurred in the ANSYS™ model when the plate spacing was increased to 10’-0” on center was found to be 3,117psi. This value gives the connection a safety factor of approximately 2.7.

7.4 Diaphragm Stresses

The diaphragms were instrumented at both ends during the actual load test. The ANSYS™ diaphragms allow the maximum normal stress values to be reported at the end (connection to the girder web) of each member. The maximum stress in each of the five instrumented diaphragms is shown in Figures 7-14 through 7-18.

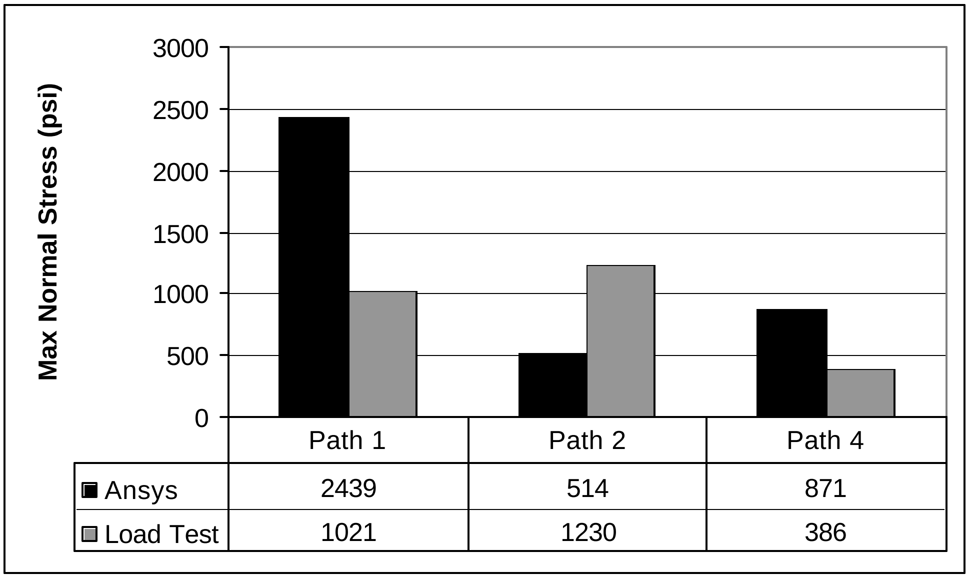

* (-) = Compression

(+) = Tension

Figure 7-14. Maximum Normal Stress - Diaphragm D1

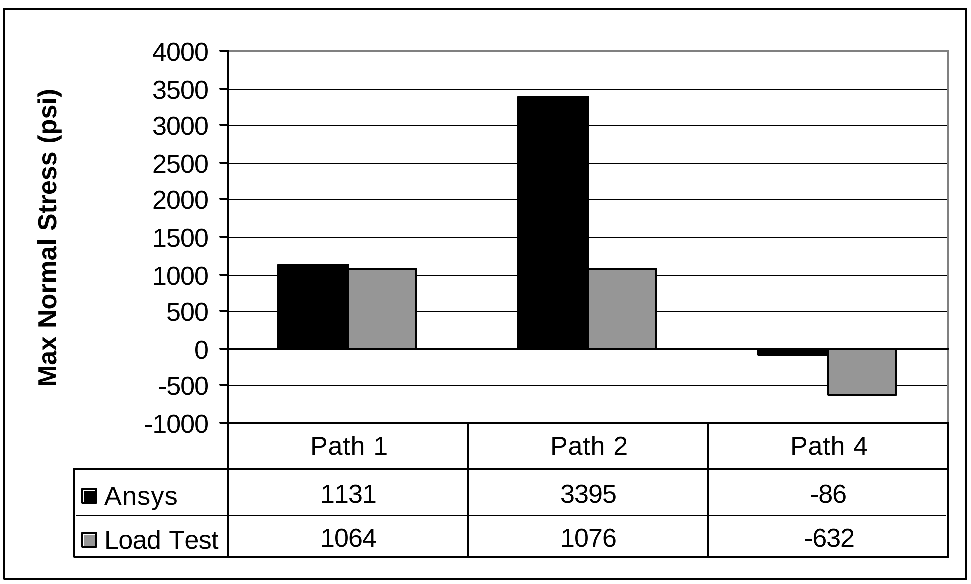

* (-) = Compression

(+) = Tension

Figure 7-15. Maximum Normal Stress - Diaphragm D2

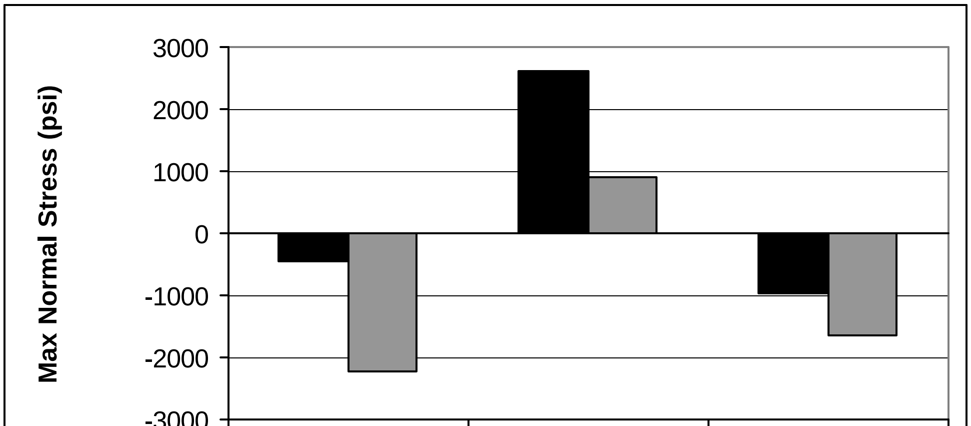

	Path 1	Path 2	Path 4
Ansys	-462	2607	-966
Load Test	-2217	916	-1647

* (-) = Compression

(+) = Tension

Figure 7-16. Maximum Normal Stress - Diaphragm D3

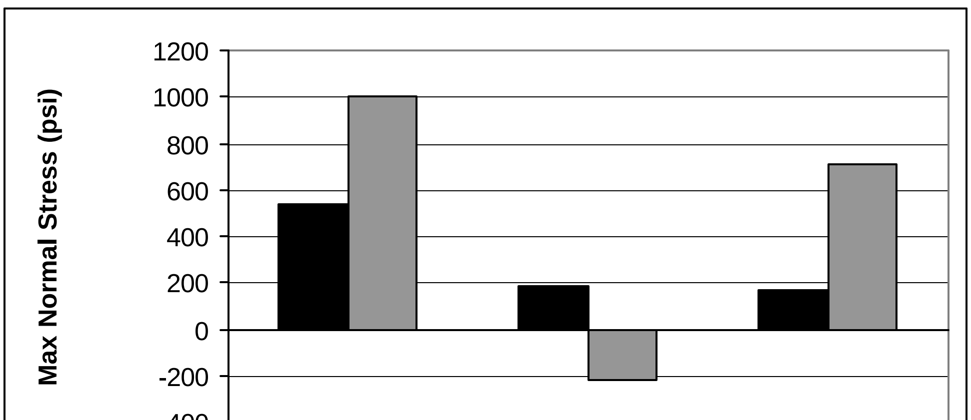

	Path 1	Path 2	Path 4
Ansys	537	184	170
Load Test	1003	-222	711

* (-) = Compression

(+) = Tension

Figure 7-17. Maximum Normal Stress - Diaphragm D5

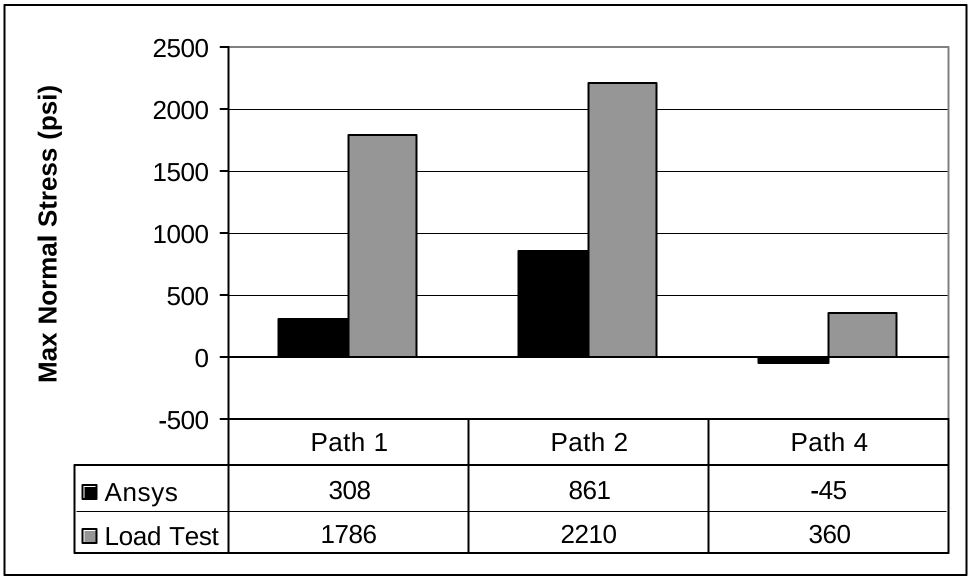

* (-) = Compression

(+) = Tension

Figure 7-18. Maximum Normal Stress - Diaphragm D6

The instrumented diaphragms were primarily in one quadrant of the bridge. The ANSYS™ model was only loaded to produce maximum effects on the five deck girders at mid-span. The diaphragms at the mid-points in the actual load test showed larger stresses. The quarter point diaphragms had larger stress values in the ANSYS™ model. The largest stress in any plate was computed by the ANSYS™ model, it was found to be 3,400psi in tension. This value is significantly less than the diaphragm yield strength of 36ksi. It is evident that the steel plates transmit the majority of the live load forces.

8 Conclusions and Recommendations

The present study focused on a new bridge deck girder obtained from a typical AASHTO Type III girder in the following areas: (1) fabrication and transportation of a new deck girder type: (2) the bridge construction, instrumentation and in-situ load testing of the finished bridge; (3) the design and FE analysis of the bridge behavior; and finally, (4) on the flange connection shear and tensile capacities and failure modes. Based on this 13-month investigation, the following conclusions and recommendations can be made:

- The fabrication of the deck girders was completed according to design specifications and few problems were encountered. The development of a new formwork that would allow the deck and the AASHTO Type III girder to be cast in one pour will expedite the fabrication and bridge construction process. The addition of more inserts to allow additional securing chains during transportation would also be beneficial.
- The construction of the bridge was completed without any major problems. The diaphragm holes proved to be too large for the collapsible washers used for the connections. A decrease in hole diameter could be a solution to this problem. Another solution could be the use of concrete diaphragms.
- Although the deck girders were installed with an acceptable tolerance with respect to vertical tolerance, in order to eliminate the need for the asphalt topping in future projects, an extra inch of concrete could be added on the top of the deck girders during fabrication, which could be ground off prior to the opening of the bridge. This would cut down on construction time, which would in turn save money.
- The bridge test was completed before the opening of the bridge, and a large number of test results were recorded. The data was analyzed and compared to the FE analysis. As expected, the girder stresses were not distributed evenly but rather distributed according to the location of the loading path. The girders that were located underneath the loading vehicle received much higher stresses than the ones away from the loading.
- During the load tests, the instruments on the plates recorded higher stresses than the diaphragms, which could be a result of the diaphragms not being tightened according

to specifications (due to oversized holes in the concrete members). The displacements recorded were very small compared to the design criteria of L/800 given by AASHTO. The end bent provided the deck girders with a fixed constraint which was the cause of the negative moment found in the girders. The impact factors were calculated using the dynamic test results. The values were proven to be fairly close to the design impact factors given by AASHTO.

- The use of Larsa 2000™ as an analysis program proved to be very precise when considering the effects (prestress, dead, and live loading) on the deck girders and analyzing multiple moving loads with multiple lane paths at any point along the bridge length. The accuracy of the program, when compared to the NCDOT design calculations, was very comparable. The construction stage option allowed a timely and accurate assessment of deck girder camber and stress values at different construction steps. The limitations of the program were encountered when the steel plate connectors were considered. The use of a more sophisticated FE program was required to analyze the smaller bridge components with more precision.
- The ANSYS™ FE model resulted in plate stress values that were comparable to the actual load test results. The load test and ANSYS™ model maximum tensile stress values were found to be approximately half of the stress that would result in a connection failure. The spacing of the plates was increased to 10'-0" on center and a noticeable increase in plate stress occurred. The diaphragm members in both the FE model and the actual load test were found to be very small compared to the diaphragm yield strength of 36ksi. The diaphragms' stresses were relatively small with both plate spacing increments. The plate spacing increase to 10"-0" appears to be viable design alternative based on the ANSYS™ model results, but only with a redesigned connection detail, and considering connection long-term performance.
- The flange connection analysis shows that the PCI handbook 6th Edition does not accurately assess all types of connections. Therefore, either different equations or analysis need to be derived, or additional experimental investigations performed. The ultimate experimental capacities for shear and tension are respectively 24.65 kips and 12.78 kips. These values vary drastically from the predicted values from the PCI Design Handbook 6th Edition.

9 Implementation and Technology Transfer

Research product: deck girder bridge fabrication/construction reports

Suggested User: Materials and Tests, and Structure Design Units

Recommended Use: to develop faster, safer, and more efficient methods to complete future deck girder bridge system projects.

Recommended Training: none

Research product: integral end-bent moment restraint

Suggested User: Structure Design Units

Recommended Use: the deck's negative reinforcement and connection detailing to the integral end bent provided a significant moment restraint at the end of the deck girders, a detail which must be designed accordingly, in order to avoid deck cracking

Recommended Training: minimal

Research product: deck girder bridge ANSYS™ and LARSA finite element (FE) models

Suggested User: Structure Design Unit

Recommended Use: to find the forces and behavior of components not covered in the current LRFD Bridge Design Manual and to analyze the behavior of the deck girder bridge as a whole.

Recommended Training: minimal training, operating the FE software

Research product: embedded stud connection laboratory testing

Suggested User: Materials and Tests, and Structure Design Units

Recommended Use: to find the capacity of headed stud connections not currently presented in the PCI Design Handbook 6th Edition.

Recommended Training: none

10 References

1. AASHTO LRFD Bridge Design Specifications, American Association of State Highway Transportation Officials (2002).

2. ACI 318-05, Building Code Requirements for Structural Concrete and Commentary (2005).

3. AISC Manual of Steel Construction, American Institute of Steel Construction (2001).

4. Anderson, Art, "Stretched – Out AASHTO – PCI Beams Types III and IV for Longer Span Highway Bridges," PCI Journal, V. 18, No. 5, September – October 1973.

5. Anderson, Neal S., and Meinheit, Donald F., "Pry out Capacity of Cast-In Headed Stud Anchors," PCI Journal, V.50, No. 2, March – April 2005.

6. Anderson, Neal S., and Meinheit, Donald F., "Design Criteria for Headed Stud Groups in Shear: Part 1 – Steel Capacity and Back Edge Effects," PCI Journal, V.45, No. 5, September – October 2000.

7. ANSYS™ Product Launcher Release 10.0, Copyright 1994-2000 SAS IP.

8. Arcview, "Arcview GIS 3.3®," software developed by Environmental Systems Research Institute, 1995.

9. Bailey, Kevin G., "Deck Bulb Tees Using Standard AASHTO I-Beams and AASHTO LRFD Specifications," Thesis Document, UNC-Charlotte, 2006.

10. Cheung, M. S., Jategaonkar, R., and Jaeger, Leslie G., "Effects of intermediate diaphragms in distributing live loads in beam-and-slab bridges," Canadian Journal of Civil Engineering, V. 13, No. 3, June 1986.

11. Concrete Technology Associates, "Segmental Construction," Technical Bulletin 73 – B12, December 1973.

12. Gergely, J., Lawrence, T.O., Prado, C.I., Ritter, C.T., Stiller, W.B. North Carolina Department of Transportation Research Project No. HWY – 2002 – 12: *Evaluation of Bridge Analysis Vis – á – vis Performance* (2004).

13. Hanks, B. C., "Hand Calculations for Pre-stressed Deck Girders," NCDOT, March 2005.

14. Larsa™, "Larsa™ 2000 4th Dimension for Bridges," software developed by Larsa™, Inc., 2005.

15. PCI Design Handbook: Precast and Prestressed Concrete (5th Edition), Precast/Prestressed Concrete Institute (1999).

16. PCI Design Handbook: Precast and Prestressed Concrete (6th Edition), Precast/Prestressed Concrete Institute (2004).

17. PCI Bridge Design Manual: Chapter 9, Section 9.4, Precast/Prestressed Concrete Institute (2003).

18. Prestressed Concrete Institute, "The Reflections of the Beginnings of Prestressed Concrete in America," PCI Journal, V. 23, No. 3, May – June 1978 through V. 25, No. 3, May – June 1980.

19. Stallings JM, Yoo CH. Tests and Ratings of Short Span Steel Bridges. *Journal of Structural Engineering.* ASCE; 119.

Appendix

A- Construction Report

A.1 Site Preparation

Once the decision was made to replace the existing bridge on Austin Road in Stanley County, site preparation began to demolish the existing bridge. The surrounding residents were notified and signs for detours were posted for the traffic on Austin Road. A detour route was created on both sides of Long Creek. Several steps were taken to keep the surrounding environment safe from the debris created during the demolition and construction of the bridge. Erosion control measures were installed to prevent contamination of Long Creek (see Figure A-1). The creek is labeled as a clean water creek; requiring no creek disturbance by the contractor.

Figure A-1. Erosion Control Measures

Once all site preparation was complete, the demolition process of the existing bridge began. Fabrication of the deck girders was being performed in Savannah, GA by Standard Concrete Products, at the same time demolition was done to the existing bridge. The existing bridge consisted of four spans at 20 feet. The superstructure consisted of steel beams with timber decking and the substructure was constructed from timber piles with concrete bent caps.

The replacement bridge consisted of five prestressed deck girders made from standard AASHTO Type III girders (see Figure A-2). The deck girders were spaced at 6.5 feet on center, with intermediate diaphragms at mid-span and quarter points along the bridge. The deck also had embedded angle connections along both sides of the interior girders and on the inner flange of the exterior girders, placed every 5 feet. The embedded angles were connected by a 3"x 4"x ½" plate. The deck girders also contained a grouted shear key along the edge of the flanges between girders. Each end of the bridge was embedded into an integral end bent that was poured at a later date. The guard rail that was attached to the parapet wall was a one-bar metal rail also shown in Figure 44. The bridge also required an average of 4½" of asphalt due to the location of the bridge: one of the abutments was located in a sag curve.

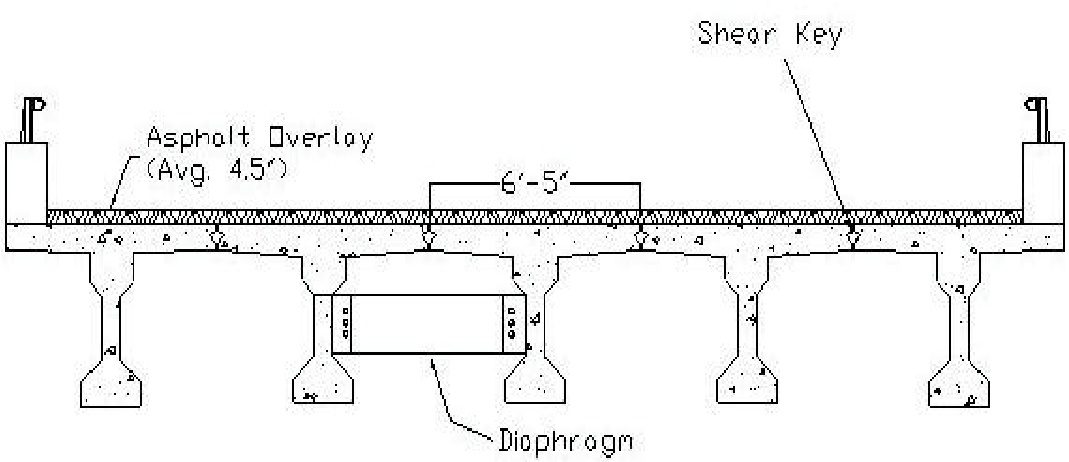

Figure A-2. Section View of Deck Girder Bridge

Once the existing bridge was removed soil was transported in to be used as fill. The proper elevation was established and the construction of the abutments began. The first step was to install the piles used in the abutments. The type of piles used was HP 12 x 53 steel piles. The piles were driven to a minimum bearing capacity of 60 tons each. The rebar for each abutment was tied, and then the formwork was constructed around the rebar. Concrete was then placed, completing the abutments. Each abutment was poured and vibrated using a mechanical vibration device. The abutments were constructed to ensure a 2% slope in the deck girders starting at the East end, sloping downward toward the West end. A 2% slope was also constructed in the transverse direction of the abutments as well (see Figure A-3).

Dowel bars were extending form the top of the abutment to connect it with the integral end bent (see Figure A-4). Once the concrete achieved a minimum compressive strength of 4,000 psi, the formwork was removed and the elastomeric bearing pads, shown in Figure A-5, were placed at the correct locations on top of the abutments. Rip rap was placed on the bank in front of the abutment for erosion control (see Figure A-6).

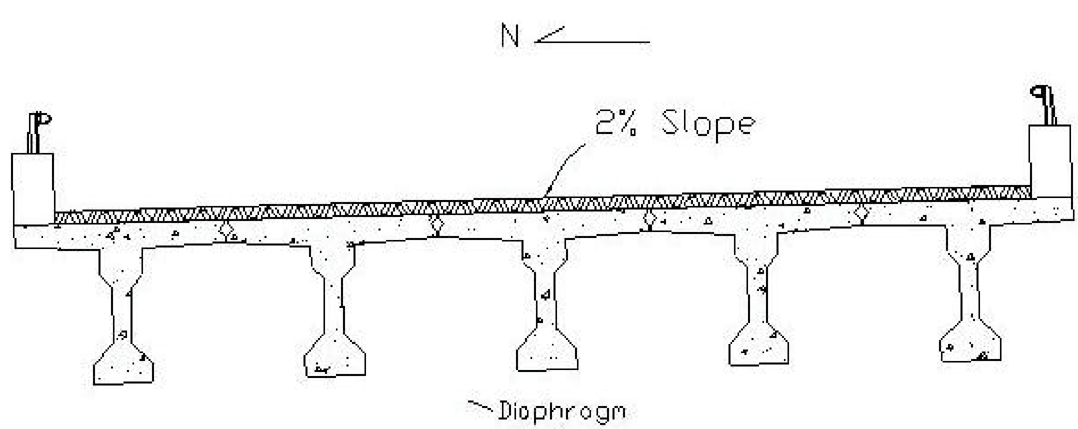

Figure A-3. Transverse Slope of New Deck Girder Bridge

Figure A-4. Vertical Rebar Protruding Out of Abutment

Figure A-5. Elastomeric Bearing Pad

Figure A-6. Rip Rap Installed Along the Creek Bank in Front of the Abutment

In order for the trucks carrying the deck girders to be able to transport them onsite, a temporary bridge system was needed. The temporary bridge system consisted of materials that were from previous construction projects. The bridge was constructed using steel beams combined with a timber deck that was installed in groups of fours (see Figure A-7). The temporary bridge system was constructed along the South side of the new bridge location.

Figure A-7. Installation of Temporary Bridge System

Once the temporary bridge system was finished, safety lines were added to provide a safe environment for the construction workers (see Figure A-8). Cranes were ordered and positioned on the site one day before the arrival of the deck girders. The contractor selected two 240 ton cranes, shown in Figure A-9, for the installation of the deck girders. The cranes were stationed at the East and West ends of the proposed bridge location. Steel beams and scaffolding were placed across Long Creek located where the bridge was going to be constructed (see Figure A-10). This provided the workers a working pad for the installation of the steel diaphragms on the bridge. The next step was installing the deck girders.

Figure A-8. Finished Temporary Bridge with Safety Lines

Figure A-9. 240 Ton Crane Used for Deck Girder Installation

Figure A-10. Steel Beam and Scaffolding for Diaphragm Installation

A.2 Girder Installation

The installation of the deck girders was a rapid, but delicate process. Each deck girder was carefully backed down onto the temporary bridge system by the trucks. The crane lines were then attached to lifting loops cast during fabrication in the deck girders shown in Figure A-11. The crane used two heavy-duty shackles to lift the deck girders off the truck.

Prior to lifting, the angles for the steel diaphragms were attached at the proper locations on the deck girder. The steel angles were only hand tightened during this initial phase (see Figure A-12). They were tightened in accordance with the plan specifications, once all the deck girders were in final position. Once the two cranes were attached and the steel angles tightened, the deck girder was lifted off of the truck in unison. The cranes then slowly rotated the deck girder above the abutments. Once the deck girder was in the correct location above the abutments, each crane slowly lowered the deck girder down (see Figure A-13). The deck girder was carefully placed onto the bearing pads.

Figure A-11. Lifting Loops Used for Deck Girder Installation

Figure A-12. Hand Tightening of the Angles Before Deck Girder Placement

The deck girder was then temporarily stabilized until the next deck girder was placed and the diaphragms were installed. This was achieved using a cable and ratchet lock system. Each end of the cable had a hook attached to it. One hook was attached to the longitudinal rebar anchored in the deck, and the other hook was attached to the rebar in the abutment as shown in Figure A-14. This additional lateral support was a precautionary measure due to the high deck girder center of gravity, as well as the 2% transverse slope of the abutment.

Figure A-13. Installation of Deck Girder

Figure A-14. Stabilizing System for Deck Girders

A.3 Superstructure Construction

Once the five deck girders were in final position, the construction for the final components of the superstructure began. The next step was to install the diaphragms between the deck girders. There were a total of twelve diaphragms used at mid-span and at quarter points along the bridge. The diaphragm installation began with the center diaphragms, then the diaphragms at the quarter and three-quarter points on the bridge. The diaphragms were placed onto the temporary work platform that was constructed underneath the bridge prior to the installation of the deck girders. The diaphragms were lifted into place using a small crane system consisting of two pulleys and a crank attached to a metal rolling frame (see Figure A-15). Next, the bolts securing the diaphragms were tightened, and the flange connector plates were welded to the embedded angles. The bolts were tightened according to the specifications using a torque wrench. Collapsible washers, shown in Figure A-16, were used to help provide assurance of the proper torque. However, the holes in the angles were too large, and the washers started to push through before the proper torque was achieved.

Figure A-15. Small Crane System Used for Diaphragm Installation

Figure A-16. Collapsible Washer Used for Tightening Bolts

The welding of the flange connections in the deck girder was performed during the same time as the tightening of the bolts (see Figure A-17). Each connection consisted of an angle embedded into the flange of each parallel deck girder and a galvanized plate. The plate was completely welded along the three edges (see Figure A-18). Once each connection was welded, the shear key was prepared for grouting. The end of each shear key was blocked out by a square piece of plywood (see Figure A-19). The bottom of the shear key was stuffed with backer rod to prevent the grout from flowing through. Some of the deck girders fit tight enough together, that the backer rod was not able to be placed. Great Stuff® Insulating Foam Sealant was used in place of the backer rod at these locations to prevent the grout from escaping through the gap in between the girders (see Figure A-20).

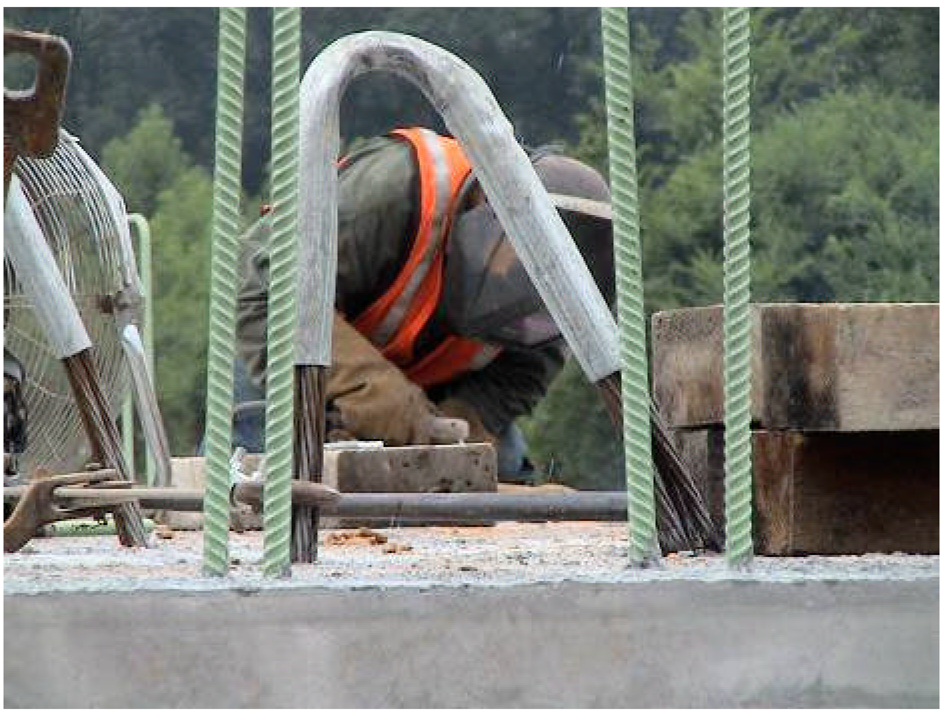

Figure A-17. Welding of Flange Connections

Figure A-18. Welded Flange Connections

Figure A-19. Plywood Used to Form the Shear Key

Figure A-20. Insulating Foam Used in Place of Backer Rod

Once completed, the grout was then mixed using a small gasoline powered rotary mixer (see Figure A-21). A gallon of water for every 50 lbs. of grout was the mixing ratio used. The grout was mixed for about 5 to 10 minutes and then poured into a wheel barrow. The wheel barrow was then transported to the West end of the bridge. At the location of the first connection the grout was poured into the connection opening. The slope of the bridge allowed the grout to flow towards the East side of the bridge. Once a connection opening was full, a trowel was used to smooth out the grout (see Figure A-22). This was performed for each line of connections. The connections were then covered with damp burlap to provide proper curing conditions for the grout (see Figure A-23).

Figure A-21. Gasoline Powered Rotary Mixer

Figure A-22. Trowel Used to Smooth Out Flange Connection Pocket

Figure A-23. Damp Burlap Used to Cover the Grouted Connections

A.4 Integral End Bent

During the grouting of the shear key, the integral end bent construction began as well. The East bent was constructed first, and then the West would follow. Rebar was tied according to the plans, and then the formwork was fabricated using plywood (see Figure A-24). The East facing of the formwork was braced using 2x4's stabilized into the fill soil. Then, the concrete was ordered and transported to the site. The concrete was poured directly from the truck into a concrete bucket. The bucket was lifted by a crane on site from the truck to the end bent location. Once the bucket was above the proper location, the release lever was pulled and the concrete was dumped into the formwork (see Figure A-25). A mechanical vibration device was used to remove any voids in the concrete (see Figure A-26). Once the concrete reached the desired elevation a trowel was used to smooth it. The same process was repeated for the West bent.

Figure A-24. Integral End Bent Rebar and Formwork

Figure A-25. Concrete Used to Pour the Integral End Bent

Figure A-26. Mechanical Vibration Device Used to Vibrate Concrete

A.5 Parapet and Guardrail

Once the construction of the integral end bents was completed, back fill was placed. Soil was delivered and compacted according to plan specifications. The construction of the parapet walls was then started. The epoxy coated reinforcement for each wall was added during the fabrication process of the deck girders. The longitudinal rebars were first tied and then the formwork was constructed. The contractor chose to use wooden formwork instead of slip forms to save money. The formwork was constructed using plywood nailed together. The drainage holes for the parapet were made using wooden box block outs (see Figure A-27). There were six total on the parapet.

Once the formwork was complete, then the concrete was ordered and placed. Once the concrete was poured, inserts were placed into the concrete to provide a template for the installation of the guardrail (see Figure A-28). Then the formwork was removed and the process was completed for the other parapet. Once the parapets were finished, the metal guard rail could be attached. The type of guard rail used for this bridge was a one bar metal rail. The rail was attached to the top of the parapet wall according to plans using ¾ inch diameter studs anchored into the concrete (see Figure A-29).

Figure A-27. Removal of Block Out for Drainage Holes

Figure A-28. Concrete Insert Placed Into the Parapet

Figure A-29. One-Bar Metal Railing

A.6 Approach Slab and Wearing Surface

The approach slab construction began during the construction of the parapets. The bridge system required an approach slab at each end of the bridge. The construction of the approach slab began by compaction of a 6 inch layer of ABC stone base. A geo-membrane, shown in Figure A-30, was then installed on top of the base to provide an impermeable surface and prevent any water from washing away the underlying soil. The rebar for the slab was then tied. The approach slab required the rebar to be epoxy coated to prevent corrosion (see Figure A-31). The rebar was supported on high chairs locating the rebar at the correct height in the slab. The formwork was then constructed around the outside edges of the rebar. The formwork consisted of 2x4s and plywood nailed together. The concrete was then ordered and delivered to the site. Each slab was poured directly from the truck and a mechanical vibration device was used to eliminate voids in the concrete. Once the desired elevation was reached, a trowel was used to smooth the concrete. The surface was then given a raked finish (see Figure A-32).

Figure A-30. Geo-Membrane Installed Underneath Approach Slab

Figure A-31. Epoxy Coated Rebar for Approach Slab

Figure A-32. Raked Finish on Top of Approach Slab

Once the approach slab was complete and the formwork was removed, the installation of the wearing surface could begin. The wearing surface on the bridge had an average thickness of 4½". The asphalt for the wearing surface was installed in one inch lifts and compacted according to specifications. Once the asphalt wearing surface was complete, the installation of the guard rail along the road side began. The first step in installing the guard rail was to lay out each piece along the road side at the proper locations (see Figure A-33). This would provide a fast and efficient installation. The posts were then driven into the ground by a hydraulic hammering device attached to a truck bed (see Figure A-34). Then, the guard rail was attached to each post.

The final step in the construction of the bridge was to clean the road and prepare it for painting. The road was washed and swept clean as well as the parapet wall. The double yellow line and two outside lines were put down and the bridge was ready for opening. The bottom and top of the final product after construction is shown in Figures A-35 and A-36.

Figure A-33. Guard Rail Placed Along Side of Roadway

Figure A-34. Hydraulic Hammer Used for Driving Posts

Figure A-35. Underside of Deck Girder Bridge

Figure A-36. Deck Girder Bridge on Austin Rd. in Stanly Co., NC

B- Connection Test Details

B.1 Concrete Specimen Log

Table B-1. 7-Day Concrete Ultimate Strength

7 - Day Strength	Test #1	Test #2	Test #3
Load (lb)	94668	94062	92398
Pressure (psi)	7537	7489	7356

Table B-2. 28-Day Concrete Ultimate Strength

28 - Day Strength	Test #1	Test #2	Test #3
Load (lb)	119200	119110	122460
Pressure (psi)	9486	9478.4	9745

Table B-3. Concrete Specimen Tensile Properties

Tensile Strength	Test #1	Test #2	Test #3
Load (lb)	31653	30900	27583
Broken Aggregate	24	18	18
Unbroken Aggregate	5	7	7

Table B-4. Concrete Properties at Pour

Slump	4"
Air Content	3.90%

C- Bridge Test Details

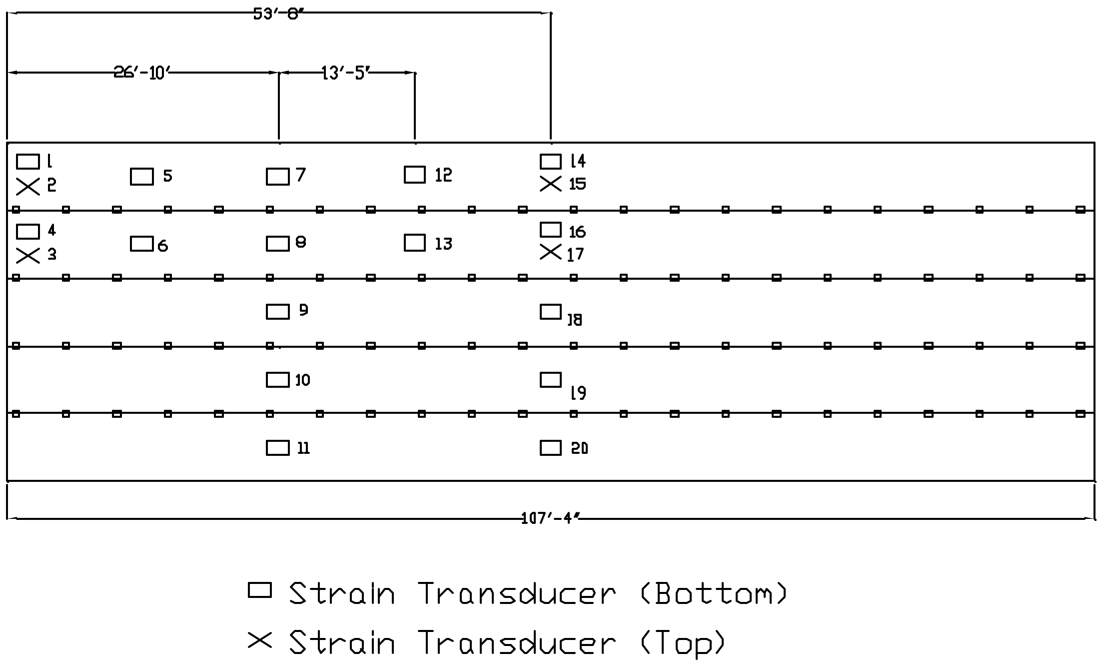

Figure C-1. Strain Transducer Layout

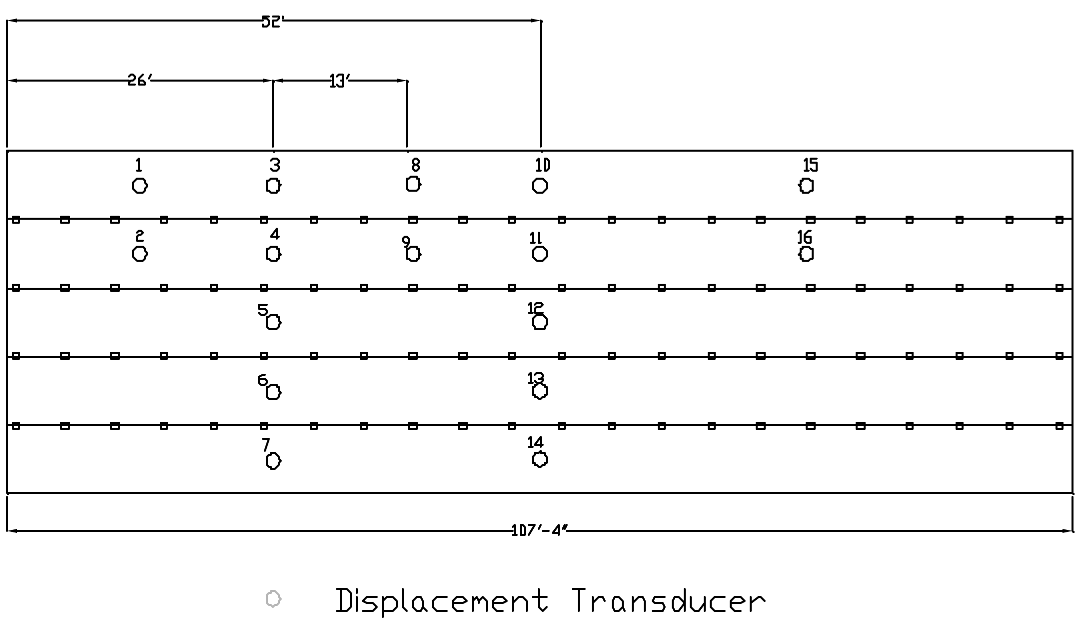

Figure C-2. Displacement Transducer Layout

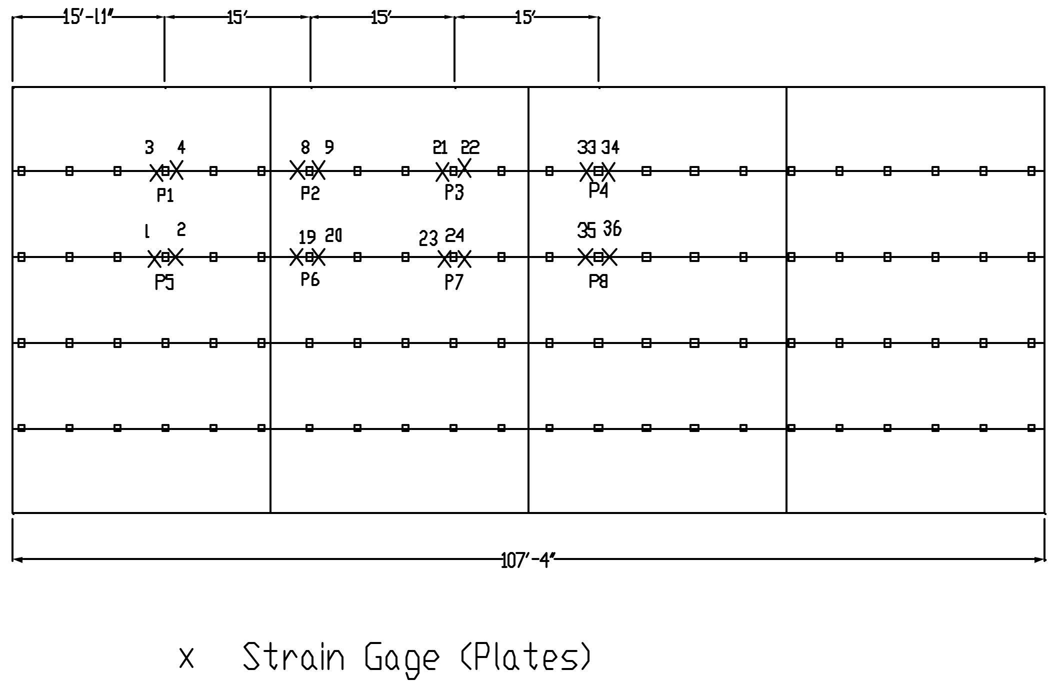

Figure C-3. Plate Connection Strain Gage Layout

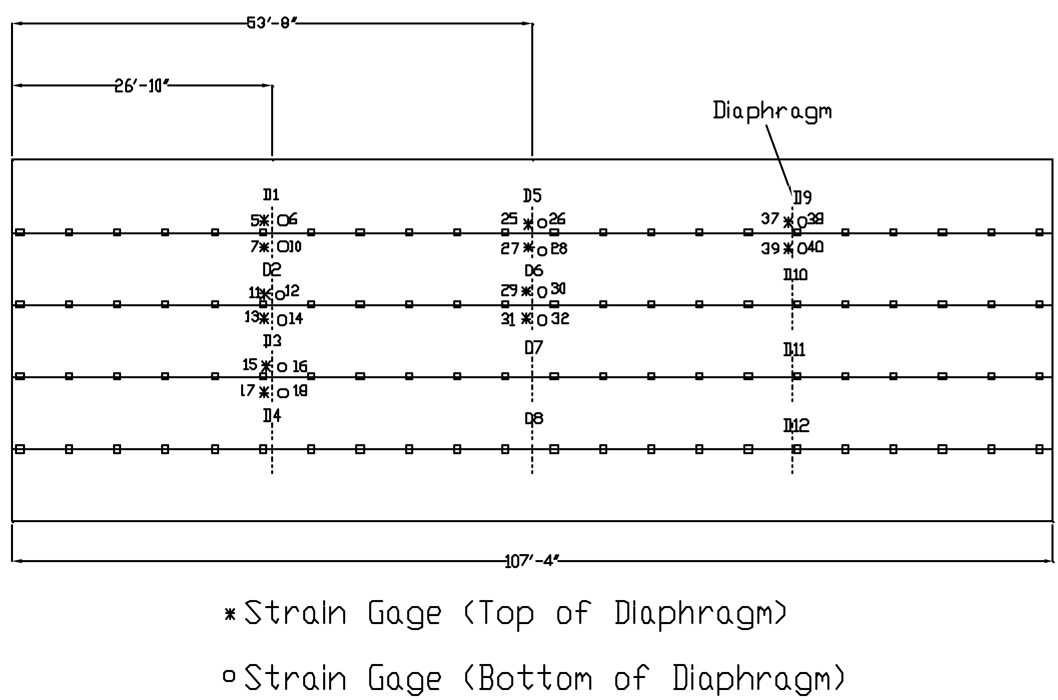

Figure C-4. Diaphragm Strain Gage Layout

D- ANSYS™ Batch Input File

```
/TITLE, Deck Girder Bridge Stanly County, NC
!
/PREP7
!
ANTYPE,STATIC,NEW
!
ET,1,SOLID65              ! 3-D Reinforced Concrete Solid
KEYOPT,1,1,0
KEYOPT,1,5,1
KEYOPT,1,6,3
KEYOPT,1,7,1
!
ET,2,LINK8                ! Prestress Cable
!
ET,3,SOLID45              ! Steel Plate
!
ET,4,BEAM4                ! Steel Diaphragms
KEYOPT,4,6,1
KEYOPT,4,9,3
!
!                          ! Girder and Deck  High-Strength Concrete Properties
MPTEMP,1,0
MPDATA,EX,1,,6620862.588
MPDATA,PRXY,1,,.2
MP,DENS,1,.0868055
TB,MISO,1,1,6,
TBTEMP,0
TBPT,,.0005982,3960.6
TBPT,,.00126,7585.305
TBPT,,.00192,10321.261
TBPT,,.00259,12063.723
TBPT,,.00326,12942.623
TBPT,,.00399,13202
TB,CONC,1,1,9,
TBTEMP,0
TBDATA,,.25,.25,-1,-1,,
!                          ! Prestress Cable Material Properties
MPTEMP,1,0
MPDATA,EX,2,,29000000
MPDATA,PRXY,2,,.3
TB,BISO,2,1,2,
TBTEMP,0
TBDATA,,270000,,,,,
```

```
!                                ! Steel Reinforcement Material Properties
MPTEMP,1,0
MPDATA,EX,3,,29000000
MPDATA,PRXY,3,,.3
TB,BISO,3,1,2,
TBTEMP,0
TBDATA,,60000,,,,,
!                                ! Steel Plate and Diaphragm Material Properties
MPTEMP,1,0
MPDATA,EX,4,,29000000
MPDATA,PRXY,4,,.3
TB,BISO,4,1,2,
TBTEMP,0
TBDATA,,36000,,,,,
!
R,1,3,.025,,90,2,.025,          ! Real Constant Non-Reinforced Concrete
!
R,2,3,.03,,90,2,.031            ! Real Constant Integral Deck Concrete Top
!
R,3,.3307,.00715                ! Real Constant Prestress Strand
!
R,4,.1653,.00715                ! Real Constant Prestress Strand
!
R,5                             ! Real Plates
!
R,6,6.3,7.15,243,18,.225        ! Real Constant End Diaphragms
!
R,7,12.6,14.3,554,18,.45        ! Real Constant Middle Diaphragms
!
!
K,1,0,0,0,                      ! Center-line Key Points
K,2,-3.5,0,0
K,3,-6.5,0,0
K,4,-9.5,0,0
K,5,-11,0,0
KSEL,ALL
KGEN,2,ALL,,,,1.875
KSEL,S,KP,,6,10,1
KGEN,2,ALL,,,,3
KSEL,S,KP,,11,15,1
KGEN,2,ALL,,,,3
KSEL,S,KP,,16,20,1
KGEN,2,ALL,,,,2.875
K,26,0,19.85,0
K,27,0,23.75,0
K,28,0,27.65,0
```

```
K,29,0,35.75,0
KSEL,S,KP,,26,29,1
KGEN,2,ALL,,,-3.5
K,34,-8,35.75,0
K,35,0,47,0
K,36,0,51.5,0
K,37,0,55,0
KSEL,S,KP,,35,37,1
KGEN,2,ALL,,,-3.5
KSEL,S,KP,,38,40,1
KGEN,2,ALL,,,-4.5
KSEL,S,KP,,41,43,1
KGEN,2,ALL,,,-6
KSEL,S,KP,,44,46,1
KGEN,2,ALL,,,-6
KSEL,S,KP,,47,49,1
KGEN,2,ALL,,,-6
KSEL,S,KP,,50,52,1
KGEN,2,ALL,,,-6
KSEL,S,KP,,53,55,1
KGEN,2,ALL,,,-3.25
KSEL,S,KP,,56,57,1
KGEN,2,ALL,,,-2.25
KSEL,S,KP,,59,60,1
KGEN,2,ALL,,,-1.25
!
KSEL,ALL
!
A,2,1,6,7
A,3,2,7,8
A,4,3,8,9
A,5,4,9,10
A,7,6,11,12
A,8,7,12,13
A,9,8,13,14
A,10,9,14,15
A,12,11,16,17
A,13,12,17,18
A,14,13,18,19
A,15,14,19,20
A,17,16,21,22
A,18,17,22,23
A,19,18,23,24
A,20,19,24,25
A,22,21,26,30
A,30,26,27,31
```

```
A,31,27,28,32
A,32,28,29,33
A,33,29,35,38
A,34,33,38,41
A,38,35,36,39
A,41,38,39,42
A,39,36,37,40
A,42,39,40,43
A,44,41,42,45
A,45,42,43,46
A,47,44,45,48
A,48,45,46,49
A,50,47,48,51
A,51,48,49,52
A,53,50,51,54
A,54,51,52,55
A,57,54,55,58
A,59,56,57,60
A,56,53,54,57
A,61,59,60,62
!
!
ASEL,ALL                        ! Girder Volume Creation and Extrusion
VEXT,ALL,,,,3
!
ASEL,S,LOC,Z,3
VEXT,ALL,,,,4
!
ASEL,S,LOC,Z,7
VEXT,ALL,,,,14
!
VSEL,S,LOC,Z,14
VGEN,4,ALL,,,,,14
!
VSEL,ALL
VSEL,U,LOC,Z,1.5
VGEN,11,ALL,,,,,60
!
VSEL,S,LOC,Z,656
VSEL,A,LOC,Z,642
VSEL,A,LOC,Z,628
VDELE,ALL,,,1
!
ASEL,S,LOC,Z,621
VEXT,ALL,,,,8
!
```

```
ASEL,S,LOC,Z,629
VEXT,ALL,,,,,7
!
!
VSEL,S,LOC,Y,53          ! Top of Deck Reinforcement
VATT,1,2,1,
!
VSEL,ALL                 ! Middle of Deck no Reinforcement
VSEL,U,REAL,,2,
VATT,1,1,1
!
!
LSEL,S,LOC,X,-3.5,       ! Prestress Strand Real Constant Assignment
LSEL,R,LOC,Y,1.875,
LATT,2,3,2,
!
LSEL,S,LOC,X,-6.5,
LSEL,R,LOC,Y,1.875,
LATT,2,3,2,
!
LSEL,S,LOC,X,-9.5,
LSEL,R,LOC,Y,1.875,
LATT,2,3,2,
!
LSEL,S,LOC,X,-3.5,
LSEL,R,LOC,Y,4.875,
LATT,2,3,2,
!
LSEL,S,LOC,X,-6.5,
LSEL,R,LOC,Y,4.875,
LATT,2,3,2,
!
LSEL,S,LOC,X,-9.5,
LSEL,R,LOC,Y,4.875,
LATT,2,3,2,
!
LSEL,S,LOC,X,-3.5,
LSEL,R,LOC,Y,7.875,
LATT,2,3,2,
!
LSEL,S,LOC,X,-6.5,
LSEL,R,LOC,Y,7.875,
LATT,2,3,2,
!
LSEL,S,LOC,X,-9.5,
LSEL,R,LOC,Y,7.875,
```

```
LATT,2,3,2,
!
LSEL,S,LOC,X,0,
LSEL,R,LOC,Y,1.875,
LATT,2,4,2,
!
LSEL,S,LOC,X,0,
LSEL,R,LOC,Y,4.875,
LATT,2,4,2,
!
LSEL,S,LOC,X,0,
LSEL,R,LOC,Y,7.875,
LATT,2,4,2,
!
!
VSEL,ALL                    ! Symmetry to Create One-Girder
VSYMM,X,ALL
ASEL,S,AREA,,9404
VEXT,ALL,,,,.5
!
ASEL,S,AREA,,18190
VEXT,ALL,,,.5
!
ASEL,S,AREA,,18192
VEXT,ALL,,,1.25
!
VSEL,S,VOLU,,4181,4183,1    ! Plate Generation
VATT,4,5,3
!
VSEL,S,REAL,,5
VGEN,11,ALL,,,,,60
!
VSEL,S,REAL,,5
VGEN,4,ALL,,,78
!
!
VSEL,ALL
VSEL,U,REAL,,5
VGEN,5,ALL,,,78
!
!
VSEL,ALL
LSEL,ALL
!
!
L,8957,15609                ! Lines for Diaphragm Elements
```

```
L,21561,27513
L,33465,39417
L,45369,51321
L,11809,18461
L,24413,30365
L,36317,42269
L,48221,54173
!
!
LSEL,S,LINE,,130372            ! Real Constant and Element Type for Diaphragms
assigned
LSEL,A,LINE,,130371
LSEL,A,LINE,,130370
LSEL,A,LINE,,130369
LATT,4,7,4
!
!
LSEL,S,LINE,,130373
LSEL,A,LINE,,130374
LSEL,A,LINE,,130375
LSEL,A,LINE,,130376
LATT,4,6,4
!
LSEL,ALL
ASEL,ALL
VSEL,ALL
KSEL,ALL
NUMMRG,ALL,,,,LOW       ! Re-number and Compress all Entities
NUMCMP,ALL
!
LESIZE,ALL,,,1,1,1,OFF,,   ! Mesh all Volumes as One Element
VSEL,ALL
MSHAPE,0,3D
MSHKEY,1
VMESH,ALL
!
LSEL,ALL
!
LSEL,S,REAL,,3,4,1     ! Mesh Lines that Represent Diaphragms and Prestress Strands
LSEL,A,REAL,,6,7,1
LMESH,ALL,
LSEL,ALL,
!
!
ASEL,S,LOC,Z,1.5       ! Fix Areas Inside Integral End-Bent
ASEL,A,LOC,Z,5
```

```
ASEL,A,LOC,Z,14
ASEL,A,LOC,Z,0
DA,ALL,UX,0
DA,ALL,UY,0
DA,ALL,ROTZ,0
DA,ALL,ROTY,0
DA,ALL,ROTX,0
NSEL,ALL
!
!
LSEL,ALL          ! Reflect Entire Model about Mid-Span in the Longitudinal Direction
ASEL,ALL
ASEL,S,LOC,Z,636
DA,ALL,SYMM
ASEL,ALL
!
!
ALLSEL,ALL,ALL
!
!
ACEL,,1
!
LSWRITE,1                 ! DEAD + PRESTRESS STRENGTH 1
!
!                         ! TRUCK PATH 4
!
ASEL,ALL
NSEL,ALL
NSEL,S,NODE,,10215
NSEL,A,NODE,,6153
F,ALL,FY,-8050
!
ASEL,ALL
NSEL,ALL
NSEL,S,NODE,,5703
NSEL,A,NODE,,9665
F,ALL,FY,-8050
!
!
ASEL,ALL
NSEL,ALL
NSEL,S,NODE,,9053
NSEL,A,NODE,,5203
F,ALL,FY,-8050
!
!
```

```
!
ASEL,ALL
NSEL,ALL
ESEL,ALL
ALLSEL,ALL,ALL
SFTRAN
SBCTRAN
LSWRITE,2
!
!                                    ! TRUCK PATH 2
!
ASEL,ALL
NSEL,ALL
NSEL,S,NODE,,10215
NSEL,A,NODE,,6153
NSEL,A,NODE,,9665
NSEL,A,NODE,,5703
NSEL,A,NODE,,9053
NSEL,A,NODE,,5203
FDELE,ALL,ALL
!
!
!
ASEL,ALL
NSEL,ALL
NSEL,S,NODE,,19187
NSEL,A,NODE,,16415
F,ALL,FY,-8050
!
ASEL,ALL
NSEL,ALL
NSEL,S,NODE,,15865
NSEL,A,NODE,,18745
F,ALL,FY,-8050
!
!
ASEL,ALL
NSEL,ALL
NSEL,S,NODE,,15253
NSEL,A,NODE,,18253
F,ALL,FY,-8050
!
!
ASEL,ALL
NSEL,ALL
ESEL,ALL
```

```
ALLSEL,ALL,ALL
SFTRAN
SBCTRAN
LSWRITE,3
!
!                                ! TRUCK PATH 1
!
ASEL,ALL
NSEL,ALL
NSEL,S,NODE,,19187
NSEL,A,NODE,,16415
NSEL,A,NODE,,15865
NSEL,A,NODE,,18745
NSEL,A,NODE,,15253
NSEL,A,NODE,,18253
FDELE,ALL,ALL
!
ASEL,ALL
NSEL,ALL
NSEL,S,NODE,,10229
NSEL,A,NODE,,12996
F,ALL,FY,-8050
!
ASEL,ALL
NSEL,ALL
NSEL,S,NODE,,9679
NSEL,A,NODE,,12554
F,ALL,FY,-8050
!
!
ASEL,ALL
NSEL,ALL
NSEL,S,NODE,,9067
NSEL,A,NODE,,12062
F,ALL,FY,-8050
!
!
ASEL,ALL
NSEL,ALL
ESEL,ALL
ALLSEL,ALL,ALL
SFTRAN
SBCTRAN
LSWRITE,4
!
!
```

```
ASEL,ALL
NSEL,ALL
ESEL,ALL
ALLSEL,ALL,ALL
!
SFTRAN
SBCTRAN
!
FINISH
!
SAVE
!
/SOLU
LSSOLVE,1,4,1
ANTYPE,STATIC
OUTPR,ALL,8
OUTRES,ALL,8
!
AUTOTS,ON
NSUBST,50,
SOLCONTROL,1.0,INCP
NCNV,0
SOLVE
!
FINISH
```